MAGNESIUM STABLE ISOTOPES AS A PROXY FOR MICROBIAL NUTRIENT UPTAKE AND BIOWEATHERING

DISSERTATION

ZUR ERLANGUNG DES GRADES EINES

DOKTORS DER NATURWISSENSCHAFTEN (DOCTOR RERUM NATURALIUM)

AM FACHBEREICH GEOWISSENSCHAFTEN

DER FREIEN UNIVERSITÄT BERLIN

vorgelegt von

Rasesh Pokharel

Berlin 2018

Prof. Friedhelm von Blanckenburg

Erstgutachter, Freie Universität Berlin

Prof. Anna Gorbushina

Zweitgutachter, Freie Universität Berlin

Tag der Disputation: 07.12.2018

Eidesstattliche Erklärung

Hiermit versichere ich, die vorliegende Dissertation selbstständig und ohne unerlaubte Hilfe angefertigt zu haben. Bei der Verfassung der Dissertation wurden keine anderen als die im Text aufgeführten Hilfsmittel verwendet. Beiträge von Koautoren zu publizierten und zur Publikation vorbereiteten Manuskripten sind im ‚Preface' dieser Arbeit dargelegt. Ein Promotionsverfahren zu einem früheren Zeitpunkt an einer anderen Hochschule oder bei einem anderen Fachbereich wurde nicht beantragt.

Berlin, 24. Oktober, 2018

_____

Rasesh Pokharel

Dedicated to my family

Ramesh Prasad Pokharel, Nirmala Pokharel, Rejina Pokharel, Rachi Pokharel, Mini Pokharel, Tirtha Raj Joshi, Ram Adhikari, Uttam Kandel, Aarnav and Aanya

FOLLOW YOUR CURIOSITY

Albert Einstein

Summary

Magnesium (Mg) is an important macronutrient for all living cells and is abundant in the environment. At the Earth's surface its stable isotopes are fractionated by both abiotic (mineral dissolution, primary and secondary mineral formation from solution) and biotic processes (uptake into and translocation through organisms). The objectives of this doctoral thesis were to investigate, in controlled laboratory experiments, the fractionation of Mg stable isotopes during (1) uptake and translocation of Mg into microbes focusing on microbial species, cell physiology, and the dependence on pH; and (2) mineral dissolution under abiotic conditions and in the presence of a fungus. Given that large Mg fluxes pass through biological pools, the fingerprints I identified is useful for Mg cycling studies, and for tracing Mg pathways through ecosystems.

To reduce the complexity of natural systems I conducted laboratory batch experiments using unicellular model organisms. Growth experiments showed a pH-dependence of Mg stable isotope fractionation during uptake by the rock-inhabiting microcolonial fungus *Knufia petricola*. The fungal cell was enriched in heavy Mg isotopes relative to the growth solution, where at pH 6 the $^{26}Mg/^{24}Mg$ ratio (expressed as $\delta^{26}Mg$) was 0.65 ± 0.10‰ higher than that in the growth solution, and at pH 3 $\delta^{26}Mg$ was 1.11 ± 0.34‰ higher. In contrast, the cyanobacterium *Nostoc punctiforme* incorporated lighter Mg isotopes from the growth solution and the cells' $\delta^{26}Mg$ was -0.27 ± 0.14‰ lower than that of the growth solution. Chlorophyll extracted from the cyanobacterium, however, preferentially incorporated the heavier Mg isotopes, with a $\delta^{26}Mg$ value that was 1.85 ± 0.14‰ higher than the growth solution. To explore how Mg metabolic pathways in these organisms set these isotope composition, a mass-balance model was designed.

The results can be explained by three fractionation processes and the mass balance associated with them: (1) during uptake, where Mg with a slightly lower $^{26}Mg/^{24}Mg$ isotope ratio is preferred by cells; (2) during incorporation of a substantial portion (>95%) of intracellular Mg into Mg-bonded compounds (ATP, ribosomes and chlorophyll) where Mg with higher $^{26}Mg/^{24}Mg$ is preferred; and (3) during efflux and, possibly, additional fractionation of the remaining free Mg that obtains the $^{26}Mg/^{24}Mg$ isotope ratio complementary to that of the Mg taken up into the bonded compounds. In the fungus *K. petricola* the efflux rate of free Mg low in $^{26}Mg/^{24}Mg$ is high; this Mg gets replenished by Mg from the growth solution that is higher in $^{26}Mg/^{24}Mg$. The bulk *K. petricola* cell Mg isotope signature is thus dominated by the isotopically heavy intracellular Mg bonded to compounds like ATP and ribosomes. The pH-dependence on Mg isotope fractionation observed in the fungus *K. petricola* cells is due to

differences in fluxes of Mg entering and leaving the cell. The cyanobacterium *N. punctiforme*, in contrast, has large intracellular Mg inventories (10 times greater than *K. petricola*) and partitions almost all Mg entering into the cell into its bonded compounds. Therefore the bulk cell obtains the isotope composition of the Mg that entered the cell. As a result, an inverse relationship arises between cellular Mg concentrations and the bulk cell Mg isotope fractionation. This model explains published field and laboratory measurements of the Mg isotope composition of leaves, roots, bulk plant, fungi and cyanobacteria, which are also characterized by an inverse relationship between Mg concentration and bulk Mg isotope fractionation. I suggest that the model of cellular processes and Mg metabolic pathways thus developed is predictive of Mg isotope fractionation in ecosystems.

Once the fractionation by the fungal cells was established, the rates and mechanisms of olivine $(Mg,Fe)_2(SiO_4)$ dissolution in the presence of the fungus *K. petricola* were determined in laboratory batch experiments. After 94 days, olivine dissolution rates (1.04×10^{-15} moles cm^{-2} s^{-1}) at pH 6 in presence of the fungus were seven-fold higher than in the abiotic control. Mg/Si ratios in the supernatant reflected an initial non-stoichiometric phase during which the dissolution rate was higher than the rate in a later stoichiometric phase. The initial non-stoichiometric phase was attributed to rapid exchange of Mg^{2+} with H^+ along with simultaneous polymerization of Si tetrahedra, whereas the stoichiometric phase was attributed to the buildup of a Si-rich amorphous layer that acts to slow dissolution rates. Mg isotopic analysis of the supernatant in both abiotic and biotic experiment showed an enrichment in ^{24}Mg relative to the mineral in the initial non-stoichiometric phase, interpreted to be due to kinetic isotope fractionation, while during the later stoichiometric phase the isotopic composition of the supernatant was similar to that of the dissolving olivine and thus dissolution was isotopically congruent. No difference in the temporal evolution of stoichiometry and isotope ratios was found between the biotic and the abiotic experiments. This similarity indicates that olivine dissolution mechanisms are identical whether fungus is present or not. However, I propose that the fungus accelerates olivine dissolution by (1) attachment of fungal cells to mineral surfaces that acidify the micro-environment of the contact zone by releasing protons; and (2) dissolving Fe(III) precipitates present in the Si-rich amorphous layer through chelation with siderophores excreted by the fungus. The accelerating effect on mineral dissolution by the fungus found in this study not only provides insights into biogenic mineral weathering but is also of relevance to the efficiency "enhanced weathering" employed as means of CO_2 sequestration.

ZUSAMMENFASSUNG

Magnesium (Mg) ist ein, für alle lebenden Zellen, wichtiger und in der Natur häufig vorkommender Makronährstoff. Die stabilen Isotope von Mg fraktionieren an der Erdoberfläche sowohl durch abiotische (Mineralauflösung, Bildung primärer und sekundärer Minerale aus Lösungen) als auch durch biotische Prozesse (Aufnahme von Zellen und Translokation). Das Ziel der vorliegenden Doktorarbeit ist es, unter experimentellen und kontrollierten Laborbedingungen, die Fraktionierung stabiler Mg Isotope bei (1) der mikrobiellen Aufnahme von Mg aus einer Wachstumslösung und dessen Translokation unter zellphysiologischen Gesichtspunkten als auch in Bezug auf pH-Wert und mikrobieller Spezies und (2) der Mineralauflösung unter abiotischen Bedingungen und in Gegenwart von Pilzen zu untersuchen. Angesichts der Tatsache, dass große Mengen Mg biologische Kompartimente passieren, ist der isotopische Fingerabdruck, den ich identifizieren konnte, auf ökosystemare Mg-Studien anwendbar.

Um die Komplexität natürlicher Systeme zu verringern, führte ich Laborexperimente mit einzelligen Modellorganismen durch. Wachstumsexperimente zeigten, dass die Fraktionierung von Mg-Isotopen während der Aufnahme durch den gesteinsbesiedelnden mikrokolonialen Pilz *Knufia petricola* vom pH-Wert abhängig ist. Das $^{26}Mg/^{24}Mg$ Verhältnis (dargestellt als $\delta^{26}Mg$) des Mg in der Pilzzelle war bei pH 6 um 0,65 ± 0,10‰ und bei pH 3 um 1,11 ± 0,34‰ isotopisch schwerer als das Mg der Wachstumslösung. Ein weiteres Wachstumsexperiment mit dem Cyanobakterium *Nostoc punctiforme* zeigte, dass dieses isotopisch leichtes Mg aufnimmt und die Zelle um -0,27 ± 0,14‰ isotopisch leichter als die Wachstumslösung war. Chlorophyll, das aus der Cyanobakterienzelle extrahiert wurde, war um 1,85 ± 0,14‰ isotopisch schwerer als die Wachstumslösung. Um zu untersuchen, wie Mg-Stoffwechselwege in diesen Organismen die Isotopenfraktionierung beeinflussen, wurde ein Massenbilanzmodell entwickelt.

Die Ergebnisse können durch dreierlei Fraktionierungsprozesse und den zugrunde liegenden Massenbilanzen erklärt werden: (1) während der Aufnahme, wobei Mg mit einem tiefen Isotopenverhältnis bevorzugt wird; (2) während des Einbaus eines wesentlichen Teils (> 95%) von intrazellulärem Mg in Mg-enthaltenden Verbindungen (ATP, Ribosomen und Chlorophyll), in denen schwere Mg-Isotope gebunden sind; und (3) während des Exports des verbleibenden freien, isotopisch komplementären und daher leichten Mg und evt. zusätzlicher Fraktionierung. In den Zellen des Pilzes *K. petricola* herrscht eine hohe Exportrate von freiem Mg, das leicht in seiner Mg-Isotopenzusammensetzung ist, vor. Dieses Mg wird anschließend mit isotopisch schwerem Mg aus der Wachstumslösung aufgefüllt. Die *K. petricola*-Zelle wird

daher von den isotopisch schwereren intrazellulären Mg enthaltenden Verbindungen wie ATP und Ribosomen dominiert. Die pH-Wert abhängige Mg-Isotopenfraktionierung in *K. petricola*-Zellen beruht auf Unterschieden in den Zuflüssen von Mg, die in die Zelle eintreten und diese verlassen. Im Gegensatz dazu verfügt das Cyanobakterium *N. punctiforme* über große intrazelluläre Mg-Vorräte (10-mal mehr als *K. petricola*) und bindet alles Mg, das in die Zelle eintritt, in ihren Mg-Verbindungen. Daher ist die Isotopenzusammensetzung der Zelle identisch mit der des Mg, das aus der Wachstumslösung in die Zelle eingetreten ist. Aus dieser Beziehung resultiert eine inverse Beziehung zwischen Mg-Konzentrationen in den Zellen und der Mg-Isotopenfraktionierungsfaktoren der Gesamtzelle. Dieses Modell erklärt bereits veröffentlichte Feld- und Labordaten zu der Mg-Isotopenzusammensetzung von Blättern, Wurzeln, Gesamt-Pflanzen, Pilzen und Cyanobakterien, die eine inverse Beziehung zwischen Mg-Konzentrationen und Mg-Isotopenfraktionierungsfaktoren aufzeigen. Das in dieser Arbeit entwickelte zelluläre Modell erlaubt nunmehr, die Isotopenfraktionierung von Mg in Ökosystemen vorherzusagen.

Nachdem die Mg-Isotopenfraktionierung durch Pilzzellen erforscht war, wurden die Raten und Mechanismen der Auflösung von Olivin $(Mg,Fe)_2(SiO_4)$ in Laborexperimenten einerseits in Gegenwart von *K. petricola* und andererseits in einem abiotischen Kontrollexperiment bestimmt. Die Auflösungsraten von Olivin ($1{,}04 \times 10^{-15}$ mol cm^{-2} s^{-1}) bei pH 6 waren in Gegenwart des Pilzes siebenmal höher als in dem abiotischen Kontrollversuch. Die Mg/Si-Verhältnisse im Überstand zeigten eine anfängliche nicht-stöchiometrische Phase, in der die Auflösungsgeschwindigkeit höher war, und eine spätere stöchiometrische Phase, bei der die Auflösungsgeschwindigkeit geringer war. Die anfängliche nicht-stöchiometrische Phase wurde einem schnellen Austausch von Mg^{2+} mit H^+ bei gleichzeitiger Polymerisation von Si-Tetraeder zugeordnet, während die stöchiometrische Phase dem Aufbau einer Si-reichen amorphen Schicht zugeordnet wurde, die die Auflösungsgeschwindigkeiten verlangsamt. Das nicht-stöchiometrische Verhalten zeigte sich auch in den Mg-Isotopenverhältnissen. Die Mg-Isotopenanalyse des Überstandes zeigte sowohl im abiotischen als auch im biotischen Experiment eine Anreicherung von ^{24}Mg relativ zum Mineral der anfänglichen nicht-stöchiometrischen Phase. Im Gegensatz dazu war während der späteren stöchiometrische Phase die Isotopenzusammensetzung des Überstands ähnlich der des auflösenden Olivins. Die bevorzugte Freisetzung von ^{24}Mg während der Anfangsphase der Auflösung von Olivin führe ich auf kinetische Isotopenfraktionierung und isotopisch kongruente Auflösung während der stöchiometrischen Phase zurück. Es wurden keine Unterschiede in der Entwicklung der chemischen Zusammensetzung und der Isotopensignatur zwischen dem biotischen und dem

abiotischen Experiment gefunden. Diese Ähnlichkeit zeigt, dass der Pilz die Freisetzung von Mg nicht direkt beeinflusst. Nur die Freisetzungsraten sind unterschiedlich. Demnach beschleunigt der Pilz die Olivinauflösung indirekt durch (1) die Anlagerung von Pilzen an Mineraloberflächen, die die Mikroumgebung der Kontaktzone durch Abgabe von Protonen ansäuert; und (2) die Auflösung von Fe(III)-Ausfällungen, die in der Si-reichen amorphen Schicht vorliegen, durch Chelatbildung mit Siderophoren. Diese Studie bietet nicht nur Einblicke in die biogene Mineralverwitterung, sondern ist auch relevant für die Effizienz der "verstärkten Verwitterung", die in Experimenten zur CO_2-Sequestrierung eingesetzt wird.

Acknowledgements

Firstly, I would like to thank Prof. Friedhelm von Blanckenburg for all his trust, support and guidance during my doctoral study. It has been an amazing learning experience working with Friedhelm. His passion for science is incredible and is an inspiration for young scientists like me. Thank you for always motivating and encouraging me in these 4 years.

Secondly, I would like to thank Ruben Gerrits for the experimental support. I appreciate your hard work and efforts in this project. Good luck with your thesis. I am also indebted to Prof. Anna Gorbushina for allowing me the opportunity to collaborate this wonderful transdisciplinary research. Thank you Anna for traveling to GFZ to attend all those super early (or very late) internal Isonose meetings, for discussing the project, and for allowing me to use your lab spaces, equipment, and your *Knufia*. I also want to express my gratitude to Dr. Roman Sobotka, Dr. Jacques Schott, Dr. Vasileios Mavromatis, and Franziska Stamm for the help on various scientific topics of my research.

I would like to thank Dr. Maja Tesmer, Isonose manager, for all the support. Thank you Maja for getting me selected for this program, for all the endless administration help and for the constant motivation to finish my research. Also thanks to all the other Isonoser's (Xu, Cristina, David, Jens, Nils, Carolina, Franziska, Danijela, Marie, Ann-Kristin, Daniel, Grant, Julien, Jérôme, Jacques, Eric, Balz, Seán, Rachael, Claudia, John and Joachim) for all the science and fun we had together.

I would also like to individually thank all my work colleagues at GFZ for their support during my time here. Thank you Jan for training me in the mass spec, and for being patient to answer all my questions during my random visits to your office. Thank you Patrick for all the spontaneous science discussions. I really appreciate all your effort and time to answer my questions, and also on editing, correcting and providing insightful feedbacks on my papers. Thank you Josi for all the help during the Neptune measurements. Thank you Jutta for organizing the clean lab. I want to confess to you that the missing 15 and 50 mL centrifuge tubes was sometimes by my doing. Thank you Renée for being the nice office mate and feeding Haribo to Patrick and me. Thank you Conni for helping me figure out all the endless and complex GFZ administrative processes. Also thanks to all my other GFZ colleagues, David, Marcus, Ralf, Di, Cai, Michael, Michael, Rene, Daniel, Sanjay, Hanna, Geerke, Ricarda, Hella, Cathrin, and Dirk, for all the wonderful time here.

I want to thank my family for all the support they provided in every step of my life. Also thanks to all my friends (Manash, Bimersha, Anil, Pranay, Samit, Abhinandan, Monita, Bishesh, Abhisekh, and others) for all the good time together in Berlin.

I also want to acknowledge FU Berlin and GFZ Potsdam for hosting my study. Finally, I would like to thank ISONOSE Marie Curie Research training network from the People Programme (Marie Curie Actions) of the European Union's Seventh Framework Programme FP7/2007-2013/ under REA grant agreement n^{o} (608068) for proving the necessary funding and support to conduct this research.

Preface

This thesis is an original work by Rasesh Pokharel. It is comprised of three manuscripts as three chapters, and an introductory chapter. The manuscripts have either been published or submitted. Below I provide a short summary of the contents of individual chapters. I also provide information as to what part of the chapter is my work and what part is from the other co-authors that I collaborated with. All chapters are prepared as independent research topics, therefore some introductory material is repeated in individual chapters.

Chapter 1: Chapter 1 is the introduction of the thesis. The chapter includes a brief introduction to microbes on rocks, Mg cycling in ecosystems, along with information on Mg isotope geochemistry, Mg isotope measurements using MC-ICP-MS and Mg stable isotope fractionation.

Chapter 2: Chapter 2 reports Mg isotope fractionation and its pH dependence during uptake by rock-inhabiting microcolonial fungus *Knufia petricola*. This chapter has been published in 2017 in the journal Environmental Science & Technology ("*Mg isotope fractionation during uptake by a rock-inhabiting, model microcolonial fungus Knufia petricola at acidic and neutral pH*" by Rasesh Pokharel, Ruben Gerrits, Jan A. Schuessler, Geerke H. Floor, Anna A. Gorbushina, and Friedhelm von Blanckenburg; DOI: 10.1021/acs.est.7b01798). Through growth experiments it was found that during uptake the fungus *K. petricola* discriminates against the light isotope ^{24}Mg and prefers heavy ^{26}Mg. Increase of ^{26}Mg/^{24}Mg in the *K. petricola* fungal cell relative to the growth media amounted to 0.65 ± 0.14‰ at pH 6 and 1.11 ± 0.35‰ at pH 3, showing a pH-dependence of Mg isotope fractionation. We suggest an equilibrium isotope fractionation during incorporation of Mg into intracellular ribosomes and ATP. Using a mass balance model we conclude that the magnitude of isotope fractionation depends on mass fluxes of Mg into and out of the fungal cell.

I, Friedhelm von Blanckenburg, Anna Gorbushina, Ruben Gerrits, Jan Schuessler and Geerke Floor developed the research idea. Anna Gorbushina provided strains of *K. petricola* to perform growth experiments and allowed access to conduct the growth experiment at Bundesanstalt für Materialforschung und -prüfung (BAM). Ruben Gerrits conducted the growth experiments. The protocol for Mg separation through column chemistry was conducted by me, Jan Schuessler and Geerke Floor. Mg isotope measurements using MC-ICP-MS was done by me and Jan Schuessler at Helmholtz Laboratory for the Geochemistry of the Earth Surface (HELGES) lab. Jan Schuessler assisted with the interpretation of isotope results. Mass balance model was developed by me and Friedhelm von Blanckenburg. I interpreted the data and wrote the manuscript with inputs from all co-authors.

Chapter 3: Chapter 3 reports Mg isotope fractionation during uptake by the cyanobacterium *Nostoc punctiforme*, and also reveals the parameters responsible for Mg isotope fractionation in other organisms like fungi and higher plants. This chapter has been published in 2018 in the journal Environmental Science & Technology ("*Magnesium stable isotope fractionation on a cellular level explored by cyanobacteria and black fungi with implications for higher plants*" by Rasesh Pokharel, Ruben Gerrits, Jan A. Schuessler, Patrick J. Frings, Roman Sobotka, Anna A. Gorbushina, and Friedhelm von Blanckenburg; DOI: 10.1021/acs.est.8b02238). The cyanobacterium *Nostoc punctiforme* becomes slightly depleted in $^{26}Mg/^{24}Mg$ by -0.27‰ ± 0.14 relative to the growth solution at roughly neutral pH. We speculate that cyanobacterial cells act as a closed system with no or low efflux of Mg from the cell and the slight negative fractionation measured may be due to either a) discriminating against ^{26}Mg during speciation, desolvation, transport across protein channels or b) slightly positive fractionation (i.e. discriminating against ^{24}Mg) in the membrane transporter during efflux. Results of this research along with a compilation of Mg isotope data on bacteria, fungi, lichens and higher plants show that Mg isotope fractionation is inversely proportional to cellular Mg concentrations.

For this research, Anna Gorbushina provided strains of *N. punctiforme*. Ruben Gerrits conducted the growth experiments. Roman Sobotka separated chlorophyll from the *N. punctiforme* cell using HPLC. I and Jan Schuessler did the Mg isotope measurements using MC-ICP-MS. Patrick Frings and Jan Schuessler assisted in interpreting the results about Mg isotopic composition of intracellular compartments of *N. punctiforme* cells. The mass balance model was developed by me and Friedhelm von Blanckenburg. I interpreted the data and wrote the manuscript with inputs from all co-authors, especially Friedhelm von Blanckenburg.

Chapter 4: Chapter 4 reports the application of Mg stable isotopes to determine olivine dissolution mechanisms by the rock-inhabiting fungus *K. petricola*. This chapter has been submitted to Chemical Geology (*"Mechanisms of olivine dissolution by rock-inhabiting fungi explored using magnesium stable isotopes"* by Rasesh Pokharel, Ruben Gerrits, Jan A. Schuessler, and Friedhelm von Blanckenburg). Results of the dissolution experiment show that olivine dissolution rates in the presence of *K. petricola* were seven-fold higher (1.04×10^{-15} moles cm^{-2} s^{-1}) than those in the abiotic experiments (1.43×10^{-16} moles cm^{-2} s^{-1}) at the end of 94 days. However, the temporal evolution of Mg isotopic composition of the solution did not differ between abiotic and biotic experiments. Supernatant solutions in both the biotic and the abiotic experiment showed a dissolution trend characterized by initial non-stoichiometric release of Mg and Si and preferential release of ^{24}Mg over ^{26}Mg, followed by a later phase of

stoichiometric Mg and Si and isotopically congruent release of Mg. Accelerated dissolution rates during the stoichiometric phase in the presence of *K. petricola* was attributed to fungal biochemical processes that acidify the micro-environment of the Si-rich amorphous surface layer to which *K. petricola* is attached. Removal of Fe precipitates from the Si-rich amorphous surface layer in the presence of fungus could also contribute to an increase in dissolution rates.

For this research, Ruben Gerrits and I designed and conducted the experiments. I conducted the Mg isotope measurements and Jan Schuessler assisted in interpretation of isotope results. Friedhelm von Blanckenburg and I interpreted the overall results of the research. I wrote the manuscript with inputs from all co-authors.

Table of Contents

Chapter 1

Introduction

1.1 Microbes on Rock

Rocks in the terrestrial environment contain a multitude of forms of life. A handful of soil from the extreme cold of the Artic would host millions of microbes (fungi, bacteria, lichens, algae, etc.) as would sediment from the hot Sahara desert or the deep oceans' high-temperature hydrothermal systems. Microbes mine rocks for mineral nutrients and energy by inducing chemical reactions (Brown et al., 2008; Gadd, 2010; Gorbushina and Broughton, 2009; Hochella, 2002; Li et al., 2016). They continuously perform physical and chemical transformations on the surface they grow on. These transformations include dissolution of minerals, mobility and cycling of elements, and transfer of nutrients to higher plants or animals in the ecosystem (Balogh-Brunstad et al., 2008; Bonneville et al., 2009; Bonneville et al., 2011). But how do microbes perform these transformations? Could these microbial mineral dissolution and nutrient uptake and transfer processes be quantified and elucidated? These are very important questions that are yet to be explored in detail.

Microbes release elements from the rock by two processes: (1) Biomechanical weathering; and (2) Biochemical weathering (Balogh-Brunstad et al., 2008; Bonneville et al., 2009; Gadd, 2010). Biomechanical weathering occurs typically by penetration or tunneling into the mineral lattice structure, thereby weakening and forming cracks. For example, fungal hyphae generate an internal turgor pressure through osmosis as high as 8 MPa, allowing them to penetrate hard rock surfaces to acquire nutrients (Bechinger et al., 1999; Bonneville et al., 2009; Harold, 2002). Biochemical weathering takes place by two processes, (I) proton-based and (II) ligand-based dissolution (Gadd, 2007, 2010; Hoffland et al., 2004). Proton-based dissolution involves the release of organic acids (like oxalic and citric acids), and the formation of carbonic acid by release of respired CO_2, all of which acidify the microenvironment near the microbes and promote mineral dissolution (Balogh-Brunstad et al., 2008; Bonneville et al., 2009; Burford et al., 2003a). Ligand-based weathering process involve the release of siderophores, carboxylic acids, amino acids, phenolic compounds, etc. that complex metals from the rock surfaces (Gadd, 2007, 2010; Hoffland et al., 2004). Microbes may not only dissolve the mineral surface but also form secondary minerals (Gadd, 2010). For example, fungi and cyanobacteria are known to precipitate $CaCO_3$ in calcareous soils, which can modify soil

conditions locally and also play a role in long-term carbon storage in rocks (Gadd, 2010; Verrecchia, 2000). Another study has shown evidence of protozoic silica (Si shells in protozoic organisms) as one of the important compartment of biogenic Si pools in soils (Sommer et al., 2006). A number of studies detail the influence of microbial redox processes on iron speciation in both sub-surface and deep geological environments (Cooper et al., 2006; Zhang et al., 2009). These microbially-induced iron precipitation or solubilization reactions not only play a role in iron speciation and bioavailability but also in various important processes like the oxidation of organic matter, availability of phosphate and trace metals in the environment, the generation of manganese minerals, uranium speciation in soils, etc. (Lovley et al., 2004). One of the largest iron sources on Earth, the Precambrian Banded Iron Formations (BIFs), are assumed to be formed by Fe(II) precipitation either by abiotic oxidation of O_2 produced by cyanobacteria and/or oxidation by chemolithrotrophic bacteria (Köhler et al., 2010). In summary, microbes exert a profound impact on geological processes like bioweathering, biotransformation, mineral alteration, mineral decomposition, sediment formation and metal accumulation.

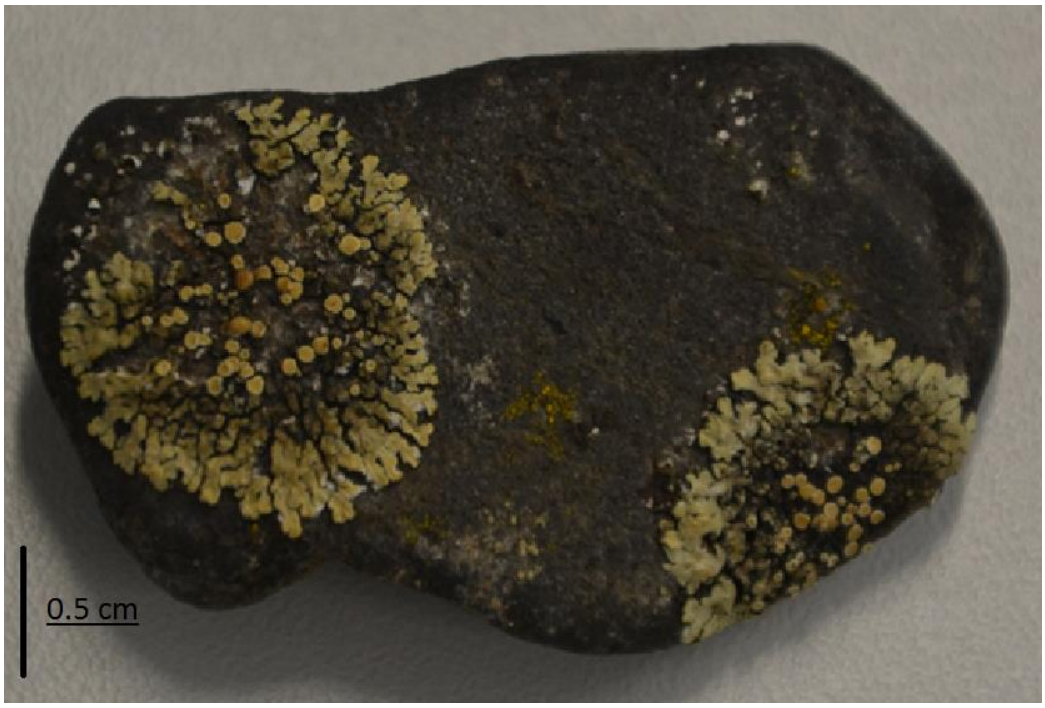

Figure 1.1: Picture of a lichen growing on the surface of a rock. Sample was obtained from the terrace of Building E (Section 3.3) at the GeoForschungsZentrum *GFZ* Potsdam.

The interaction between microbes and higher plants determines the availability of mineral nutrient to plants (Jacoby et al., 2017; Müller et al., 2016). In turn, the roots of plants release carbohydrates, organic and amino acids that provide suitable conditions for microbes to

prosper (Bardgett et al., 1998; Lareen et al., 2016). Therefore, the amount of microbes in the rhizosphere is considerably higher than in bulk soil (Kennedy and de Luna, 2005; Liu et al., 2015). It is estimated that 80% of terrestrial plants are in symbiosis with mycorrhizal fungi (Landeweert et al., 2001; Schüßler et al., 2007). Through their extensive hyphae network, fungi increase the surface area of plants thus maximizing their ability to capture nutrients and water (Johnson and Gilbert, 2015). Another important symbiotic relationship observed in nature is lichens, occupying about 8% of earth's terrestrial surface (Chen et al., 2000). Lichens are a symbiosis of a fungus with cyanobacteria, where the cyanobacteria provides fungus with sugar produced by photosynthesis and the fungus in turn provides nutrients to the cyanobacteria. Another example are ubiquitous sub-aerial biofilms (SABs): microbial communities (cyanobacteria, algae, heterotrophic bacteria, and microcolonial fungi) in symbiosis at the interface between rocks and atmosphere (Gorbushina, 2007). The interactions of these SABs with rocks can result in formation of coatings, and new biogenic minerals at the surface of rocks (Gadd, 2017). Microbes therefore are not only responsible for nutrient availability but through these symbiosis relationships transfer nutrients to other species in the ecosystem.

1.2 Magnesium cycling in the environment

Magnesium is the 8th most abundant element in the Earth's crust with approximately 2% by weight. Understanding biogeochemical cycling of Mg is crucial as it is not only an important bio-essential element but is also associated with long-term regulation of atmospheric CO_2 (Maroto-Valer et al., 2005; Opfergelt et al., 2014). It is therefore important to identify Mg fluxes in the environment and also distinguish the magnitude of abiotic fluxes from the biotic ones. Typically, magnesium fluxes at the Earth's surface arise primarily from silicate and carbonate mineral dissolution, from atmospheric deposition like dust, rain, and snow. For example, weathering of silicate rocks releases cations like Mg, Fe and Ca that eventually get transported to the ocean. It is one of the dominant control on Mg fluxes, especially in basaltic catchments (Opfergelt et al., 2014; Sigfusson et al., 2008). However, it is well observed that presence of microbes and higher plants releases Mg more rapidly from silicate rocks than in the absence of these species (Balogh-Brunstad et al., 2008; Drever, 1994; Li et al., 2016; Moulton et al., 2000). A study by Schwartzman and Volk (1989) concluded that biotic enhancement of Mg release from silicate minerals could be up to 1000 times higher than abiotic release. Although such a high figure is not universally accepted (Drever, 1994), most studies agree that the presence of vegetation enhances Mg release. A significant portion of the Mg released by abiotic and biotic fluxes ultimately precipitates as carbonate minerals, that in turn is stored in rocks or buried on

the sea floor (Walker et al., 1981). The transformation of CO_2 to dissolved bicarbonate ions as a result of silicate mineral weathering has long been considered an important sink for atmospheric CO_2 in models of the natural global carbon cycle on geological time-scales (Schuiling et al., 1986; Schuiling and Krijgsman, 2006). Some of the Mg released by silicate rock weathering is incorporated during formation of secondary mineral products like clay. While others are taken up by microbes and higher plants as nutrients for chlorophyll production, adenosine triphosphate (ATP), RNA and DNA synthesis and activating numerous enzymatic reactions in the cells (Flatman, 1984; Pasternak et al., 2010; Wolf and Cittadini, 2003). After uptake, a substantial fraction of Mg consumed by plants is released back to the soils as litter fall (Kimmig et al., 2018; Uhlig et al., 2017).

1.3 Mg stable isotope fractionation

Magnesium has three stable isotopes: ^{24}Mg, ^{25}Mg and ^{26}Mg, with natural abundances of 78.992%, 10.003%, and 11.005% respectively. Due to their large relative mass difference, Mg isotopes are easily fractionated in the environment. As with other stable isotope systems, Mg isotope ratios are commonly expressed in the δ-notation as per mil (‰) deviation from an international reference material. In the case of Mg isotopes, the international δ-zero reference material is DSM3 is commonly used. The Mg isotope composition of a given sample is thus expressed as:

$$\delta^{x}Mg_{sample} = [(({}^{x}Mg/{}^{24}Mg)_{sample} / ({}^{x}Mg/{}^{24}Mg)_{DSM3}) - 1 \times 1000] \qquad \text{(eq. 1.1)}$$

Where, *x* is 25 or 26. The most fractionated materials on Earth are found in low-temperature environments, with $\delta^{26}Mg$ values of -5.6‰ in carbonates and the highest $\delta^{26}Mg$ value of +1.8‰ in weathered silicates (Liu et al., 2014; Shalev et al., 2018; Wombacher et al., 2011).

1.4 Mg isotope measurements

Magnesium stable isotope measurements throughout this thesis were performed using a Multi Collector-Inductively Coupled Plasma Mass Spectrometry (MC-ICP-MS, Thermo Scientific Neptune), at the Helmholtz Laboratory for the Geochemistry of the Earth Surface (HELGES) at GFZ Potsdam (von Blanckenburg et al., 2016). Magnesium isotope analysis was done for two types of samples: (1) solid samples (mineral, and microbes) and (2) liquid samples (i.e. solutions containing Mg). Acid digestion for all samples was done in capped screw-top PFA bottles. All samples were processed simultaneously with blanks and reference materials to quantify potential cross contamination and method accuracy. The reference material for solid sample used in this study was BHVO-2 basalt, whereas the reference material for liquid sample was dissolved BHVO-2 basalt, Cam1, and dissolved BHVO-2 basalt doped (doped with glucose

or microbial growth solution without Mg). All samples were treated with mixture of concentrated HNO_3, HCl, and H_2O_2 on a hotplate at 150°C in multiple steps until complete dissolution. HF was additionally added during the procedure to volatilize Si in the samples containing minerals. Finally the samples were dissolved in 1M HNO_3 prior to Mg purification by column chemistry.

Magnesium separation was done using Spectrum 104704 MiniColumns filled with 2.8 mL of cation exchange resin Bio Rad AG-50W-X12 200-400 mesh (37-74μm) similar to the procedure described in Pogge von Strandmann et al. (2011). Samples and standards with 5 - 15 μg Mg along with procedural blanks were processed through the columns. Sample matrices were eluted with 32 ml of 1M HNO_3 before collecting the Mg fraction with 10 ml of 2M HNO_3. The separated Mg fraction was further treated with H_2O_2, evaporated, and redissolved in 0.3 M HNO_3. Magnesium recovery, Mg purity and Mg content in the procedural blank were checked using Inductively Coupled Plasma Optical Emission Mass Spectrometer (ICP-OES; Varian 720ES). ICP-OES results showed that >90% of Mg was recovered. Most of the samples contained in total less than 10% impurities after column separation (elements other than Mg). However, for a few samples the column chemistry failed to completely separate elements like Zn, Mn, Ni, K, and Na as they elute very close or with Mg during column chemistry. These samples were tested for potential bias effects during isotope measurements by preparing reference materials doped with these residual elements at the element:Mg ratios observed in the sample. The results showed no bias on Mg isotope ratios within analytical uncertainty.

The separated samples were diluted to a concentration of 500 ng/mL using 0.3 M HNO_3 acid. Standard-sample-standard bracketing technique with DSM3 as bracketing standard was used to correct for instrumental mass bias. For samples where elements (Zn, Mn, Ni, K and Na) were not separated the DSM3 bracketing standard was doped with the exact concentrations of the impurities present in the sample. All the sample and standards were analyzed using the MC-ICP-MS equipped with a Neptune Plus Jet Interface. The solutions were introduced to the mass spectrometer through a quartz-glass spraychamber (double pass cyclon-scott type, Thermo SIS) equipped with a self-aspirating PFA nebulizer with an uptake rate of ca. 100 μL/min. Mg isotope signals (^{24}Mg, ^{25}Mg, ^{26}Mg) were measured in medium resolution simultaneously on Faraday detectors (L2, C, and H2) with 10^{11} Ohm amplifiers with an integration time of 4 s for each cycle (20 cycles measured per sample). To avoid potential interference from $^{12}C^{14}N^+$, the H2 cup was moved slightly towards higher masses so that $^{26}Mg^+$ was measured on the interference-free low mass side of the flat-top peak. Faraday detectors H4 and L4 were used to monitor $^{27}Al^+$ and $^{23}Na^+$, respectively, to monitor any potential bias from contamination of

samples with these elements. The 500 ng/mL Mg sample corresponds to a signal intensity of about 10V on ^{24}Mg. Background intensities for ^{24}Mg on 0.3 M HNO_3 acid were typically lower than 8 mV. Blanks (0.3M HNO_3) were measured before and after each block of standard-sample-standard and the signal intensities were subtracted from both the sample and the standards. Linear drift of <0.2‰ $\delta^{26}Mg$ values between the two bracketing standard (before and after the sample) were accepted. Measurements where the linear drift was higher than 0.2‰ were considered to be unstable (instrumental mass bias) and therefore neglected. The analytical uncertainty was based on repeated measurements of reference materials (both pure and doped) and was estimated at ± 0.1‰ (2SD) in $\delta^{26}Mg$ and ± 0.06‰ (2SD) in $\delta^{25}Mg$. For details about method descriptions and uncertainty see Chapters 2, 3 and 4.

1.5 Isotope Fractionation

Variability in reaction kinetics of isotopes of the same element during a chemical or physical reaction results in enrichment of one isotope in a compartment over another causing isotope fractionation. There are two types of mass-dependent stable isotope fractionation process, (1) Equilibrium Isotope Fractionation and (2) Kinetic Isotope Fractionation (Criss, 1999). Equilibrium isotope fractionation happens when isotope ratios differs between chemical substances (reactants and products) in a reaction at chemical equilibrium (Sulzman, 1995). Isotopic equilibrium is governed by differences in the binding energy between reactant and product. These are sensitive to isotope mass of the constituents involved (Schauble, 2004; Wiederhold, 2015). A rule of thumb for equilibrium exchange reactions is that heavier isotopes tend to accumulate in compounds with the strongest chemical bond (Bigeleisen and Mayer, 1947b; Johnson et al., 2004). An example of equilibrium isotope fractionation is the reaction between carbon dioxide and water in a closed container (Sulzman, 1995).

$$C^{16}O_2 + 2H_2{}^{18}O \leftrightarrow C^{18}O_2 + 2H_2{}^{16}O \qquad \text{(eq. 1.2)}$$

Kinetic isotope fractionation is caused by unidirectional or incomplete chemical reactions due to unequal atomic weight of isotopes (Criss, 1999; Schauble, 2004). Kinetic isotope fractionation occurs in processes like evaporation, diffusion, dissociation reactions, adsorption, precipitation, and enzymatic processes (Sulzman, 1995). There are two types of kinetic isotope fractionation, (1) transport-limited and (2) reaction-limited. Kinetic isotope fractionations that occur during transport of isotopes, for example along a diffusion gradient, are transport-limited. For example, during diffusion lighter isotopes travels faster than the heavier isotopes causing depletion in heavier isotopes in the product (Bindeman et al., 2013). Reaction-limited kinetic isotope fractionation occurs during a fast chemical forward reaction.

Due to differences in zero point energy for different isotopes, the energy barrier that needs to be overcome in a chemical reactions varies causing isotope fractionation (Schauble, 2004). For example, breaking bonds of a compounds favors release of lighter isotopes, because less energy is needed compared to bonds involving heavier isotopes.

1.5.1 Reporting isotope fractionation

Typically, the measured isotopic difference between two compartments is expressed in terms of capital delta (Δ) (Coplen, 2011). The definition is:

$$\Delta_{A-B} = \delta_A - \delta_B \qquad \text{(eq. 1.3)}$$

where Δ_{A-B} is the isotopic difference between two compartments A and B; δ_A and δ_B are the isotopic compositions of the species in compartments A and B respectively. This isotopic difference does not imply the cause or the mechanism by which this isotopic difference was generated.

Isotope fractionation (caused by kinetic or equilibrium processes) between two compartments can be expressed as isotope fractionation factor (α) (Coplen, 2011; Johnson et al., 2004). The definition is:

$$\alpha_{A-B} = R_A/R_B \qquad \text{(eq. 1.4)}$$

where α_{A-B}, is the isotope fractionation factor between two compartments A and B; R is the isotope ratio in the compartment A and B, respectively. Since α_{A-B} is mostly very close to 1, a term ε_{A-B} is used to express the isotope fractionation in per mil (‰) (Coplen, 2011; Johnson et al., 2004). The definition is:

$$\varepsilon_{A-B} = \alpha_{A-B} - 1 \qquad \text{(eq. 1.5)}$$

1.5.2 Closed and Open system isotope fractionation

The isotopic composition of an element transferred from one compartment to another is also dependent on the elements' amounts in these compartments. There are two types of compartment separation: Open system and closed system (Johnson et al., 2004; Kendall and Caldwell, 1998). An open system is a system where the reactants and products are separated and no further chemical or isotope exchange takes place. Both equilibrium and kinetic isotope fractionation can take place in an open system. The open system is modeled using the Rayleigh equation. A closed system is a system where reactants and products remain in physical contact and the isotopic difference between the reactant and the product directly corresponds to the isotope fractionation factor. Typically closed system isotope fractionations are associated with equilibrium isotope fractionation. The mass balance equation for a closed system is:

$$\delta_T = \delta_A f_A + \delta_B (1-f_A) \quad \text{(eq. 1.6)}$$

Rearranging the equation, we get

$$\delta_B = \delta_T - f_A \times \varepsilon_{A-B} \quad \text{(eq. 1.7)}$$

$$\delta_A = \delta_T + f_B \times \varepsilon_{A-B} \quad \text{(eq. 1.8)}$$

where f_A and f_B are mass fraction of phase A and B; δ_T is the weighted average isotope composition of A and B or the total systems' isotope composition; ε_{A-B} is the equilibrium isotope fractionation between phases A and B (in permil).

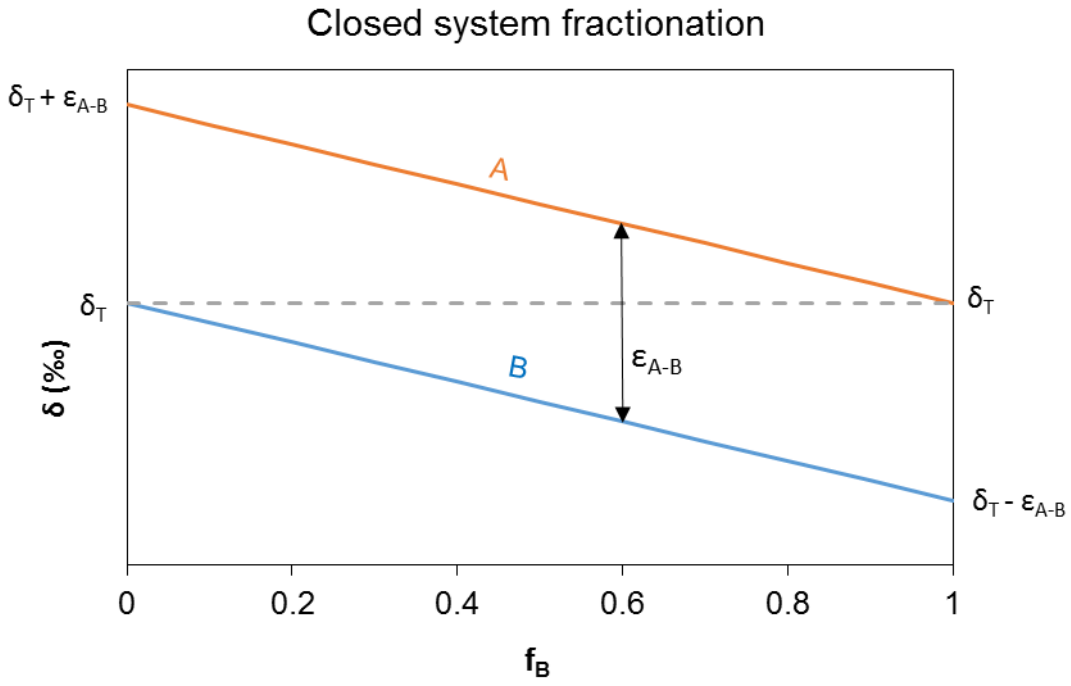

Figure 1.2: General diagram representing isotopic composition of two phases A and B in a closed system equilibrium isotope fractionation. In the figure, f_B is the fraction of phase B, δ_T is the weighted average isotope composition of A and B (i.e. the total systems' composition) and ε_{A-B} is the equilibrium isotope fractionation between A and B.

1.6 Magnesium isotope fractionation in the environment

All the four major fluxes of Mg (mineral dissolution, carbonate precipitation, secondary mineral formation and uptake by an organism) previously discussed in Section 1.2 fractionate Mg isotopes (Black et al., 2008; Black et al., 2006; Bolou-Bi et al., 2010; Bolou-Bi et al., 2012; Fahad et al., 2016; Kimmig et al., 2018; Maher et al., 2016; Mavromatis et al., 2014; Moynier and Fujii, 2017; Opfergelt et al., 2014; Pearce et al., 2012; Pokharel et al., 2017; Ra and Kitagawa, 2007; Ra et al., 2010; Ryu et al., 2016; Schmitt et al., 2012; Shirokova et al., 2011; Tipper et al., 2010; Uhlig et al., 2017; Wimpenny et al., 2014; Wimpenny et al., 2010). For

example, an experimental study by Wimpenny et al. (2010) has shown that during olivine dissolution at pH 2-3 the ^{24}Mg isotope is preferentially enriched over ^{26}Mg in the dissolved phase (-0.36‰ lower in $^{26}Mg/^{24}Mg$ than that of the olivine after 3 days). Maher et al. (2016) also observed a kinetic effect during the early stages of olivine dissolution, where the bulk solution was enriched in ^{24}Mg (-0.36‰ lower in $^{26}Mg/^{24}Mg$ than the original olivine), but at the later stages the bulk solution attained the isotopic composition of the dissolving olivine as a steady state dissolution rate was attained. Precipitation of Mg bearing carbonates (limestones, dolomites, speleothems and magnesites) incorporate lighter Mg isotopes with respect to the source (Chang et al., 2004; Galy et al., 2002; Gao et al., 2016; Mavromatis et al., 2012; Pearce et al., 2012). In contrast, experimental studies show that during secondary mineral formation like clays, heavier Mg isotopes are incorporated into the structure (Opfergelt et al., 2012; Ryu et al., 2016; Wimpenny et al., 2014).

Different biological processes incorporating Mg vary the way they fractionate Mg isotopes. For example, both laboratory and field experiments show bulk higher plants are typically enriched in heavier Mg isotopes compared to their source material (Black et al., 2008; Bolou-Bi et al., 2010; Bolou-Bi et al., 2012; Mavromatis et al., 2014; Opfergelt et al., 2014; Uhlig et al., 2017). Within plant tissues, however, Bolou-Bi et al. (2010) and Bolou-Bi et al. (2012) showed that the leaves of plants are enriched in the lighter Mg isotopes relative to their roots, indicating isotope fractionation during translocation. Another example are the chlorophyll molecules extracted from cyanobacteria by Black et al. (2006) that shows depletion of heavier Mg isotopes relative to the growth solution (i.e., chlorophyll is 0.71‰ lower in $^{26}Mg/^{24}Mg$). In contrast, Ra and Kitagawa (2007) observed that the chlorophyll molecules of marine red algae are enriched in the heavier isotopes relative to seawater by 0.58‰. Mg isotope measurements in fungi by Fahad et al. (2016) showed ectomycorrhizal fungi are slightly enriched in lighter Mg isotopes (about -0.15‰ lower in $^{26}Mg/^{24}Mg$) relative to the substrate Mg, while non-mycorrhizal fungi are enriched in heavier Mg isotopes (about 0.3‰ higher in $^{26}Mg/^{24}Mg$). In context of microbial weathering, enrichment of the dissolved phase in heavier Mg isotopes, was observed by Oelkers et al. (2015) in a 5-year olivine dissolution laboratory experiment in the presence of microbes at neutral pH. Overall, Mg isotope fractionations are associated with considerable unexplained variability.

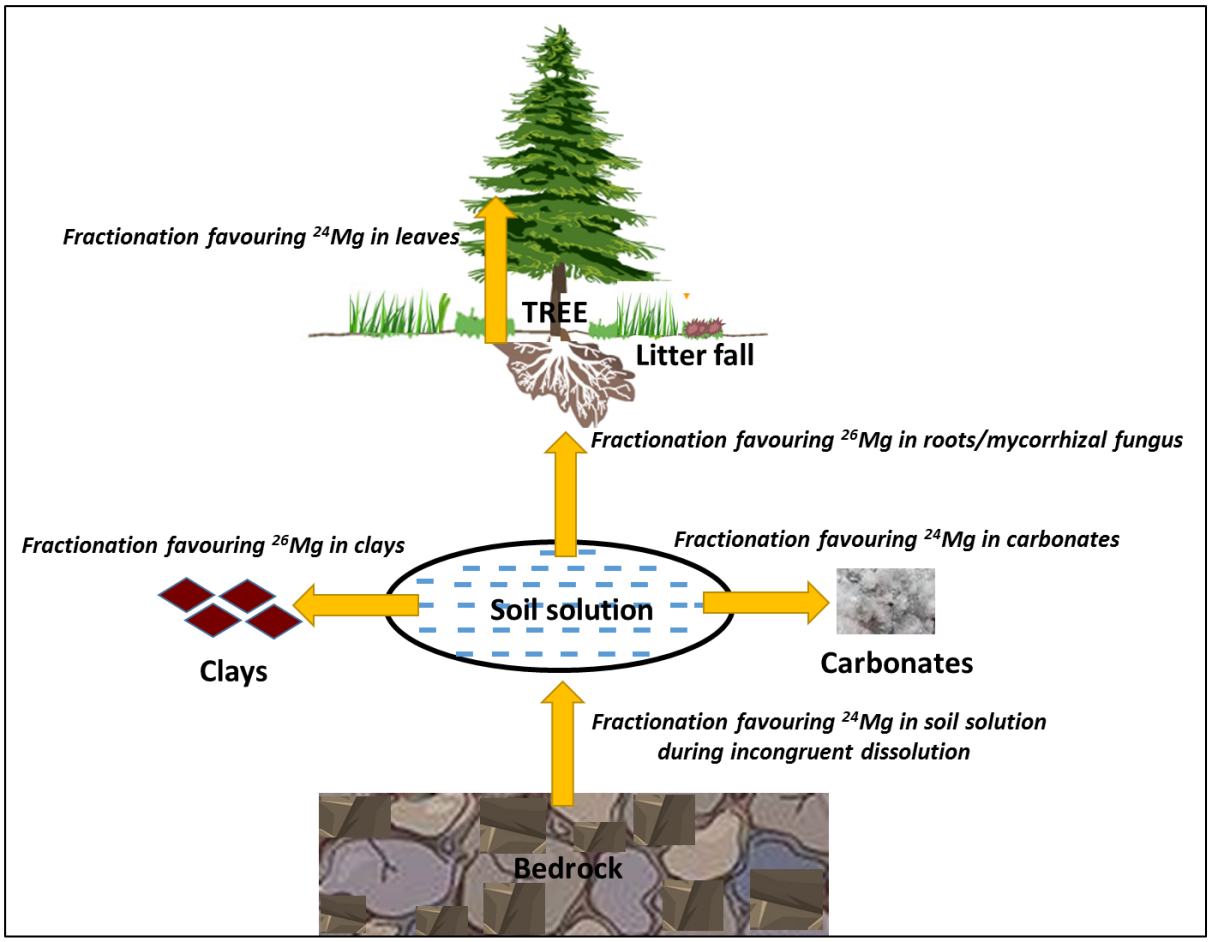

Figure 1.3: Major magnesium (Mg) fluxes and isotopic pathways in the ecosystem.

One of the recent uses of Mg stable isotopes is their application in tracing nutrient uptake and translocation studies in unicellular organisms. Mg entering in a cell could be potentially fractionated by three processes: (1) during uptake through the cellular Mg protein channels (2) during formation of intracellular Mg compounds and (3) during efflux of Mg from the cell. In Chapter 2, (see also Pokharel et al. (2017)) I show the application of Mg stable isotopes to a rock-inhabiting fungus *K. petricola*. The study revealed that the two compartments of intracellular Mg, free cytosolic Mg^{2+} (<5%) and Mg bonded in organic compounds like ATP and ribosomes (>90%), are in isotopic equilibrium (Figure 1.3). The study also showed that Mg uptake in a species is not associated with a single unique isotope fractionation factor. Rather, the isotope fractionation factor depends on Mg mass fluxes into and out of a cell which in turn are set by environmental parameters like pH. Chapter 2 and Chapter 3 of the thesis aims to determine the Mg pathways in unicellular organisms like cyanobacteria and fungi and reveal parameters that causes isotope fractionation in cells.

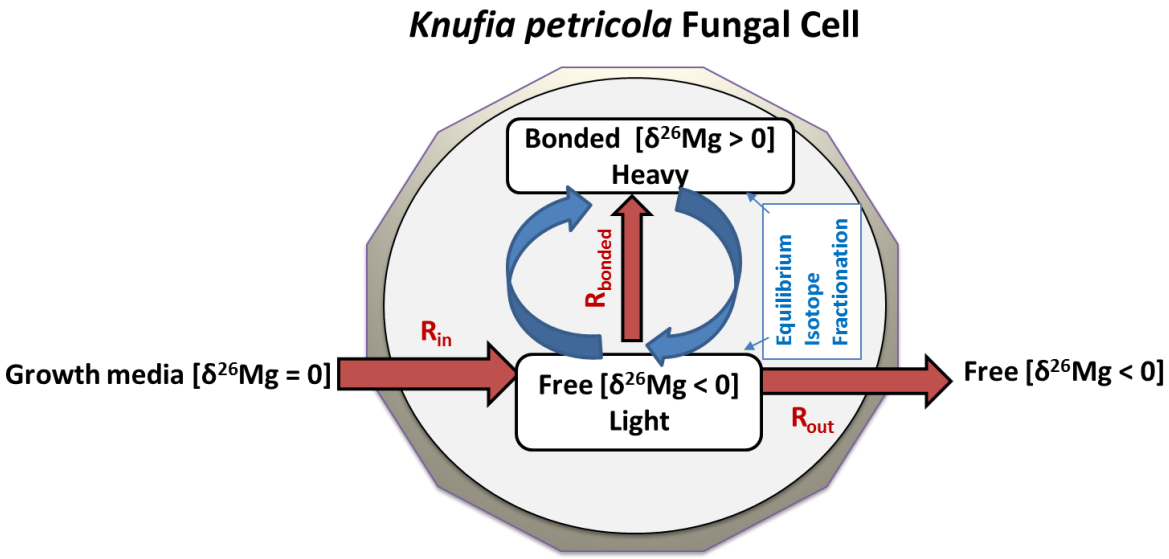

Figure 1.4: Simplified model of Mg transport pathways into and out of fungus *Knufia petricola* cell. The figure represents cellular Mg homeostasis, showing the balance between input of Mg into the cell, Mg bonded to the organic molecules ATP and ribosomes, free Mg in the cytoplasm, and efflux of Mg from the cell. δ^{26}Mg shows isotopic pathways of different Mg compartment of the cell with respect to the growth solution. Figure is modified from Pokharel et al. (2017) and the details of this figure are discussed in Chapter 2 of the thesis.

1.7 Model microbiological species

Natural systems are dynamic and complicated. In order to understand complex processes like microbial nutrient uptake and mineral dissolution, a controlled laboratory experiment set up using model microbiological organisms is ideal. For this research we chose the unicellular rock-inhabiting fungus *Knufia petricola* as a model fungal species and a unicellular cyanobacterium *Nostoc punctiforme* as a model cyanobacterium species. These particular species were chosen in this study primarily for the following reasons:

1. Both these species are ubiquitously found in the terrestrial environment (Meeks, 1998; Meeks et al., 2001; Sand-Jensen, 2014; Selbmann et al., 2015; Zhang et al., 2016).
2. Both these species are able to form subaerial microbiological communities through symbiotic processes in both natural and laboratory conditions (Ekman et al., 2013; Gorbushina and Broughton, 2009; Gorbushina et al., 2008; Nai et al., 2013; Noack-Schönmann et al., 2014).
3. The genomes of both species have been sequenced (Meeks et al., 2001; Nai et al., 2013).
4. Together both species are known to weather rocks (Seiffert et al., 2014; Seiffert et al., 2016).
5. The metabolic pathway of the heterotrophic *K. petricola* and autotrophic *N. punctiforme* cells might serve as a model for roots (chlorophyll-lacking) and leaves (chlorophyll-containing), respectively, of higher plants.

Rock-inhabiting microcolonial fungi were originally discovered in the early 1980s (Krumbein and Jens, 1981; Staley et al., 1982). Due to their stress resistance and survival capacity in nutrient-limited environments they are typically found in some of the most extreme environments on Earth, including the Antarctica glacial valleys, hot deserts and nuclear radiation-contaminated areas (Yurlova et al., 2008). The stress-resistant survival abilities in environments hostile to life could be due to the presence of melanised cell walls that provides defense against environmental stresses such as ultraviolet (UV) and ionizing radiation, as well as desiccation and oxidizing agents (Nai et al., 2013; Noack-Schönmann et al., 2014). *K. petricola* A95 (formerly known as *Sarcinomyces petricola*) is a relatively fast growing, rock-inhabiting ascomycete and can be easily cultivated in the lab. It belongs to an early-diverging lineage of the pathogen-rich ascomycetes order Chaetothyriales (class Eurotiomycetes) and is a predecessor of lichens. *Knufia petricola* strain A95 (CBS 123872) used in this study was isolated from a marble surface in Athens, Greece. The strain was cultivated in the laboratory by following the procedure described in Noack-Schönmann et al. (2014) and Nai et al. (2013). Detailed information on cultivation and incubation are described in these articles and Chapter 2.

Nostoc punctiforme ATCC 29133 is an aerobic, filamentous and motile cyanobacterium that is commonly found at the Earth surface. It has been intensively studied to understand microbial carbon and nitrogen dynamics (Campbell and Meeks, 1992). Colonies of *Nostoc* exist in a wide variety of geographical conditions, from hot to cold regions and from acidic to alkaline soils (Meeks et al., 2001; Sand-Jensen, 2014). They are capable of forming symbiotic relationships with fungi, providing carbohydrates to them and in return receiving nutrients from the fungi. *Nostoc* is also the dominant organism in cyanobacteria-plant symbiosis (Ekman et al., 2013). *N. punctiforme* used in this study was supplied by J.M. Meeks (University of California, Davis, CA, USA). Chlorophyll for Mg isotope analysis was extracted from *N. punctiforme* with methanol and separated using a High Performance Liquid Chromatography (HPLC) system at Centre Algatech, Třebon, Czech Republic. Detailed information on cultivation of the *N. punctiforme* strain, and the chlorophyll extraction and separation protocol, is provided in Chapter 3

For this study, two different type of growth solutions were prepared. For Mg growth experiments, the growth solution used was a nutrient-rich modified BG-11 media. Original BG-11 media was modified to stimulate biomass growth (additional glucose and ammonium nitrate) and to detect both concentration and isotopic changes in Mg (adjusting the amount of $MgSO_4.7H_2O$). MES (2-(*N*-morpholino)ethanesulfonic acid) buffer was used as a pH buffer.

Magnesium isotopic composition of the growth media was pre-determined. For dissolution experiments, a growth media with minimal nutrient solution containing all essential elements except the metal(loid)s, which should be obtained by dissolving olivine, was made. The solution comprised 0.3 mM Na_2SO_4, 0.173 mM K_2HPO_4, 9.95 µM thiamine hydrochloride, and 18.5 mM NH_4NO_3. 9.96 mM glucose*H_2O and 18.50 mM of NH_4NO_3. MES was used to buffer the pH around 6. Detailed compositions of the growth media for both the growth and dissolution experiments are given in Chapter 2, 3, and 4.

1.8 Scope of the project

The overall goal of this doctorate project is to develop the Mg stable isotope tool as a means to improve our understanding on the impact of microbes (fungi and cyanobacteria) on weathering processes. Here, I applied Mg stable isotopes in the field of cell physiology and biogenic weathering. To achieve the objective an interdisciplinary team combining the microbiological facilities and expertise of Bundesanstalt für Materialforschung und -prüfung (BAM) with the geochemical tools of HELGES lab at GFZ Potsdam was formed. Specifically, I designed laboratory batch experiments to investigate processes known to fractionate Mg stable isotopes; the uptake and translocation of elements into model organisms (fungus *K. petricola* and cyanobacterium *N. punctiforme*) from the growth solution and fungal mineral dissolution.

The first aim was to provide understanding of the uptake and translocation of Mg in plants by exploring Mg metabolic processes on a cellular level. With these sets of laboratory experiments, I explored the relationship between cell physiological processes and isotope fractionations factors, and reveal whether they depend on environmental controls like species and pH. These experiments are the first to report a dependence of Mg isotope fractionation on pH during fungal uptake and the first to quantify Mg isotope fractionation during uptake by a cyanobacterium. I applied mass balance models constrained by the experimental results to pinpoint where exactly Mg isotopes fractionate in fungus *K. petricola* and cyanobacterium *N. punctiforme* (for example, during uptake through the transport channels or during formation of Mg incorporation organic compounds like ATP and chlorophyll, etc.). I extrapolated the results to higher plants and explained the previously unknown mechanisms of Mg isotope fractionation during uptake and translocation from roots to leaves. This part of the doctorate project is presented on Chapters 2 and 3.

The second part of the doctorate project aimed at separating abiotic and biotic factors associated with biogenic weathering of the silicate mineral olivine $(Mg, Fe)_2(SiO_4)$ by the fungus *K. petricola,* and to test whether the isotope fractionation found during fungal uptake

can be traced in mineral dissolution experiments. Here we apply the stable isotopes of Mg in laboratory batch experiments with a fungus growing on a silicate mineral to investigate biologically driven dissolution processes. With this setup, I determined abiotic and biotic olivine dissolution rates. In addition, with the application of Mg isotopes I was able to predict abiotic and biotic olivine dissolution mechanisms. These mechanisms include the biogeochemical transformations at the mineral surface that reveal processes controlling olivine dissolution. The outcome of this study has important applications on CO_2 sequestration. This part of the doctorate project is presented on Chapter 4.

Chapter 2

Mg isotope fractionation during uptake by a rock-inhabiting, model microcolonial fungus Knufia petricola at acidic and neutral pH

Abstract

The model rock-inhabiting microcolonial fungus *Knufia petricola* fractionates stable Mg isotopes in a time- and pH-dependent manner. During growth, the increase of $^{26}Mg/^{24}Mg$ in the fungal cells relative to the growth media amounted to 0.65 ± 0.14‰ at pH 6 and 1.11 ± 0.35‰ at pH 3. We suggest a constant equilibrium fractionation factor during incorporation of Mg into ribosomes and ATP as a cause of enrichment of ^{26}Mg in the cells. We suggest too that the proton gradient across the cell wall and cytoplasmic membrane controls Mg^{2+} transport into the fungal cell. As the strength of this gradient is a function of extracellular solution pH, the pH-dependence on Mg isotope fractionation is thus due to differences in fungal cell mass fluxes. Through a mass balance model we show that Mg uptake into the fungal cell is not associated with a unique Mg isotope fractionation factor. This Mg isotope fractionation dependence on pH might also be observed in any organism with cells that follow similar Mg uptake and metabolic pathways, and serves to reveal Mg cycling in ecosystems.

2.1 Introduction

In the past 15 years metal and metalloid stable isotope ratios (e.g. Mg, Fe, Si, Li, Ca, Zn, etc.) have been developed as novel source and process tracers in ecological and Earth surface systems. Mg isotopes in particular are a promising tool to decipher both biological and Earth surface processes as Mg is a mineral nutrient that is ubiquitous in rocks. Mg stable isotopes change their relative abundances during biogeochemical transformations (e.g. precipitation and secondary mineral formation from fluids, uptake and translocation by plants), hence producing distinct isotope fingerprints (Schmitt et al., 2012; Shirokova et al., 2011; Uhlig et al., 2017). Biological processes vary in the way they fractionate Mg isotopes (Black et al., 2008; Black et al., 2006; Bolou-Bi et al., 2010; Bolou-Bi et al., 2012; Fahad et al., 2016; Ra and Kitagawa, 2007). However, the metabolic processes controlling Mg isotope fractionation are not well-quantified. This knowledge gap is a significant obstacle to interpreting data from complex and dynamic natural ecosystems. As mediators of metal and mineral transformations as well as element cycling, fungi in particular play an important role in rock weathering and deliver large amounts of Mg and other nutrients to higher plants and other phototrophs (Finlay et al., 2009; Gadd, 2007, 2017; Hoffland et al., 2004). Therefore, if the Mg processed by fungi has a unique isotopic fingerprint, this fingerprint serves to interpret Mg elemental mass fluxes at the soil, ecosystem, and river catchment scale. To this end, we still need to explore how cell physiology and isotope fractionation factors are related and whether these in turn depend on environmental controls (pH, speciation, etc.). Addressing these questions will reveal how metal isotope tracers can be used to explore the role of fungi in ecosystem nutrient turnover studies.

The study of Mg isotopes in biology is at an early stage compared to the lighter traditional stable isotope systems of H, C, O, N and S. All studies to date show that biological processes linked with incorporation of Mg induce isotope fractionation. Black et al. (2006) demonstrated that chlorophyll molecules extracted from cyanobacteria are depleted in the heavier Mg isotopes relative to the growth solution (i.e., chlorophyll is 0.71‰ lower in $^{26}Mg/^{24}Mg$ compared to the solution). In contrast, Ra and Kitagawa (2007) observed that the chlorophyll molecules of marine red algae are enriched in the heavier isotopes relative to seawater by 0.58‰ in $^{26}Mg/^{24}Mg$. Two laboratory studies by Black et al. (2008) and Bolou-Bi et al. (2010) showed that the plants are enriched in heavier Mg isotopes relative to the growth solution. These studies discovered that heavier Mg isotopes are preferred during plant uptake, while the lighter Mg isotopes were enriched from roots to shoots during translocation. To date, only one experimental study on Mg isotope fractionation in fungi has been conducted (Fahad et al., 2016). This study revealed that an ectomycorrhizal fungus showed only minor Mg isotope

fractionation, whereas a non-mycorrhizal fungus distinctly incorporated heavier Mg isotopes when grown on a growth media. This pioneering study showed the direction of Mg isotope fractionation in different types of fungus. However, an explanation for the biological processes that cause this fractionation is still missing.

In this study we conducted laboratory experiments under controlled conditions that offered the opportunity to isolate selected parts of the system and test the influence of important geochemical parameters, in our case the effect of pH, on Mg isotope fractionation by a single fungal species. We conducted growth experiments to show for the first time a pH dependence of the Mg isotope fractionation during uptake by a model black fungus. Black microcolonial fungi are ubiquitous world-wide and colonize sub-aerial rock surfaces and exposed natural or man-made structures in diverse climates ranging from hot to cold deserts, acidic metal-enriched mine waters, neutral to alkaline soils in the high Artic, limestone monuments, saltpans, and acidic exposed rocks (Selbmann et al., 2015; Zhang et al., 2016). We chose *Knufia petricola* A95 as a model black fungus because of its capacity to interact with phototrophic algae and cyanobacteria to form stable subaerial microbial communities at acidic and neutral pH in both natural and laboratory conditions (Gorbushina and Broughton, 2009; Gorbushina et al., 2008; Nai et al., 2013; Noack-Schönmann et al., 2014). Due to their short torulose hyphae, they have a smaller surface area compared to mycorrhizae fungus (Nai et al., 2013), but possess the capacity of interacting with mineral surfaces (Seiffert et al., 2014). We suggest that chemical equilibrium during formation of ribosomes and ATP causes Mg isotope fractionation within *K. petricola* cells. Furthermore, we use a mass balance model to explain that the magnitude of isotopic fractionation depends on differences in mass fluxes of Mg into and out of the fungal cell is controlled by pH-dependent transport gradients.

2.2 Material and Methods

2.2.1 Knufia petricola A95

The fungus used in the study was *Knufia petricola* strain A95 (CBS 123872). Rock-inhabiting microcolonial fungi were originally discovered in the early 1980s (Krumbein and Jens, 1981; Staley et al., 1982). They are the predominant and permanent settlers of some of the most extreme environments on Earth, like Antarctica glacial valleys, hot deserts and nuclear radiation-contaminated areas (Yurlova et al., 2008). *K. petricola* A95, is a relatively fast growing rock inhabiting ascomycete and can be easily handled in the lab. The strain was isolated from a marble surface in Athens, Greece. It belongs to an early-diverging lineage of the pathogen-rich ascomycetes order Chaetothyriales (class Eurotiomycetes) and is a

predecessor of lichens. The *K. petricola* strain and a melanin-minus mutant of *K. petricola* (ΔPKS) were cultivated in the lab following the procedure described in Noack-Schönmann et al. (2014) and Nai et al. (2013). A melanin-minus mutant of *K. petricola* was used in order to test potential Mg isotope fractionation effects during adsorption on the cell wall of the fungus. Melanin is a cell wall-bound protective pigment that provides defense against environmental stresses such as ultraviolet (UV) and ionizing radiation as well as desiccation and oxidizing agents.

2.2.2 Growth media

Modified BG-11 media was used to obtain a favorable growth condition for the fungus. Compared to normal BG-11 media, half the amount of $MgSO_4$ was added. The aim of this reduction was to allow detection of changes in Mg concentrations and isotope ratios in the growth solution during uptake. Moreover, additional glucose, and NH_4NO_3 were added to stimulate biomass growth. However, we show below that biomass growth was too low to resolve changes in the solution's Mg isotope composition. A buffered BG-11 media at pH 6 was also prepared by adding about 55 mM of MES (2-(*N*-morpholino)ethanesulfonic acid) buffer. The detailed composition of the modified BG-11 media is given in Table 1.

Table 1: Composition[a] of modified BG-11 media

Species	Concentration (mM)
NaEDTA	0.0027
NH_4Fe citrate	0.0229
Citrate*H_2O	0.0204
$CaCl_2$*$2H_2O$	0.2449
$MgSO_4$*$7H_2O$	0.15
K_2HPO_4*$3H_2O$	0.1753
H_3BO_3	0.0463
$MnCl_2$*$4H_2O$	0.0058
$ZnSO_4$*$7H_2O$	0.0008
$CuSO_4$*$5H_2O$	0.0003
$CoCl_2$*$6H_2O$	0.0002
$NaMoO_4$*H_2O	0.0019

[a]The components of the BG 11 media were diluted to 1 L with MilliQ water. Then 0.75 g of $NaNO_3$ (8.82 mM), 0.75 g of NH_4NO_3 (9.37 mM) and 0.02 g of Na2CO3 (0.189 mM) was added. The pH of the solution was adjusted to 6 and then autoclaved. Finally after autoclaving, 2000 mg filtered, sterilized glucose*H_2O (11.22 mM) was added. For buffered BG-11 media, 10662 mg filter sterilized MES*H_2O (54.62 mM) was further added.

2.2.3 Growth Experiment

The experiments conducted here are biologically as well as geochemically reproducible. We conducted independent growth experiments in triplicate to verify repeatability. Also all the components of the experimental system are precisely quantifiable. All batch experiments with *K. petricola* and abiotic controls were performed under aerobic and sterile conditions in triplicate. 500 mL polycarbonate Erlenmeyer flasks (with sterile vented caps) were cleaned with HCl and HNO_3 acid, washed four times with deionized water (MilliQ), and autoclaved to avoid chemical and microbial contamination. 400 mL of BG-11 media, either with or without MES buffer, was transferred into each Erlenmeyer flask. The flasks with the MES buffer are hereafter called the "buffered experiment" and the flasks without MES buffer are called the "unbuffered experiment". The melanin-minus mutant was not included in the unbuffered experiment because, as will be shown below, results from the wild type and melanin-mutant strains did not differ in the buffered experiment.

Before transfer of cultures of *K. petricola* from the stationary growth phase to the flasks for the time-series growth experiments, they were separated from the MEB media by centrifugation (15 min, 7500 RPM) and then homogenized using an oscillating mill. The cultures were then washed with 5 mM EDTA and BG-11 media to minimize risk of surficial contamination from the original liquid malt-extract media (MEB). The cell number was measured just before inoculation (hemocytometer and quantitative PCR) and a small aliquot of the culture was taken to determine the initial elemental and Mg isotopic compositions (see methods below). Then, between 0.002 g and 0.006 g dry biomass weight of *K. petricola* were incubated in the experiments. The Erlenmeyer flasks with modified BG-11 media and *K. petricola* were placed in a climate chamber under constant temperature (25°C), constant light source (90 µmol photons/m^2s) and were shaken at 150 RPM. Experiments were ran for 10 days for the buffered experiment and 11 days for the unbuffered experiment. Periodic sampling (5 mL) was done using a volumetric pipet whilst manually shaking the flasks to homogenize the culture. The sampled supernatant mixed with biomass was filtered using 0.2 µm sterile filters, acidified with concentrated HNO_3 acid and stored at 4^{o}C until Mg concentration and isotope analysis. The biomass was separated from the supernatant to determine growth at each sampling point. Finally, the experiment was terminated by centrifuging to separate the remaining biomass in the Erlenmeyer flasks. Part of the biomass was used for cell number measurements and the residual was stored at -80^{o}C until used for Mg concentration and isotope analysis.

2.2.4 Analysis

Elemental concentrations of the filtered supernatant and the digested biomass were analyzed by Inductively Coupled Plasma Optical Emission Spectrometry (ICP-OES, Varian 720-ES). Quantitative PCR (qPCR) method was used to quantify the cell number of *K. petricola* by measuring the amount of fungal DNA (Martin-Sanchez et al., 2016). For information about sample preparation and analysis by ICP-OES and qPCR see the supplement.

Sample preparation and Mg purification for isotope measurements were done in the Helmholtz laboratory for the geochemistry of the earth surface (HELGES) at GFZ Potsdam. The pre- and post-experiment dried fungal biomass, and supernatant samples, were acid-digested along with references materials (BHVO-2, BHVO-2 with glucose and Cambridge-1) and blanks in capped screw-top PFA beakers. Mg was purified by cation exchange column chromatography (see supplement for detailed information).

Mg isotope analysis was performed on a Multicollector-Inductively Coupled Plasma Mass Spectrometer (MC-ICP MS, Thermo Scientific Neptune). Analytical results are reported relative to the international measurement standard DSM3 in the delta notation according to

Coplen (2011), $\delta^{x}Mg_{sample} = [\ (^{x}Mg/^{24}Mg)_{sample} / (^{x}Mg/^{24}Mg)_{DSM3}\ ] - 1\ ]$, where x = 26 or 25. Multiplication with a factor 1000 gives the per mil (‰) deviation relative to DSM3. Based on repeated measurements of reference materials, the uncertainty in $\delta^{26}Mg$ is ± 0.1‰ (2SD). For all cell number, pH, and concentrations (Mg, P, K, and Fe) results in Figure (1), the analytical uncertainty or the repeatability of independent experiments was used for interpretation, whichever was larger. See supplement for detailed information on sample preparation, instrument setting and reference material used for MC-ICP MS analysis.

2.3 Results and Discussion

2.3.1 Growth of K. petricola

The acidic pH in the unbuffered experiments favored the growth of *K. petricola*. The dry weight of *K. petricola* biomass after the unbuffered experiment was 0.27 ± 0.03 g, whereas after the buffered experiment it was 0.03 ± 0.01 g, suggesting about 10 times more growth in the unbuffered condition (Table 2). This favored growth of *K. petricola* under acidic conditions has been previously observed (Nai et al., 2013). The melanin-minus mutant experiment showed slightly greater biomass growth (0.06 ± 0.03 g) than the corresponding wild type in the buffered experiment. The number of cells determined by qPCR with respect to experimental runtime for both the experiments is shown in Figure 1.

2.3.2 Evolution of growth solution and incorporation of nutritive metals

Figure 1 shows the evolution of pH, Mg, P, K, and Fe concentration and Mg isotope ratios in the growth solution and biomass with respect to time. pH measurements of the unbuffered experiment with *K. petricola* showed a rapid decrease from 6 to 3 and then remained stable after 6 days. This rapid acidification of the solution in the presence of fungi is well-known from past studies, and is caused by the excretion of protons, release of organic acids, and formation of carbonic acid by respiration of CO_2 by the fungi (Gadd, 2010). As expected, Mg concentrations of the abiotic control experiment remained unchanged (within uncertainty) at both buffered and unbuffered conditions. Mg concentrations in the supernatant solution in the *K. petricola* and melanin-minus mutant experiments at both buffered and unbuffered condition also did not vary outside the analytical uncertainty (Figure 1). This implies that the Mg uptake by the fungus was small relative to the Mg in the initial growth media.

Measurements of Mg in the fungal biomass yielded differences in the final amount of Mg in the biomass between the buffered and unbuffered experiments (Table 2). In the unbuffered experiment about 4.5 % of the total Mg of the growth solution was taken up by *K.*

petricola, compared to only 0.65 % in the buffered experiment. However, as mentioned above, the resulting decrease in the growth solution's Mg mass was not analytically resolvable. The concentration of Mg per gram of dry cells was slightly higher in the buffered experiment (365.28 ± 65.25 µg/g) compared to the unbuffered experiment (245.84 ± 22.46 µg/g) (Table 2). This minor difference suggests that the concentration of Mg inside *K. petricola* does not strongly depend on growth rate. This was already shown in previous studies, i.e. the concentration of intracellular Mg tends to be homeostatic or tightly regulated inside the fungal cell (Flatman, 1984; Okorokov et al., 1975). Less of the nutrients phosphorous and potassium were consumed in the buffered than in the unbuffered experiment. The change in the nutrient concentrations with respect to the initial media amounted to 0.02 mM for P and 0.01 mM for K in the buffered experiment, and 0.04 mM P and 0.13 mM K in the unbuffered experiment, respectively. Due to the greater biomass growth in the melanin-minus mutant experiment compared to the wild type under buffered conditions, a slightly higher uptake of P (a change of 0.05 mM in the growth solution concentration) and K (a change of 0.03 mM) was found. The BG-11 media contains iron as ammonium iron(III) citrate. This iron precipitated, presumably as iron oxyhydroxides, in the abiotic and biotic buffered experiments and the abiotic unbuffered experiment, due to a stable pH at around 6 in these experiments. In the unbuffered biotic experiment where the pH changed from 6 to 3, iron precipitated in the beginning, but then redissolved when acidic conditions were reached. The relevance of iron precipitation as iron oxyhydroxides lies in their potential to sorb and thus fractionate Mg isotopes. However, we did not observe a decline in Mg concentration in the growth solution during the unbuffered abiotic control experiment, suggesting that Mg sorption onto precipitated Fe oxides was negligible. Information on measured elemental concentrations in the supernatant of individual experiments can be found in Table S3 in the supplement.

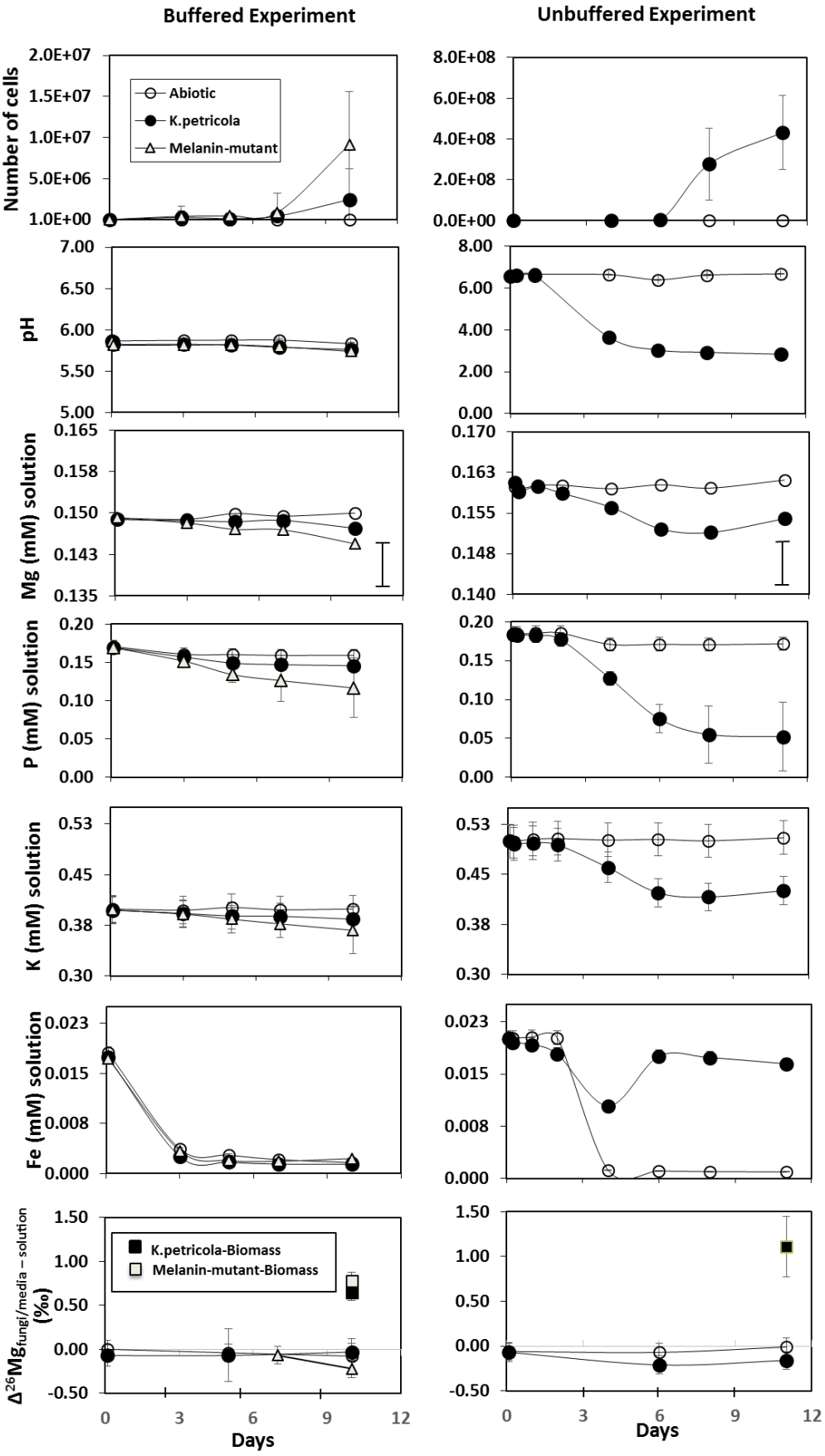

Figure 1: Analysis of various components of the buffered (left column) and unbuffered (right column) experiment as a function of experimental run time. Open circles (○) represent abiotic experiments, closed circles (●) represent *K.petricola* experiments, open triangles (Δ) represent melanin-minus mutant

experiments, closed squares (■) represent Mg isotopic composition of *K.petricola* biomass and open squares represent (□) Mg isotopic composition of melanin-minus mutant biomass. All error bars represents 2SD. For graphs of number of cells, pH (growth solution), and concentration (Mg, P, K, and Fe of growth solution), the analytical uncertainty or the repeatability of independent experiments was used for interpretation, whichever was larger. $\Delta^{26}Mg_{fungi/media\ -\ solution}$ is the isotopic difference between either the biomass of fungi or the growth solution at respective sampling time and the initial growth solution. The error on the graph of $\Delta^{26}Mg_{fungi/media\ -\ solution}$ represent the error propagation of analytical uncertainties for individual measurement analyzed by MC-ICPMS or uncertainty derived from the repeatability of independent experiments, whichever was larger. Detailed information on both types of uncertainties for all data points are given in the supplement (Table S3). For plots where no error bars are shown, the uncertainties are smaller than the symbols.

2.3.3 Mg isotopic composition

All the measured isotopic shifts showed mass-dependent isotope fractionation (Figure S1). No significant variations were observed in the Mg isotopic evolution of the supernatant solutions (all results are identical within analytical uncertainties). Replicate measurements for Mg isotopes of the supernatant were not performed since mass balance calculations verify that a change of less than 5% in Mg amount over the course of the experiment will not significantly change the initial Mg isotope composition of the growth media. Mass balance shows that the slight change are within the analytical uncertainty of 0.1‰ (2SD) for $\delta^{26}Mg$ (see supplement for mass balance calculation). In contrast, at the end of both experiments, the biomass of *K. petricola* showed significant enrichment in the heavier Mg isotopes relative to the growth media. The measured isotopic difference between fungi (*K. petricola* or melanin-mutant) and growth solution (BG-11) was calculated as:

$$\Delta^{26}Mg_{fungi-\ solution} = (\delta^{26}Mg_{fungi} - \delta^{26}Mg_{growth\ solution})\ (‰)$$

In the buffered experiment the calculated isotopic difference between fungus and growth solution was 0.65 ± 0.06 ‰ (2SD, n = 3 full experimental replicates, whereas in the unbuffered experiment the value was higher at 1.11 ± 0.35‰ (2SD, n = 3). Mg isotope fractionation for the melanin-minus mutant buffered experiment was 0.78 ± 0.1‰ (2SD), which is similar to the value obtained for the wild type within the given uncertainty (Table 2). This similarity suggests the absence of Mg isotope fractionation due to adsorption of Mg into melanin in the cell wall and verifies that adsorption is not a large term in the mass balance of Mg. The above uncertainties are derived from the external repeatability of the three independent growth experiments. However, there is also an analytical uncertainty of 0.1‰ (2SD) for individual $\delta^{26}Mg$ measurements. Therefore, the error bars shown for $\Delta^{26}Mg_{fungi\ -\ solution}$ values in Figure 1 and Table 2 represent either the error propagation of analytical uncertainties for individual measurement or external repeatability, whichever is higher. Information on individual Mg

isotope analyses in supernatant and biomass and their respective analytical and external repeatability uncertainties for all experiments can be found in Table S3.

Table 2: Mg Concentration and isotope analysis of the growth solution and biomass

Species	Experimental condition	Mg amount in initial BG-11 media (µg)	Mg amount in initial biomass (µg)	Dry weight of final biomass (g) ± SD[b]	Mg amount in final BG-11 media (µg) ± SD[b]	Mg amount in final biomass (µg) ± SD[b]	Mg concentration in final biomass (µg of Mg/gram of dry cells) ± SD[b]	Mg isotopic difference ($\Delta^{26}Mg_{fungi-solution}$) ± 2SD[c]
K.petricola	Buffered	1449	0.44	0.03 ± 0.01	1429 ± 10	9.37 ± 0.73	365.28 ± 65.25	0.65 ± 0.14
[a]Mutant	Buffered	1449	0.37	0.06 ± 0.03	1400 ± 29	25.48 ± 9.85	401.50 ± 11.48	0.78 ± 0.14
K.petricola	Unbuffered	1556	0.89	0.27 ± 0.03	1497 ± 10	66.83 ± 0.17	245.84 ± 22.46	1.11 ± 0.35

[a]Mutant is the melanin-minus mutant of *K. petricola*.
[b]SD represents standard deviation from the triplicate measurements.
[c]2SD represents the error propagation of analytical uncertainties for individual measurement analyzed by MC-ICPMS or uncertainty derived from the repeatability of three independent experiments, whichever was larger.
The $\delta^{26}Mg_{DSM3}$ value of BG-11 during the experiments was constant over time, i.e., measured at -4.50 ± 0.1 (2SD, n=11) for the buffered and -4.45 ± 0.1 (2SD, n=3) for the unbuffered experiments.

2.3.4 Isotope fractionation during desolvation?

In the unbuffered experiment, PHREEQC speciation calculations predict that the most dominant species was Mg^{2+}(aq) (Figure S2). Before uptake, the cell membrane proteins that transport Mg must be able to recognize the very large hydrated molecule of Mg^{2+}(aq), strip the tightly bound hydration shell from the cation, and then only transport the dehydrated form (Kehres and Maguire, 2002; Moomaw and Maguire, 2008). Mass balance dictates that the resulting quantitative transfer does not allow any isotope fractionations to be manifested. Hence, desolvation in the unbuffered experiment is unlikely to be a dominant control of the observed Mg isotope fractionation in the experiments.

However, in the buffered experiment, PHREEQC speciation calculations predict that the most dominant aqueous species (>99%) was Mg-MES along with trace amounts of Mg^{2+}(aq). A potential mechanism to explain the enrichment of ^{26}Mg in the fungus is a change in the Mg speciation in solution prior to uptake. Schott et al. (2016) have shown that at equilibrium there is an enrichment of ^{26}Mg in $MgSO_4^0$ or $Mg(citrate)^-$ compared to dissolved Mg^{2+} (Mg^{2+}(aq)). In contrast, there is a depletion of ^{26}Mg in $Mg(EDTA)^{2-}$ or $Mg(citrate)_2^{4-}$ compared to Mg^{2+}(aq). The associated isotope fractionation depends on the bond strength of the dissolved chemical species, with stronger bonds favoring incorporation of the heavier isotopes (Schauble, 2007). For the buffered experiment, we can envisage a scenario in which after complexing with MES, a small Mg^{2+}(aq) compartment remains that is lighter than the bulk growth solution. To explain the isotopic difference $\Delta^{26}Mg_{fungi-solution}$ of 0.65‰ observed in the buffered experiment and 1.11‰ in the unbuffered experiment, the composition of the small Mg^{2+}(aq) pool not complexed with MES would be 0.46‰ lower than the isotopic composition of Mg complexed with MES. This scenario can only be verified by comparing the bond strength of Mg-MES and Mg^{2+}(aq) and calculating the respective equilibrium fractionation factors, but no such fractionation factors have been determined.

The scenario that we discuss instead is one in which the reaction between Mg-MES and Mg^{2+}(aq) is not associated with major isotope fractionation. We can further assume that after stripping from Mg-MES, quantitative uptake of Mg^{2+}(aq) species by the fungus is likely, similar to the unbuffered experiment. If uptake of Mg from Mg^{2+}(aq) is complete in both experiments then isotopic fractionation during desolvation can explain neither the presence of fractionation itself, nor the observed difference between the buffered and the unbuffered experiment.

2.3.5 Isotope fractionation during cell uptake and transport?

Previous studies have shown that the concentration of Mg is constant or tightly regulated within a fungal cell, even though there is exchange of extracellular and intracellular Mg during growth (Flatman, 1984; Nelson and Kennedy, 1971; Okorokov et al., 1975). The continuous exchange of Mg between the cell and the external solution excludes Rayleigh-type isotope effects and is consistent with a steady-state (quasi-equilibrium) closed system isotopic exchange (Johnson et al., 2004).

Three different proteins ALR1, ALR2 and MRS2 have been identified as major Mg transporters for eukaryotes (Gardner, 2003). All the three proteins are homologs of the CorA protein. CorA protein is an ion channel that mediates transport of divalent ions across cell membranes in prokaryotic organisms. All three Mg transporters for eukaryotes independently

mediate the translocation of free Mg^{2+} across the cytoplasmic membrane by an electrochemical gradient (Groisman et al., 2013; Hawkesford et al., 2012; Maguire, 2006; Shaul, 2002). The electrochemical gradient is established in the plasma membrane of the fungus. The proton pump (H^+-ATPase) releases protons and thus forms a negative membrane potential inside the cytoplasm. Protons accumulate on the outside of the cell making the cell wall more acidic than the cytoplasm. This electrochemical gradient across the cell wall and cytoplasm barrier leads to Mg^{2+} transport into the cytoplasm.

A unidirectional Mg^{2+} transport could, in principle, be associated with kinetic Mg isotope fractionation. A kinetic isotope fractionation involves enrichment of lighter isotopes in the product relative to the source compartment. However, *K. petricola* is isotopically heavier than the growth solution in both experimental setups, suggesting that kinetic fractionation does not play a dominant role in our experiments. Furthermore, we can safely assume that all Mg ions attracted to the transporter are shuttled into the protein channel and finally into the cytoplasm. If this Mg mass transfer from the cell wall into the cytoplasm is complete, any potential isotope fractionation during transport within the protein channels is not preserved.

2.3.6 Isotope fractionation within the fungus?

A substantial percentage (~95 %) of the intracellular Mg^{2+} transported by the protein transporter is bound to ribosomes, ATP and other polyanionic cell constituents; the remainder consists of tightly regulated free Mg^{2+} at a concentration of 1-5 mM Mg^{2+} (Alatossava et al., 1985; Gardner, 2003; Moncany and Kellenberger, 1981). The bonding of Mg^{2+} in the organic compounds occurs as highly coordinated or strong covalent bonds (Kirkby, 2012). Nierhaus (2014) has shown that in a cell, bonded and free Mg^{2+} are in equilibrium with each other. Various laboratory experiments conducted on free Mg^{2+} and RNA-bound Mg have suggested chemical equilibrium between these species (Stein and Crothers, 1976; Zitomer and Flaks, 1972). Thus in a closed, well-mixed system at chemical equilibrium, isotope equilibrium between free Mg^{2+} and bonded magnesium is likely established. As a general rule, at chemical and isotope equilibrium, the heavier isotopes (^{26}Mg) are enriched in the stronger bonds (in this case e.g. the ATP or ribosomes) (Bigeleisen and Mayer, 1947a; Schauble, 2007). The process of Mg bonding into organic molecules as a likely cause of isotope fractionation leading to higher $\delta^{26}Mg$ signatures in plants has also been suggested by Schmitt et al. (2012) and Bolou-Bi et al. (2010). The Mg^{2+} effluxed from the fungus is depleted in ^{26}Mg because of preferential partitioning of ^{26}Mg into Mg-ATP and ribosomes at equilibrium. Continuous removal of this isotopically light Mg from the cell results in fungal biomass enriched in ^{26}Mg. Thus the net isotope fractionation

between growth solution and the bulk cell is governed, in addition to the individual isotope fractionation factors, by the relative fluxes into, within, and from the cell.

2.3.7 Isotope fractionation dependence on pH?

Previous work has demonstrated that net biological isotope fractionations can be modeled as a function of cellular influx/efflux rate ratios of the element in question, so that the parameter that controls these rates can control the isotope fractionation. For example, dissolved Si uptake and efflux rates involving marine sponges are related to ambient dissolved Si concentrations, so silicon isotope fractionation by these organisms varies predictably as a function of Si concentration (Hendry and Robinson, 2012; Wille et al., 2010). Similarly, the ratio of calcification to organic carbon fixation fluxes has been related to carbon isotope fractionation in coccolithophores (McClelland et al., 2017). In the following, we present a mass balance model showing how observed Mg isotope fractionation can vary with Mg uptake rate into the cell, and address how the pH of the solution might control this flux.

Under acidic conditions (pH 3), more H^+ ions are present in the cell wall compared to neutral pH. Acidic conditions thus increase the proton gradient between the cell wall and the cytoplasm, resulting in a higher input rate of (isotopically unfractionated) Mg from the growth solution into the cell. About 95% of the Mg within the cell is in the form of isotopically fractionated Mg-bearing compounds (e.g. ATP, ribosome, referred to as "$Mg_{ribo+ATP}$"), which have a higher $\delta^{26}Mg_{ribo+ATP}$ relative to the growth solution. As dictated by mass balance, at equilibrium in a closed system this remaining 5% free Mg^{2+} (Mg^{2+}_{free}) obtains a lower isotope ratio (defined as $\delta^{26}Mg_{free}$). This isotopically light Mg^{2+}_{free} will eventually be exported from the cell. There, it is mixed into the large pool of Mg in the growth solution (without significantly affecting its isotopic composition), to be replaced with an influx of fresh unfractionated Mg from the growth solution. Thus the $\delta^{26}Mg_{free}$ depends on the rate of replenishment of Mg^{2+}_{free} versus the rate of Mg bonding into $Mg_{ribo+ATP}$ compounds. Because of mass conservation in the cell, influx and efflux are coupled. At low pH, this coupling results in higher efflux of isotopically fractionated Mg^{2+}_{free} low in $\delta^{26}Mg_{free}$. Thus the total fungal cell Mg (Mg^{2+}_{free} + $Mg_{ribo+ATP}$) will be isotopically enriched in heavy Mg isotopes. In contrast, in the buffered experiment at higher pH, the gradient is smaller, and thus the rate of Mg influx is small too. This results in lower efflux of isotopically fractionated Mg^{2+}_{free} causing the fungal cell to have lower positive total $\delta^{26}Mg_{fungi}$ values than in the unbuffered experiment.

We model these scenarios with a simple mass balance following a similar approach taken for Si isotope fractionation during uptake in marine organisms (Hendry and Robinson, 2012; Milligan et al., 2004; Wille et al., 2010). To determine the pH dependency on the

fractionation factor, the cell was treated as a continuous batch reactor (Figure 2). A continuous batch reactor is a setup where there is a continuous flow of reactant in and out of the reactor.

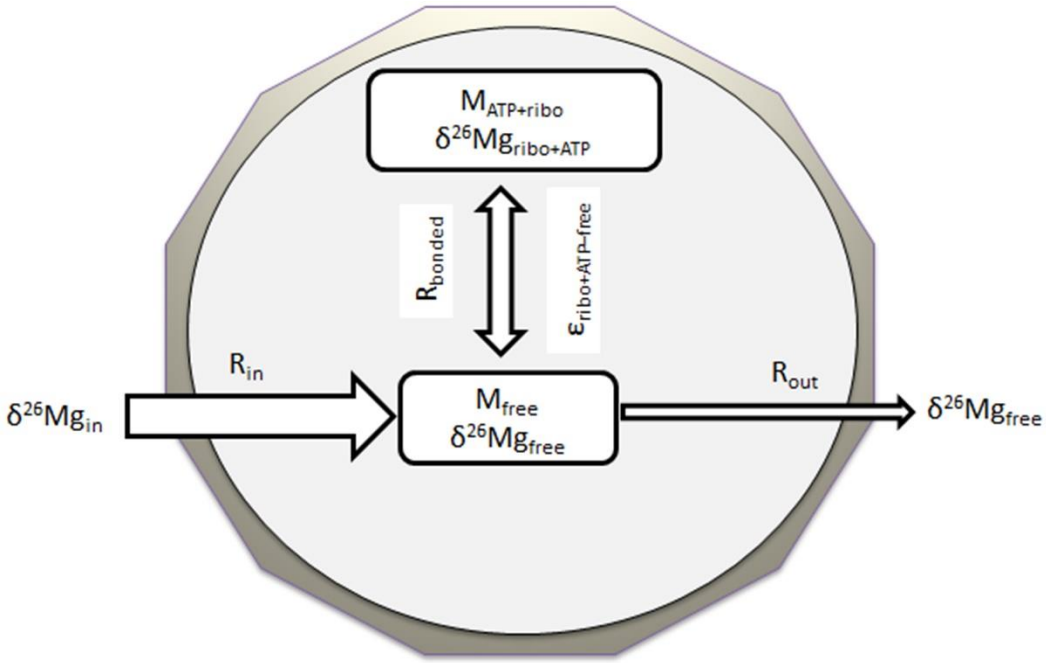

Figure 2: Simplified model of Mg transport pathways into and and out of the fungal cell. The figure represents cellular magnesium homeostasis, showing the balance between input of Mg into the cell, Mg bonded to the organic molecules ATP and ribosomes, free magesium in the cytoplasm, and efflux of magnesium from the cell. Detailed information of the individual compartments and the corresponding δ-values are given in the main text.

In this model, R_{in} is the input rate of Mg into the cell [moles sec^{-1}]; R_{bonded} is the bonding rate of Mg into $Mg_{ribo+ATP}$ [moles sec^{-1}]; R_{out} is the rate of Mg efflux [moles sec^{-1}]; R_{free} is the rate of free Mg formation [moles sec^{-1}]; $\delta^{26}Mg_{solution}$ is the Mg isotopic composition of the unfractionated influx of BG-11 growth solution; $\delta^{26}Mg_{ribo+ATP}$ is the isotopic composition of $Mg_{ribo+ATP}$ [‰]; $\delta^{26}Mg_{free}$ is the Mg isotope composition of Mg^{2+}_{free} in the cell [‰]; $M_{ribo+ATP}$ = amount of Mg in $Mg_{ribo+ATP}$ [moles]; M_{free} = amount of Mg^{2+}_{free} in the cell [moles].

The mass balance equation for the total cell is

$$\delta^{26}Mg_{fungi} \bullet M_{cell} = \delta^{26}Mg_{free} \bullet M_{free} + \delta^{26}Mg_{ribo+ATP} \bullet M_{ribo+ATP} \quad \text{(eq. 1)},$$

where M_{cell} is the total amount of Mg in fungal cell [moles]. As mentioned above, the partitioning of Mg between Mg^{2+}_{free} and $Mg_{ribo+ATP}$ (5:95) is constant but the rate of change in the Mg mass in a growing cell is not constant, and given by

$$\frac{dM_{cell}}{dt} = R_{in} - R_{out} = R_{bonded} + R_{free} \approx R_{bonded} \quad \text{(eq. 2)}$$

The simplification on the right hand side of equation 2 can be done because 95% of the Mg is contained in $Mg_{ribo+ATP}$.

And thus,

$$R_{in} = R_{out} + R_{bonded} \quad \text{(eq. 3)}$$

Introducing corresponding δ-values into equation 3,

$$R_{in} \bullet \delta^{26}Mg_{solution} = R_{out} \bullet \delta^{26}Mg_{free} + R_{bonded} \bullet (\delta^{26}Mg_{free} + \varepsilon_{ribo+ATP-free}) \quad \text{(eq. 4)}$$

where $\varepsilon_{ribo+ATP-free} = \delta^{26}Mg_{ribo+ATP} - \delta^{26}Mg_{free}$, is the equilibrium isotope fractionation between Mg^{2+}_{free} and $Mg_{ribo+ATP}$

Now, substituting $R_{out} = R_{in} - R_{bonded}$ in equation 4, we then solve for $\delta^{26}Mg_{free}$

$$\delta^{26}Mg_{free} = \delta^{26}Mg_{solution} - (R_{bonded}/R_{in}) \bullet \varepsilon_{ribo+ATP-free} \quad \text{(eq. 5)}$$

Substituting equation 5 in equation 1:

$$\delta^{26}Mg_{fungi} - \delta^{26}Mg_{solution} = \varepsilon_{ribo+ATP-free}\,[f_{bonded} - (R_{bonded}/R_{in})] \quad \text{(eq. 6)}$$

$$\Delta^{26}Mg_{fungi-solution} = \varepsilon_{ribo+ATP-free}\,[f_{bonded} - (R_{bonded}/R_{in})] \quad \text{(eq. 7)}$$

where f_{bonded} is $(M_{ribo+ATP}/M_{cell})$, which is ca. 0.95. In this model we assume that the fractionation factor between the species Mg^{2+}_{free} and $Mg_{ribo+ATP}$ i.e. $(\varepsilon_{ribo+ATP-free})$ is a constant that does not depend on the growth solution pH. This assumption is based on the fact that the external pH does not affect the intracellular pH due to the homeostatic nature of the cell. In other words, the conditions for formation of $Mg_{ribo+ATP}$ compounds are independent of external pH.

From equation 6, we can infer that the isotopic difference between fungi and solution ($\Delta^{26}Mg_{fungi-solution}$) is inversely proportional to (R_{bonded}/R_{in}). We show this dependence for two different $\varepsilon_{ribo+ATP-free}$ in Figure 3. Since data on equilibrium fractionation factors for $Mg_{ribo+ATP}$ compounds are unavailable, we chose two values of 2‰ and 4‰. These fractionation factors were chosen because they are comparable to the equilibrium fractionation factors between Mg organic complexes (Mg oxalate and Mg citrate) and $Mg(H_2O)_6^{2+}$ calculated by Schott et al. (2016). To conserve mass, the ratio of (R_{bonded}/R_{in}) during growth has to be between 0 and 1. In general, $\Delta^{26}Mg_{fungi-solution}$ ranges between $0.95 \cdot \varepsilon_{ribo+ATP-free}$ (when $R_{bonded}/R_{in} = 0$) and $-0.05 \cdot \varepsilon_{ribo+ATP-free}$ (when $R_{bonded}/R_{in} = 1$).

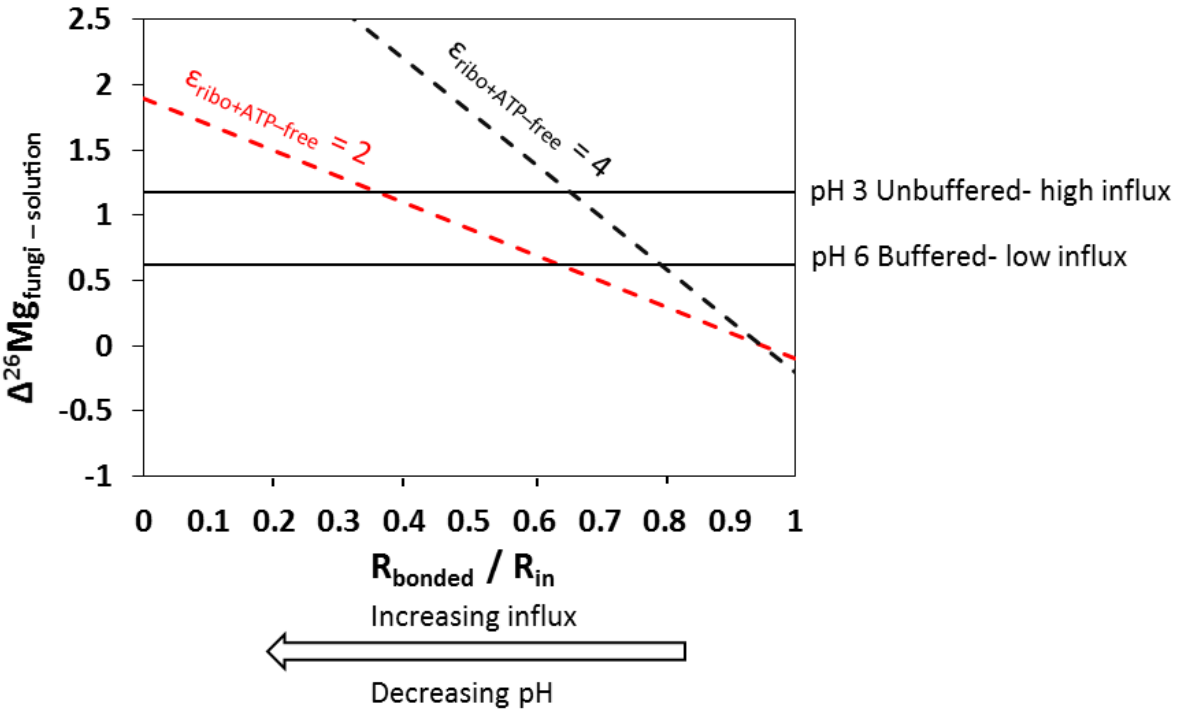

Figure 3: The figure shows the dependence of $\Delta^{26}Mg_{fungi-solution}$ on the ratio of (R_{bonded} / R_{in}) at two assumed equilibrium fractionation factors $\varepsilon_{ribo+ATP-free}$, i.e., for $\varepsilon_{ribo+ATP-free}$ = 2 (red dashed line) and 4 (black dashed line) in equation 4. Solid horizontal lines represent the measured isotopic difference between fungi and growth solution ($\Delta^{26}Mg_{fungi-solution}$) at buffered and unbuffered conditions.

Using the fractionation factor $\varepsilon_{ribo+ATP-free}$ of 2‰, R_{bonded}/R_{in} ratios for the buffered and unbuffered experiment are 0.64 and 0.36, respectively. Assuming a $\varepsilon_{ribo+ATP-free}$ of 4‰, the R_{bonded}/R_{in} ratios for the buffered and unbuffered experiments are 0.80 and 0.66, respectively. Because we do not know $\varepsilon_{ribo+ATP-free}$, we cannot assign actual R_{bonded}/R_{in} to a given pH value. However, we conclude that the relationship between isotopic difference (between fungi and solution) and pH observed in our experiments can be explained by variations in (R_{bonded}/R_{in}).

2.4 Environmental Implications

The ubiquitous distribution of fungi in ecosystems makes them an important component of soil microbial communities that are responsible for a large amount of nutrient transfer, in particular mineral nutrients that can limit plant productivity. We have chosen a representative species of microcolonial rock-inhabiting fungi to investigate Mg isotope fractionation and elucidate the responsible cellular processes under acidic and neutral conditions. Selecting a representative

primary coloniser on bare rocks which is proven to interact with mineral substrates at various environmental conditions increases the relevance of our findings if placed into the context of how Mg cycles in the critical zone at the interface between the atmosphere, biosphere and lithosphere.

Equally important is that 80 % of terrestrial plant species are associated with mycorrhizal fungi (Landeweert et al., 2001). This implies that the Mg isotope fractionations derived for plant uptake in previous studies (Bolou-Bi et al., 2012; Tipper et al., 2010; Tipper et al., 2012; Uhlig et al., 2017) might actually reflect the prior uptake of Mg into the symbiotic fungi. Our study pertains to this suggestion as for the first time we show that the same species of black fungi fractionates Mg isotopes differently at two different pH levels. This is important information for ecosystem studies where Mg isotopes are used to trace Mg uptake pathways from the soils or soil pore water to fungi and then to plants, for example. We now know that using a single fractionation factor for fungal uptake in these types of studies is incorrect, as the net isotopic factor varies with the environment in which the fungi are growing.

Previous studies on Mg isotopes in plants in both laboratory and natural settings have shown a wide variety of fractionation between the root of the plant and respective growth solution at both acidic and neutral conditions (Black et al., 2008; Bolou-Bi et al., 2010; Bolou-Bi et al., 2012). The general trend observed in some studies is that the roots of the plants grown in acidic conditions are slightly heavier in ^{26}Mg than the roots of plants grown in neutral conditions (Bolou-Bi et al., 2010; Bolou-Bi et al., 2012). However until now there was no explanation provided for this trend. We suggest that Mg undergoes equilibrium isotopic fractionation during incorporation of Mg into ATP and ribosomes inside the fungal cell, and observe that the degree of isotope fractionation is dependent on the initial rate of Mg uptake. For plants that are not associated with symbiotic fungi, the same mechanism for varying isotope fractionation during uptake may be relevant as some of the Mg transport proteins for plants have been identified to belong to the same CorA superfamily as the fungi (Li et al., 2001). We therefore speculate that higher plants follow similar metabolic pathways for Mg uptake, and the pH-dependence of Mg isotope fractionation we observed in *K. petricola* might also be observed in other organisms.

2.5 Supporting Information

2.5.1 PCR Analysis

Quantitative PCR (qPCR) was used to quantify the cell numbers of *K. petricola* by measuring the amount of fungal DNA (Martin-Sanchez et al., 2016). First, the DNA was extracted by using

phenol:chloroform:isoamylalcohol (25:24:1, v/v/v). The product was then purified and precipitated using chloroform:isoamylalcohol (24:1, v/v) and ethanol respectively. Finally the purity and concentration of DNA was checked with spectrophotometry (Nanodrop 2000C, Thermo Scientific). qPCR was performed using a Real Time PCR Cycler CFX96 (Bio-Rad), an iTaq Supermix (Bio-Rad) and the following primers:

NL1f: 5′-ATATCAATAAGCGGAGGAAAAG-3′

LS2r: 5′-ATTCCCAAACAACTCGACTC-3′

Each sample was analyzed in duplicate with a standard series (in triplicate) at the beginning of each run.

2.5.2 ICP-OES Analysis

Elemental concentrations of the filtered supernatant and the digested biomass were analyzed by Inductively Coupled Plasma Optical Emission Spectrometry (ICP-OES, Varian 720-ES). Sample dilutions of 1:3 were made using 0.3 M quartz distilled HNO_3 with 1000 ppm Cs, 1.3 ppm In and 1.4 ppm Sc as internal standards. The detection limit for Mg was 0.5 µM and the analytical uncertainty was estimated at 5 %, based on repeat analyses of quality control solutions. A linear response in signal intensity was observed for the calibration standards over four orders of magnitude of concentration ($R^2 > 0.999$). Instrument stability was confirmed by checking blanks and quality control samples (Multi or single element ICP standards with or without glucose, of known concentrations) after every 12 samples (Table S1).

2.5.3 Mg Column Separation

All the biomass, supernatant, blanks and reference material were acid-digested in capped screw-top PFA beakers. All samples were treated with mixture of concentrated HNO_3, HCl, H_2O_2 and HF on a hotplate at 150^{o}C in multiple steps until complete dissolution. Finally the samples were taken up in 1M HNO_3 acid prior to column chemistry for Mg separation.

Mg separation was performed in Spectrum 104704 MiniColumns filled with 2.8 mL of cation exchange resin Bio Rad AG-50W-X12 200-400 mesh (37-74µm) similar to the procedure described in Pogge von Strandmann et al. (2011) and Uhlig et al. (2017). About 15 µg of Mg (samples and reference material) along with blanks were processed through columns. Matrix elements ware eluted by subsequent washing with 1M HNO_3 acid and Mg was collected with 2M HNO_3. The purified Mg fractions were evaporated to almost dryness and taken up in 1 mL of 0.3N HNO_3. Check for purity and quantitative yield of the Mg fraction was done by ICP-OES.

2.5.4 MC-ICP MS analysis

Multicollector-Inductively Coupled Plasma Mass Spectrometer (MC-ICP MS, Thermo Scientific Neptune) was used for Mg isotope analysis. Samples and standards were diluted to a Mg concentration of 500 ppb in 0.3M HNO_3, corresponding to about 10 V signal on ^{24}Mg using a 10^{11} Ohm Faraday cup current amplifier. The solutions were introduced to the mass spectrometer via a quartz-glass spraychamber (double pass cyclon-scott type, Thermo SIS) equipped with a self-aspirating PFA nebulizer with an uptake rate of ca. 100 µL/min. Mg isotope signals (^{24}Mg, ^{25}Mg, ^{26}Mg) were measured simultaneously on Faraday detectors with an integration time of 4 s for each cycle (20 cycles measured per sample). All samples and reference materials were measured by MC-ICP-MS using the standard-sample-standard bracketing technique with DSM3 as bracketing standard to correct for instrumental mass bias.

Reference materials Cambridge-1 (pure Mg solution, both processed and unprocessed through Mg columns), pure BHVO-2 and BHVO-2-Glucose (basaltic rock doped with glucose, processed through Mg columns) were periodically measured and yielded values of $\delta^{26}Mg_{Cam\text{-}1}$ = -2.65 ± 0.1‰ (2SD, n= 74), $\delta^{26}Mg_{BHVO\text{-}2}$ = -0.23 ± 0.1‰ (2 SD, n = 18), and $\delta^{26}Mg_{BHVO\text{-}2\text{-}Glucose}$ = -0.26 ± 0.1‰ (2 SD, n = 6) respectively, in good agreement with results reported in the literature (Bolou-Bi et al., 2009; Pogge von Strandmann et al., 2011). In some cases Mg fractions contained residual amounts of other elements, such as Ni, Mn, Zn, K and Na that were not completely removed by the column chromatography protocol. To test for any potential bias on Mg isotope results induced by the presence of these impurities, we analyzed reference materials doped with these residual elements at element to Mg ratios observed in samples. The results showed no effect on measured Mg isotope ratios within analytical uncertainty (Table S2).

2.5.5 Closed System Mass Balance Calculations

Here we verify that a change in Mg amount by ≤5% does not resolvably change the initial Mg isotope composition of the growth solution. The closed system mass balance equation is given by:

$$\delta^{26}Mg_{initial} = f \bullet \delta^{26}Mg_{final} + (1\text{-}f)\ \delta^{26}Mg_{fungi} \qquad \text{(eq. 1)}$$

Here, $\delta^{26}Mg_{initial}$ is the initial growth solution isotope composition; $\delta^{26}Mg_{final}$ is the final growth solution isotope composition; $\delta^{26}Mg_{fungi}$ is the isotope composition of the fungi and f is the fraction of Mg remaining in the solution at the end of experiment (≥ 95% in our case). Solving equation 1 for $\delta^{26}Mg_{final}$:

$$\delta^{26}Mg_{final} = (\delta^{26}Mg_{initial} - 0.05 \bullet \delta^{26}Mg_{fungi})/0.95 \quad \text{(eq. 2)}$$

Now, substituting, $\delta^{26}Mg_{fungi} = (\delta^{26}Mg_{initial} + \Delta^{26}Mg_{fungi-solution})$ in equation 2, we get

$$\delta^{26}Mg_{final} = [\delta^{26}Mg_{initial} - 0.05\ (\delta^{26}Mg_{initial} + \Delta^{26}Mg_{fungi-solution})]/0.95 \quad \text{(eq. 3)}$$

where $\Delta^{26}Mg_{fungi-solution}$ is the measured isotopic difference. Now substituting $\delta^{26}Mg_{initial}$ = -4.5‰ and $\Delta^{26}Mg_{fungi-solution}$ = 1.11‰, we get $\delta^{26}Mg_{final}$ = - 4.56‰, which is within analytical uncertainty (0.1‰, 2SD) of the initial solution isotope composition ($\delta^{26}Mg_{initial}$ = -4.5‰).

Table S1: Analysis of quality control standards for ICP-OES

Name	In (µg/g)	Sc (µg/g)	Mg (µg/g)	K (µg/g)	P (µg/g)	Fe (µg/g)	Glucose (g/L)
Reference value (Stock: Merck ICP Single Element Standard)	1.32	1.41	0.96				
Measured value (n=12)	1.33	1.40	1.00				
2SD	0.01	0.02	0.05				
Measured deviation from reference value (%)	**0.1**	**-0.5**	**3.4**				
Reference value (Stock: Merck ICP Multi Element Standard)			0.96	0.96		0.96	
Measured value (n=4)			0.97	0.96		1.018	
2SD			0.00	0.01		0.00	
Measured deviation from reference value (%)			**1.75**	**0.52**		**5.70**	
Reference value (GFZ-R1)	1.32	1.41	1.29	6.48	1.90	0.38	0.66
Measured value (n=10)	1.33	1.41	1.29	6.46	1.88	0.38	
2SD	0.01	0.02	0.10	0.05	0.05	0.00	
Measured deviation from reference value (%)	**0.5**	**0.1**	**0.1**	**-0.3**	**-1.3**	**-0.3**	

Results of concentration analysis of reference material by ICP-OES in our laboratory. Reference materials without glucose were prepared from manually diluting and weighing the Merck ICP single or multiple element standard solutions. Reference material GFZ-R1 is a synthetically prepared multi element standard with glucose. The mean results of n replicates are given together with 2 standard deviations (2SD; representing 95% of the population). The measured deviation from the reference value is a quantitative indication of accuracy.

Table S2: Mg isotope analysis of pure and doped reference materials

Reference material	Ni/Mg (%)	Mn/Mg (%)	Zn/Mg (%)	K/Mg (%)	Na/Mg (%)	$\delta^{26}Mg_{DSM3}$ (‰)	n
Pure Mg solution (not processed through column chemistry)							
Cambridge-1						-2.65 ± 0.10	74
Basalt reference material processed through column chemistry							
BHVO-2						-0.23 ± 0.10	18
Reference material doped with glucose and processed through column chemistry							
BHVO-2-Glucose						-0.26 ± 0.10	6
Pure Mg solution doped with different contaminant elements (not processed through column chemistry)							
Cambridge-1-doped			29			-2.64 ± 0.10	8
Cambridge-1-doped	181	22				-2.72 ± 0.10	8
Cambridge-1-doped	13	17	30			-2.63 ± 0.10	4
DSM3-doped		7	5	13	7	-0.07 ± 0.10	8
DSM3-doped		7		27		-0.07 ± 0.10	8

All reference material solutions were diluted to 500 ng/ml Mg for MC-ICP-MS analysis and were measured by sample-standard bracketing with DSM3 solution of the same concentration. Doped solutions indicate that pure Mg solutions (500 ng/ml Mg) were doped with different elements to achieve the given element to Mg mass concentrations ratios that represent maximum concentrations of impurities left in some sample Mg fractions after column separation. The mean $\delta^{26}Mg$ values of n replicate analysis is given relative to DSM3 (= 0‰). Analytical repeatability of each reference material was within the uncertainty of the MC-ICP-MC analytical method, estimated at ± 0.10‰ for $\delta^{26}Mg$.

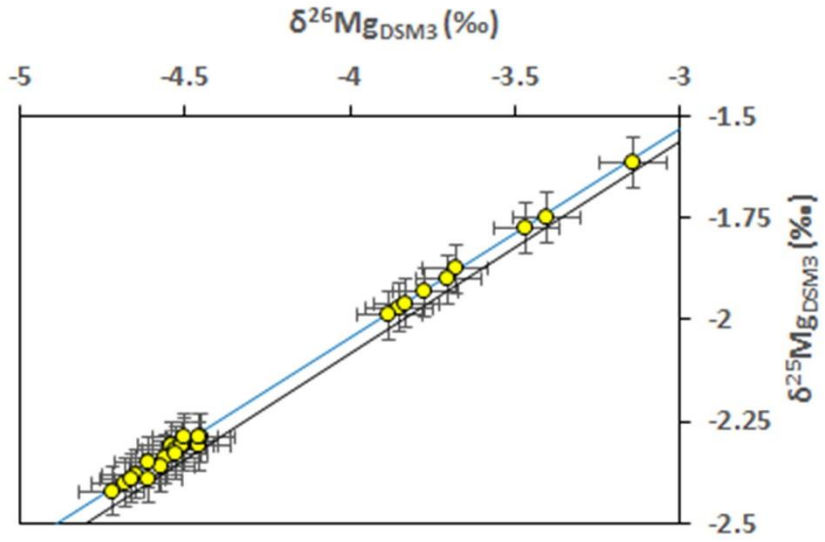

Figure S1: Mg isotope composition of all samples (yellow circles) measured in this study in a three isotope plot of $\delta^{26}Mg_{DSM}$ vs $\delta^{25}Mg_{DSM}$. The solid black line and solid blue line represent the mass dependent equilibrium fractionation line (slope = 0.521) and kinetic fractionation line (slope = 0.511), respectively. Error bars are based on repeat reference material measurements processed through the Mg column chemistry and are ±0.10‰ (2SD, $\delta^{26}Mg_{DSM3}$) and ±0.06‰ (2SD, $\delta^{25}Mg_{DSM3}$).

Figure S2: Results of PHREEQC calculations for Mg speciation and relative amounts in the initial BG-11 media at unbuffered and buffered conditions. The pie chart shows that the dominant Mg species in the unbuffered condition is the Mg^{2+}(aq) (Mg+2 in graph), whereas Mg bonded with MES (MesMg+ in graph) is the dominant species in the buffered condition.

Table S3: Concentration and Mg isotope measurements of biomass and growth solution

			Growth solution							Biomass (fungi *K.petricola*)		Isotopic difference (biomass – solution)
Experiment	Replicate experiment number	Time (Days)	pH	Mg^c (mM)	Fe^c (mM)	K^c (mM)	P^c (mM)	$\delta^{25}Mg_{DSM3}$ (‰)	$\delta^{26}Mg_{DSM3}$ (‰)	$\delta^{25}Mg_{DSM3}$ (‰)	$\delta^{26}Mg_{DSM3}$ (‰)	$\Delta^{26}Mg_{fungi-solution}$[d] (‰)
Abiotic-Buffered	1- (Initial BG-11)	0	5.86	0.149	0.017	0.397	0.169	-2.31 ± 0.06[a]	-4.50 ± 0.10[a]			
	Exp 1	0.08	5.89	0.150	0.018	0.401	0.170	-2.31 ± 0.06[a]	-4.46 ± 0.10[a]			
	Exp 2	0.08	5.86	0.149	0.018	0.401	0.171	-2.31 ± 0.06[a]	-4.54 ± 0.10[a]			
	Exp 3	0.08	5.85	0.149	0.018	0.396	0.172					
	Mean		**5.87**	**0.149**	**0.018**	**0.399**	**0.171**	**-2.31**	**-4.50**			
	2SD[b]		**0.04**	**0.001**	**0.000**	**0.006**	**0.002**	**0.00**	**0.10**			
	Exp 1	3	5.9	0.149	0.004	0.398	0.160					
	Exp 2	3	5.87	0.149	0.003	0.400	0.160					
	Exp 3	3	5.85	0.149	0.004	0.395	0.163					
	Mean		**5.87**	**0.149**	**0.004**	**0.398**	**0.161**					
	2SD[b]		**0.06**	**0.000**	**0.000**	**0.006**	**0.004**					
	Exp 1	5	5.90	0.150	0.002	0.403	0.160					
	Exp 2	5	5.87	0.150	0.003	0.404	0.160	-2.31 ± 0.06[a]	-4.54 ± 0.10[a]			
	Exp 3	5	5.86	0.149	0.003	0.398	0.161					
	Mean		**5.88**	**0.150**	**0.003**	**0.402**	**0.160**					
	2SD[b]		**0.04**	**0.002**	**0.000**	**0.006**	**0.002**					
	Exp 1	7	5.90	0.149	0.002	0.396	0.157					
	Exp 2	7	5.87	0.150	0.002	0.401	0.160					
	Exp 3	7	5.86	0.150	0.002	0.398	0.161					
	Mean		**5.88**	**0.149**	**0.002**	**0.398**	**0.159**					
	2SD[b]		**0.04**	**0.001**	**0.000**	**0.007**	**0.003**					
	Exp 1	10	5.86	0.150	0.001	0.399	0.158	-2.38 ± 0.06[a]	-4.65 ± 0.10[a]			
	Exp 2	10	5.83	0.151	0.002	0.403	0.160	-2.31 ± 0.06[a]	-4.51 ± 0.10[a]			
	Exp 3	10	5.81	0.149	0.002	0.396	0.160					
	Mean		**5.83**	**0.150**	**0.002**	**0.399**	**0.159**	**-2.35**	**-4.58**			
	2SD[b]		**0.05**	**0.001**	**0.000**	**0.007**	**0.003**	**0.10**	**0.20**			
K. petricola-Buffered	Exp 1	0.08	5.84	0.149	0.018	0.399	0.169	-2.32 ± 0.06[a]	-4.53 ± 0.10[a]			
	Exp 2	0.08	5.84	0.149	0.018	0.398	0.169	-2.39 ± 0.06[a]	-4.61 ± 0.10[a]			
	Exp 3	0.08	5.84	0.149	0.018	0.395	0.171					
	Mean		**5.84**	**0.149**	**0.018**	**0.398**	**0.170**	**-2.35**	**-4.57 ± 0.10[a]**			
	2SD[b]		**0**	**0.001**	**0.000**	**0.004**	**0.002**	**0.10**	**0.12**			
	Exp 1	3	5.83	0.150	0.006	0.394	0.158					
	Exp 2	3	5.83	0.150	0.002	0.396	0.155					
	Exp 3	3	5.84	0.147	0.009	0.388	0.158					
	Mean		**5.83**	**0.149**	**0.006**	**0.393**	**0.157**					
	2SD[b]		**0.01**	**0.003**	**0.007**	**0.008**	**0.003**					
	Exp 1	5	5.84	0.149	0.002	0.388	0.149	-2.40 ± 0.06[a]	-4.68 ± 0.10[a]			
	Exp 2	5	5.85	0.149	0.001	0.392	0.149	-2.31 ± 0.06[a]	-4.46 ± 0.10[a]			
	Exp 3	5	5.84	0.148	0.001	0.387	0.149					

		Mean		**5.84**	**0.148**	**0.001**	**0.389**	**0.149**	**-2.35**	**-4.57**		
		2SD[b]		**0.01**	**0.002**	**0.000**	**0.005**	**0.001**	**0.12**	**0.30**		
	Exp 1		7	5.83	0.149	0.001	0.389	0.147				
	Exp 2		7	5.84	0.148	0.001	0.390	0.146				
	Exp 3		7	5.83	0.148	0.001	0.387	0.148				
		Mean		**5.83**	**0.149**	**0.001**	**0.388**	**0.147**				
		2SD[b]		**0.01**	**0.001**	**0.000**	**0.003**	**0.002**				
	Exp 1		10	5.78	0.148	0.002	0.386	0.146	-2.34 ± 0.06[a]	-4.56 ± 0.10[a]	-1.97 ± 0.06[a]	-3.85 ± 0.10[a]	0.65 ± 0.14[d]
	Exp 2		10	5.78	0.147	0.001	0.386	0.145	-2.30 ± 0.06[a]	-4.50 ± 0.10[a]	-1.96 ± 0.06[a]	-3.83 ± 0.10[a]	0.67 ± 0.14[d]
	Exp 3		10	5.78	0.146	0.002	0.381	0.147			-1.99 ± 0.06[a]	-3.88 ± 0.10[a]	0.62 ± 0.14[d]
		Mean		**5.78**	**0.147**	**0.002**	**0.384**	**0.146**	**-2.32**	**-4.53**	**-1.97**	**-3.85**	**0.65**
		2SD[b]		**0**	**0.002**	**0.000**	**0.005**	**0.002**	**0.06**	**0.08**	**0.02**	**0.06**	**0.06**
Mutant-Buffered	Exp 1		0.08	5.82	0.149	0.017	0.401	0.169				
	Exp 2		0.08	5.82	0.149	0.017	0.396	0.170				
	Exp 3		0.08	5.81								
		Mean		**5.82**	**0.149**	**0.017**	**0.398**	**0.169**				
		2SD[b]		**0.01**	**0.000**	**0.001**	**0.007**	**0.001**				
	Exp 1		3	5.82	0.148	0.003	0.392	0.152				
	Exp 2		3	5.81	0.148	0.003	0.391	0.151				
	Exp 3		3	5.82								
		Mean		**5.82**	**0.148**	**0.003**	**0.392**	**0.152**				
		2SD[b]		**0.01**	**0.000**	**0.000**	**0.001**	**0.001**				
	Exp 1		5	5.81	0.147	0.002	0.387	0.138				
	Exp 2		5	5.82	0.147	0.002	0.381	0.131				
	Exp 3		5	5.83								
		Mean		**5.82**	**0.147**	**0.002**	**0.384**	**0.134**				
		2SD[b]		**0.01**	**0.00**	**0.000**	**0.009**	**0.01**				
	Exp 1		7	5.79	0.148	0.002	0.382	0.136	-2.36 ± 0.06[a]	-4.57 ± 0.10[a]		
	Exp 2		7	5.79	0.146	0.002	0.372	0.117				
	Exp 3		7	5.81								
		Mean		**5.80**	**0.147**	**0.002**	**0.377**	**0.126**				
		2SD[b]		**0.01**	**0.003**	**0.000**	**0.014**	**0.027**				
	Exp 1		10	5.71	0.142	0.003	0.355	0.103	-2.42 ± 0.06[a]	-4.72 ± 0.10[a]	-1.88 ± 0.06[a]	-3.68 ± 0.10[a]	0.82 ± 0.14[d]
	Exp 2		10	5.75	0.147	0.002	0.380	0.130			-1.93 ± 0.06[a]	-3.77 ± 0.10[a]	0.73 ± 0.14[d]
	Exp 3		10	5.76							-1.90 ± 0.06[a]	-3.70 ± 0.10[a]	0.80 ± 0.14[d]
		Mean		**5.74**	**0.144**	**0.002**	**0.368**	**0.117**			**-1.90**	**-3.72**	**0.78**
		2SD[b]		**0.03**	**0.006**	**0.001**	**0.035**	**0.039**			**0.06**	**0.10**	**0.10**
Abiotic-Unbuffered	1-(Initial BG-11)		0	6.58	0.160	0.020	0.501	0.186	-2.29 ± 0.06[a]	-4.45 ± 0.10[a]			
	Exp 1		0.08		0.160	0.020	0.504	0.185	-2.31 ± 0.06[a]	-4.51 ± 0.10[a]			
	Exp 2		0.08		0.159	0.020	0.496	0.184					
	Exp 3		0.08		0.160	0.020	0.496	0.184					
		Mean			**0.160**	**0.020**	**0.499**	**0.061**					
		2SD[b]			**0.001**	**0.000**	**0.009**	**0.000**					
	Exp 1		0.25	6.63	0.159	0.020	0.501	0.185					
	Exp 2		0.25	6.59	0.160	0.020	0.498	0.184					
	Exp 3		0.25	6.63									
		Mean		**6.62**	**0.159**	**0.020**	**0.499**	**0.185**					
		2SD[b]		**0.05**	**0.000**	**0.000**	**0.004**	**0.001**					
	Exp 1		1	6.66	0.159	0.020	0.502	0.185					
	Exp 2		1	6.61	0.161	0.020	0.503	0.185					

	Exp 3		1	6.64						
		Mean		**6.64**	**0.160**	**0.020**	**0.503**	**0.185**		
		2SD[b]		**0.05**	**0.002**	**0.000**	**0.002**	**0.000**		
	Exp 1		2		0.160	0.020	0.503	0.186		
	Exp 2		2		0.161	0.020	0.504	0.185		
	Exp 3		2							
		Mean			**0.160**	**0.020**	**0.504**	**0.186**		
		2SD[b]			**0.001**	**0.000**	**0.002**	**0.001**		
	Exp 1		4	6.64	0.159	0.001	0.500	0.171		
	Exp 2		4	6.63	0.160	0.001	0.503	0.171		
	Exp 3		4	6.63						
		Mean		**6.63**	**0.160**	**0.001**	**0.502**	**0.171**		
		2SD[b]		**0.01**	**0.001**	**0.000**	**0.003**	**0.000**		
	Exp 1		6	6.40	0.161	0.001	0.507	0.172	-2.33 ± 0.06[a]	-4.53 ± 0.10[a]
	Exp 2		6	6.53						
	Exp 3		6	6.56	0.160	0.001	0.498	0.170		
		Mean		**6.50**	**0.160**	**0.001**	**0.502**	**0.171**		
		2SD[b]		**0.17**	**0.001**	**0.000**	**0.013**	**0.003**		
	Exp 1		8	6.62	0.159	0.001	0.498	0.170		
	Exp 2		8	6.60	0.160	0.001	0.503	0.171		
	Exp 3		8	6.59						
		Mean		**6.60**	**0.160**	**0.001**	**0.500**	**0.171**		
		SD[b]		**0.03**	**0.001**	**0.000**	**0.007**	**0.001**		
	Exp 1		11	6.68	0.162	0.001	0.509	0.172	-2.29 ± 0.06[a]	-4.46 ± 0.10[a]
	Exp 2		11	6.71	0.161	0.001	0.505	0.172		
	Exp 3		11	6.71	0.161	0.001	0.501	0.171		
		Mean		**6.70**	**0.161**	**0.001**	**0.505**	**0.172**		
		SD[b]		**0.03**	**0.001**	**0.000**	**0.009**	**0.001**		
***K.petricola*-Unbuffered**	Exp 1		0.08		0.160	0.020	0.503	0.185	-2.29 ± 0.06[a]	-4.50 ± 0.10[a]
	Exp 2		0.08		0.160	0.020	0.500	0.184		
	Exp 3		0.08		0.162	0.020	0.496	0.183		
		Mean			**0.161**	**0.020**	**0.500**	**0.184**		
		SD[b]			**0.002**	**0.000**	**0.008**	**0.002**		
	Exp 1		0.25	6.62	0.160	0.020	0.501	0.185		
	Exp 2		0.25	6.64	0.158	0.019	0.490	0.181		
	Exp 3		0.25	6.62						
		Mean		**6.63**	**0.159**	**0.020**	**0.496**	**0.183**		
		2SD[b]		**0.02**	**0.003**	**0.000**	**0.014**	**0.006**		
	Exp 1		1	6.60	0.160	0.019	0.500	0.184		
	Exp 2		1	6.59	0.159	0.019	0.494	0.181		
	Exp 3		1	6.60						
		Mean		**6.60**	**0.160**	**0.019**	**0.497**	**0.183**		
		2SD[b]		**0.01**	**0.001**	**0.000**	**0.008**	**0.004**		
	Exp 1		2		0.160	0.018	0.496	0.179		
	Exp 2		2		0.158	0.018	0.492	0.176		
	Exp 3		2							
		Mean			**0.159**	**0.018**	**0.494**	**0.178**		
		2SD[b]			**0.002**	**0.000**	**0.007**	**0.004**		
	Exp 1		4	3.66	0.156	0.010	0.461	0.128		
	Exp 2		4	3.52	0.156	0.011	0.459	0.126		

Exp 3		4	3.52								
	Mean		**3.57**	**0.156**	**0.010**	**0.460**	**0.127**				
	2SD[b]		**0.16**	**0.00**	**0.002**	**0.003**	**0.003**				
Exp 1		6	3.04	0.152	0.018	0.422	0.065	-2.39 ± 0.06[a]	-4.66 ± 0.10[a]		
Exp 2		6	3.05	0.152	0.018	0.425	0.080				
Exp 3		6	3.05	0.152	0.018	0.420	0.081				
	Mean		**3.05**	**0.152**	**0.018**	**0.422**	**0.075**				
	2SD[b]		**0.01**	**0.001**	**0.000**	**0.004**	**0.018**				
Exp 1		8	2.93	0.150	0.017	0.410	0.042				
Exp 2		8	2.92	0.153	0.018	0.422	0.068				
Exp 3		8	2.92								
	Mean		**2.92**	**0.151**	**0.017**	**0.416**	**0.055**				
	2SD[b]		**0.01**	**0.003**	**0.001**	**0.018**	**0.037**				
Exp 1		11	2.84	0.153	0.016	0.413	0.027	-2.35 ± 0.06[a]	-4.61± 0.10[a]	-1.62 ± 0.06[a]	-3.14 ± 0.10[a]	1.31 ± 0.14[d]
Exp 2		11	2.89	0.155	0.017	0.435	0.066			-1.75 ± 0.06[a]	-3.40 ± 0.10[a]	1.04 ± 0.14[d]
Exp 3		11	2.88	0.154	0.017	0.429	0.064			-1.78 ± 0.06[a]	-3.47 ± 0.10[a]	0.98 ± 0.14[d]
	Mean		**2.87**	**0.154**	**0.016**	**0.425**	**0.052**			**-1.71**	**-3.34**	**1.11**
	2SD[b]		**0.05**	**0.001**	**0.001**	**0.022**	**0.044**			**0.18**	**0.35**	**0.35**

[a]Uncertainties given after each individual result are analytical uncertainties for each individual experiment analyzed by MC-ICP-MS. These are estimated based on repeat reference material measurements processed through the Mg column chemistry and are ±0.10‰ (2SD, $\delta^{26}Mg$) and ±0.06‰ (2SD, $\delta^{25}Mg$). Multiple MC-ICP-MS measurements of each sample solution were always repeatable within the stated uncertainties. All δ-values are reported relative to the international measurement standard DSM3.

[b]Each type of experiment (abiotic, *K. petricola*, buffered, unbuffered) was repeated multiple times and each batch contained triplicate batch reactor bottles run in parallel (indicated by exp. 1, …2, …3). For each experiment type, where more than one of the triplicates was analyzed by MC-ICP-MS after Mg column separation, the experimental mean and 2SD is reported.

[c]Element concentrations were measured by ICP-OES with analytical uncertainties estimated to be ± 5% relative (95% confidence) based on repeat measurements of quality control standards. The following emission wavelengths were used: Mg (280.270 nm), Fe (238.204 nm), K (766.491 nm) and P (213.618 nm) and calibration of the ICP-OES was made with matrix-matched multi-elements standard solutions.

[d]$\Delta^{26}Mg_{fungi-solution}$ represents the isotopic difference between the $\delta^{26}Mg$ value of fungi biomass (*K. petricola*) samples at the end of each experiment and the $\delta^{26}Mg$ value of the growth solution. The growth solution stayed constant in $\delta^{26}Mg_{DSM3}$ over the entire experiment duration with a mean $\delta^{26}Mg_{DSM3}$ of -4.50 ± 0.1‰ (2SD) for buffered and -4.45 ± 0.1 ‰ (2SD) for unbuffered experiment. Uncertainty in $\Delta^{26}Mg_{fungi-solution}$ is derived from error propagation of individual measurement uncertainties.

Chapter 3

Magnesium stable isotope fractionation on a cellular level explored by cyanobacteria and black fungi with implications for higher plants

Abstract

In a controlled growth experiment we found that the cyanobacterium *Nostoc punctiforme* has a bulk cell $^{26}Mg/^{24}Mg$ ratio (expressed as $\delta^{26}Mg$) that is -0.27‰ lower than the growth solution at a pH of ca. 5.9. This contrasts with recently published $\delta^{26}Mg$ value that was 0.65‰ higher than growth solution for the black fungus *Knufia petricola* at similar laboratory conditions, interpreted to reflect loss of ^{24}Mg during cell growth. By a mass balance model constrained by $\delta^{26}Mg$ in chlorophyll extract we inferred the $\delta^{26}Mg$ value of the main Mg compartments in a cyanobacteria cell: free cytosolic Mg (-2.64‰), chlorophyll (1.85‰), and the non-chlorophyll-bonded Mg compartments like ATP and ribosomes (-0.64‰). The lower $\delta^{26}Mg$ found in *Nostoc punctiforme* would thus result from the absence of significant Mg efflux during cell growth in combination with either a) discrimination against ^{26}Mg during uptake by desolvation of Mg or transport across protein channels; or b) discrimination against ^{24}Mg in the membrane transporter during efflux. The model predicts the preferential incorporation of ^{26}Mg in cells and plant organs low in Mg, and the absence of isotope fractionation in those high in Mg, corroborated by a compilation of Mg isotope ratios from fungi, bacteria, and higher plants.

3.1 Introduction

Magnesium (Mg) is a macronutrient for all living organisms and has a wide range of cellular functions. It plays a vital role as a cofactor in many enzymes, is responsible for ATP production and is also a requirement for protein synthesis in ribosomes (Maguire and Cowan, 2002; Moomaw and Maguire, 2008; Pasternak et al., 2010). Further, it is essential for photosynthesis as Mg is bound as a central atom in the porphyrin ring of the chlorophyll molecule (Bohn et al., 2004; Katz, 1968). Intracellular Mg exists either as free (cytosolic) Mg^{2+}, or as Mg bonded in organic compounds like ATP and ribosomes (Quamme, 2010; Silver, 1969). The level of free cytosolic Mg^{2+} is kept within narrow limits through cellular transport mechanisms, but a clear picture of the regulation process involved has not yet emerged (Alatossava et al., 1985; Grubbs, 2002). The stable isotopes of Mg offer a new approach to exploring cellular Mg metabolism. Mg has three stable isotopes: ^{24}Mg, ^{25}Mg and ^{26}Mg, with relative abundances of approximately 79, 10 and 11%, respectively. The relative mass differences (ca. 8% between ^{26}Mg and ^{24}Mg) cause subtle variations in the Mg isotope ratios (i.e. isotope fractionation) that can be resolved by mass-spectrometric measurements. It is now well established that biological processes induce Mg isotope fractionation, but the detailed cellular mechanisms causing the observed isotopic shifts have not yet been identified (Black et al., 2008; Bolou-Bi et al., 2010; Bolou-Bi et al., 2012; Chapela Lara et al., 2017; Fahad et al., 2016; Kimmig et al., 2018; Mavromatis et al., 2014; Moynier and Fujii, 2017; Opfergelt et al., 2014; Pokharel et al., 2017; Schmitt et al., 2012; Tipper et al., 2010; Uhlig et al., 2017).

Cell Mg concentrations and isotope ratios measured in previous studies require that the bonded and free Mg compartments are in chemical and isotopic equilibrium (Nierhaus, 2014; Pokharel et al., 2017). Mg incorporating cell components like ATP, ribosomes or chlorophyll - with strong covalent or highly coordinated bonds - tends to bind the heavier ^{26}Mg isotope preferentially over ^{24}Mg from the free cytosolic Mg^{2+}(Pokharel et al., 2017). The bonded Mg compartment is therefore enriched in the heavier Mg isotopes. The bonded Mg compartment also dominates total cellular Mg, amounting to >95% of total cellular Mg (Alatossava et al., 1985; Froschauer et al., 2004; Nierhaus, 2014; Romani and Scarpa, 1992). The enrichment of heavier Mg isotope in the dominant portion of total intracellular Mg suggests that in a system where Mg in the cell freely exchanges with its growth environment, bulk cell Mg should be isotopically heavier than the Mg in the growth solution. In reality, this is not always observed. For example, the Mg isotopic composition of the bulk ectomycorrhizal fungi measured by Fahad et al. (2016) shows slight enrichment in the lighter Mg isotopes relative to the substrate Mg (about -0.15‰ lower in $^{26}Mg/^{24}Mg$ than that of the growth solution), while that measured

in a non-mycorrhizal fungi in the same study did show the expected enrichment of ^{26}Mg (0.3‰ higher in $^{26}Mg/^{24}Mg$ than that of the growth solution). Mg isotope compositions within higher plants show significant variability (Black et al., 2008; Bolou-Bi et al., 2010; Bolou-Bi et al., 2012). In general, roots are isotopically heavier than shoots. Assessments of Mg isotope fractionation between chlorophyll and the growth solution have also yielded variable results. For example, Black et al. (2006) demonstrated enrichment of lighter Mg isotopes with respect to the growth solution in chlorophyll extracted from a cyanobacterium (0.71‰ lighter in $^{26}Mg/^{24}Mg$), whereas Ra and Kitagawa (2007) showed that the chlorophyll of marine red algae incorporates heavier Mg isotopes from the growth solution (0.58‰ heavier in $^{26}Mg/^{24}Mg$). Ra et al. (2010) further showed that chlorophyll extracted from a cultured coccolithophore (*Emiliania huxleyi*) is slightly depleted in heavier Mg isotopes than the growth solution, although their observations were complicated by a dependence on the simultaneous intracellular production of coccoliths.

The aim of this study is to apply the stable Mg isotope system to investigate the relationship between cell physiology and Mg cellular cycling and to identify mechanisms that explain the differing Mg isotope compositions of various biological systems. To this end we investigated Mg isotope fractionation by a model phototrophic cyanobacterium *Nostoc punctiforme* ATCC 29133 in a well-controlled laboratory growth experiment. *N. punctiforme* is an aerobic, diazotrophic, gram-negative, filamentous and motile cyanobacterium that is ubiquitous at the land surface and that has been intensively studied to understand microbial carbon and nitrogen dynamics (Lindberg et al., 2002; Meeks et al., 2001). It is important in ecological studies as it forms symbiotic relationships with plant and fungal species in a wide variety of environmental conditions and across large temperature and pH gradients (Ekman et al., 2013; Meeks, 1998; Sand-Jensen, 2014). In symbiotic relationships with fungi, *N. punctiforme* provides carbohydrates produced by photosynthesis to fungi that in turn supply nutrients and ensure structural support to the *Nostoc* cells (Ekman et al., 2013; Meeks et al., 2001). *N. punctiforme* also acts as a biological weathering agent even in vegetation-free environments and is successfully used in laboratory biofilm and weathering studies (Gorbushina and Broughton, 2009; Seiffert et al., 2016). In this study we determined the Mg isotope composition of the bulk cell *N. punctiforme*, and of the chlorophyll molecules extracted from them. These data and experimental results from the growth experiments were combined with mass balance models to predict the parameters that control isotope fractionation in a cyanobacterial cell. Finally, we explored the applicability of these predictions using and

analysing a compilation of published Mg isotope data from higher plants and fungi. We thereby aim to identify the unifying mechanisms underlying stable Mg isotope fractionation in cells.

3.2 Material and Methods

3.2.1 Nostoc punctiforme ATCC 29133

N. punctiforme used in this study was supplied by J.M. Meeks (University of California, Davis, CA, USA). As described in Seiffert et al. (2016) the axenic cultures were pre-grown in a BG-11 media at pH 7.5 25°C and 90 µmole photons of photosynthetically active light m^2 s^{-1} for 24 h d^{-1} and shaking (160 rpm). They were transferred weekly by diluting 1:100 into fresh media. After having been grown for 2 weeks, cultures were harvested and used in our Mg uptake experiments.

3.2.2 Mg uptake experiments and analytical methods

In this paper we use the same experimental conditions, growth media, sampling procedures and analytical techniques as described in detail in Pokharel et al. (2017). The major difference is the exchange of the fungus *Knufia petricola* for the cyanobacterium *N. punctiforme*. Further, the experiments were performed only under pH-buffered conditions since the acidic conditions employed in the *Knufia petricola* study are not favourable for the growth of *N. punctiforme*. A brief description of the experimental setup, sample strategies and the analytical procedure is given below; more details can be found in Pokharel et al. (2017).

All growth experiments were conducted in triplicate to verify repeatability. Experiments were conducted in an aerobic climate chamber (Percival LT-36VL, Percival, USA) under constant temperature (25°C) and constant light source (90 µmol photons/m^2s). Acid-cleaned 500 mL Erlenmeyer flasks were used to perform the growth experiments. The growth solution was a modified BG-11 media buffered to pH of 5.9 using the MES buffer (Table S1). About 0.002 g (dry weight) pre-grown biomass of *N. punctiforme* (as described above) was inoculated in these media under aseptic conditions. An abiotic control experiment (without *N. punctiforme*) was run in parallel with the biotic experiments. The Erlenmeyer flasks with *N. punctiforme* biomass were shaken at 150 rpm in the aerobic climate chamber and the experiments were ran for 10 days. Periodic sampling during the experiment was done with a volumetric pipette while manually shaking to mix the growing biomass with the supernatant. The aliquots obtained were then filtered through sterile 0.2 µm filters (MF-Millipore, Merck) to separate the supernatant from the biomass. The filtered supernatant solution was used for pH measurements, multi-element concentration and Mg isotope analysis and the biomass for growth quantification at the

time of sampling. At the end of the experiments the entire biomass of *N. punctiforme* was separated by centrifugation and analyzed for biomass growth. Elemental concentrations and Mg isotope compositions of the final biomass were determined after its dissolution in $HNO_3/H_2O_2/HCl/HF$ in screw-top PFA vials on a hotplate at 150°C for >24 hours. The dissolution process was repeated several times until the biomass was completely dissolved.

The growth of *N. punctiforme* cells at different sampling intervals was determined by extracting DNA followed by quantitative PCR (qPCR) analysis (Martin-Sanchez et al., 2016). Analytical protocols for elemental concentrations and Mg isotopes are identical to those described in Pokharel et al. (2017). Briefly, elemental concentrations (Mg, Fe, K, and P) in the supernatant solution and in the dissolved biomass were analyzed with an Inductively Coupled Plasma Optical Emission Spectrometer (ICP-OES, Varian 720-ES). The analysis was performed following the procedure described in Schuessler et al. (2016). Mg isotope analysis was achieved with Multicollector Inductively Coupled Plasma Mass Spectrometry (MC-ICP-MS, Thermo Fisher Scientific Neptune) after Mg purification by column chromatography (cation exchange resin Bio Rad AG-50W-X12 200-400 mesh). Analytical results are expressed in the δ-notation as the parts per thousand (‰) deviation of the $^{26}Mg/^{24}Mg$ ratio from the international measurement standard DSM3, $\delta^{x}Mg = [(({}^{x}Mg/{}^{24}Mg)_{sample} / ({}^{x}Mg/{}^{24}Mg)_{DSM3}) - 1 \times 1000]$, where x = 26 or 25. Based on repeated measurements of reference materials processed together with the samples, the uncertainty in $\delta^{26}Mg$ is estimated at ± 0.1‰ (2SD) and ± 0.06‰ (2SD) in $\delta^{25}Mg$. Further details on sample preparation and instrumental setup for qPCR, ICP-OES and MC-ICPMS along with quality control results on reference materials and blanks are provided in Pokharel et al. (2017) and their Supporting Information.

The Mg isotope fractionation by chlorophyll molecules in *N. punctiforme* was determined in a separate growth experiment conducted in triplicate. The experimental conditions were identical to those of the experiment described above, with the only difference being that no periodic sampling of the supernatant was undertaken. At the end of the experiment after 10 days, the *N. punctiforme* biomass was centrifuged. Since the amount of chlorophyll-bound Mg is low in cells, the biomass from the three experiments was combined and stored at -20°C before chlorophyll extraction. A detailed description of the chlorophyll pigment extraction procedure, separation by HPLC, and Mg isotope analysis is provided in the Supporting Information.

3.3 Results and Discussion

3.3.1 Evolution of pH, cell growth, and uptake of nutrients by N. punctiforme

As expected under the buffered conditions, the pH of the experiment remained stable and the acids excreted during the growth of *N. punctiforme* were buffered by the MES at a pH of ca. 5.9 (Figure 1b). This circum-neutral condition is favorable for growth of *N. punctiforme* as evidenced by the increase in biomass during the experiment (Figure 1a). During the experiment *N. punctiforme* consumed about 21 % of Mg from the initial solution (Figure 1e). The measured amount of Mg per gram of dry cells of *N. punctiforme* was 3004 µg/g (Table 1). The major nutrients in the growth solution, including K and P, were also consumed during the growth of *N. punctiforme* (Figure 1d and 1f). All Fe initially contained in the growth solution was precipitated as iron (III) oxyhydroxide (Figure 1f), the stable form of Fe at the pH of ca. 5.9, and the fully oxygenated conditions of the growth solution.

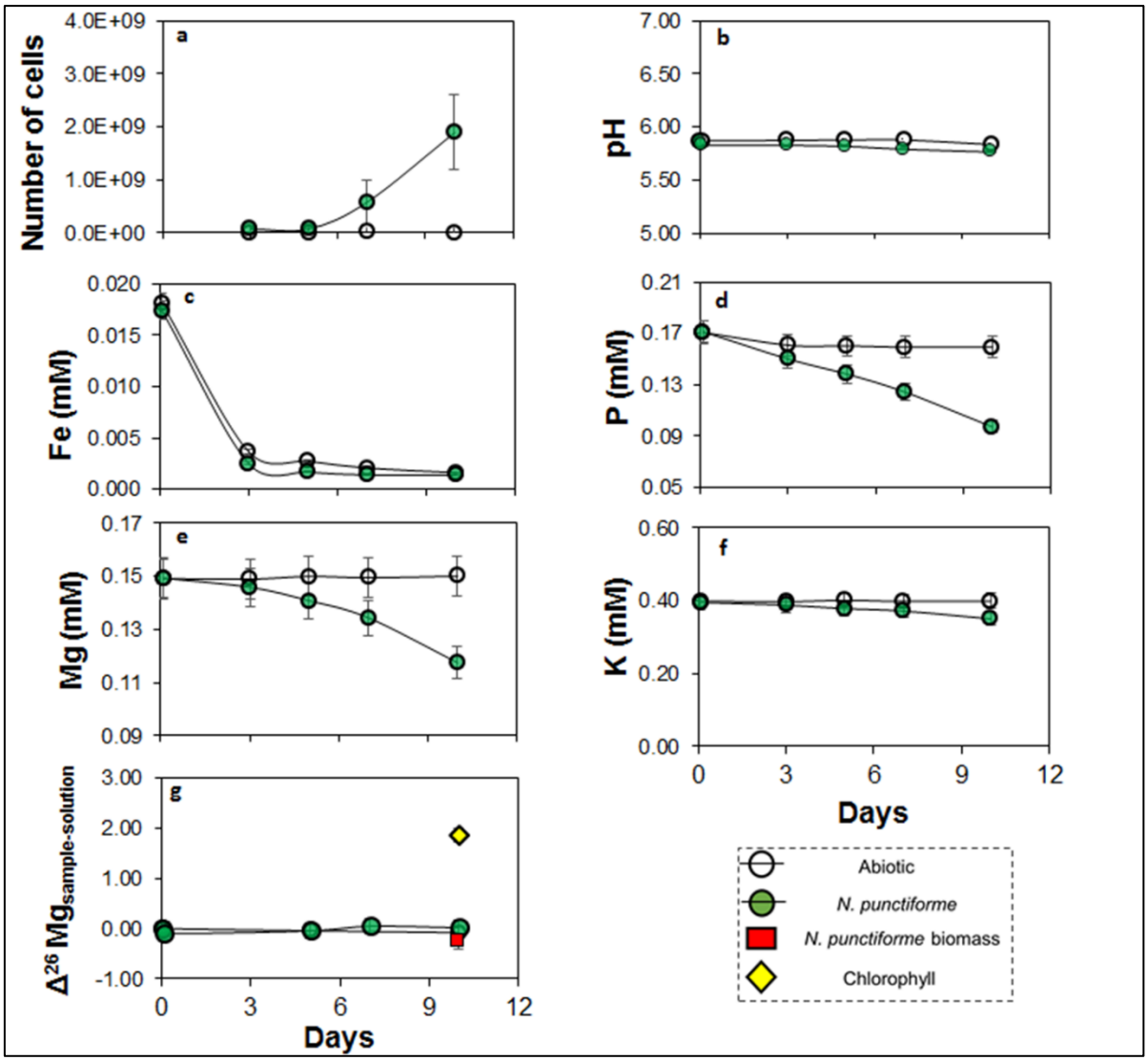

Figure 1: Documentation of parameters of the growth experiment as a function of run time. Open circles represent parameters of the solution in the abiotic experiments, the green circles represent solution parameters of *N. punctiforme* experiments, the red square represents the difference in δ^{26}Mg between *N. punctiforme* biomass and growth solution, and the yellow diamond the difference in δ^{26}Mg between chlorophyll extracted from *N. punctiforme* and the growth solution. All uncertainty bars represent 2SD. The uncertainty of the graphs a, b, c, d, e, and f was derived from the analytical uncertainty or the repeatability of independent growth experiments, whichever was larger. The uncertainty on the graph g represent the error propagation of individual measurements analyzed by MC-ICP-MS. Detailed information on both types of uncertainty on all data points are given in the Supporting Information (Table S3 and S4). In graph g, the $\Delta^{26}Mg_{sample-solution}$ is the isotopic difference between either the biomass of *N. punctiforme* or the growth solution at respective sampling time or the chlorophyll extracted and the initial growth solution. For plots where no uncertainty is shown, the uncertainty is smaller than the symbols.

Table 1: Mg concentration and isotope composition analysis of growth media and biomass

Mg mass in initial BG-11 media (µg) ± 2SD[a]	Mg mass in initial biomass (µg)	Dry weight of final biomass (g) ± 2SD[c]	Mg amount in final BG-11 media (µg) ± 2SD[a]	Mg amount in final biomass (µg) ± SD[a]	Mg concentration in final biomass (µg of Mg/gram of dry cells) ± 2SD[a]	Mg isotopic difference ($\Delta^{26}Mg = \delta^{26}Mg_{chlorophyll} - \delta^{26}Mg_{solution}$[d]) (‰) ± 2SD[b]	Mg isotopic difference ($\Delta^{26}Mg = \delta^{26}Mg_{N.punctiforme} - \delta^{26}Mg_{solution}$[e]) (‰) ± 2SD[b]
1449 ± 72	1.27	0.07 ± 0.02	1142 ± 57	208 ± 44	3004 ± 190	1.85± 0.14	-0.27 ± 0.14

[a]2SD represents analytical uncertainties from the triplicates measurements of each individual experiments or the uncertainties derived for individual measurements by ICP-OES, whichever was larger. [b]2SD represents the error propagation of individual measurements analyzed by MC-ICP-MS. [c]2SD represents uncertainties derived from repeatability of three independent experiments. [d]The $\delta^{26}Mg_{solution}$ value of –1.05 ± 0.1‰ (2SD, n=3) relative to DSM3 was measured for the input solution of the independent chlorophyll experiment (Table S4). [e]The $\delta^{26}Mg_{solution}$ value of -4.50 ± 0.1‰ (2SD, n=11) relative to DSM3 was measured for the initial input solution and time-series sampling confirmed that it stayed constant over the time of the experiment.

3.3.2 Mg isotope fractionation

All isotope measurements reported follow the expected mass-dependent isotope fractionation line in a three-isotope ($\delta^{26}Mg$ vs $\delta^{25}Mg$) plot (Figure S1), demonstrating the absence of any resolvable mass-independent isotope effect, or polyatomic interferences during measurement. Hence, we discuss all further Mg isotope data in terms of $\delta^{26}Mg$ values. Because the growth solution differs in its Mg isotope composition from the reference material DSM3 (used as isotope measurement standard during MC-ICP-MS analysis, Table S3), we report and discuss all measured sample data as net isotopic difference to $\delta^{26}Mg$ of the initial growth solution:

$$\Delta^{26}Mg_{sample-solution} = (\delta^{26}Mg_{sample} - \delta^{26}Mg_{initial\ solution})\ (‰)$$

Here, sample can refer to the growth solutions at different sampling times, *N. punctiforme* biomass, or the extracted chlorophyll. *N. punctiforme* cell at the end of the experiment was enriched in the lighter Mg isotopes relative to the growth solution. The calculated $\Delta^{26}Mg_{N.punctiforme-solution}$ is -0.27 ± 0.14‰ (2SD, n = 3) (Figure 1g, Table 1, and Table S3). No significant changes in isotopic composition of the supernatant solution were observed, despite 21% Mg uptake (Figure 1e and 1g). This observation is consistent with a Rayleigh isotope fractionation model: Mg uptake of 21% and a fractionation of $\Delta^{26}Mg_{N.punctiforme-solution}$ of -0.27‰ predicts an increase in $\delta^{26}Mg$ of the growth solution by only +0.07‰, which is analytically not resolvable. The absence of changes in the composition of the growth solution in both the abiotic control experiments and the *N. punctiforme* growth experiments demonstrates that any potential Mg isotope fractionation induced during Mg co-precipitation with iron oxides is not analytically resolvable. Mg isotope measurements of chlorophyll extracted from the *N. punctiforme* biomass

resulted in a $\Delta^{26}Mg_{chlorophyll\text{-}solution}$ value of 1.85 ± 0.14‰ (2SD) (Figure 1g, Table 1, and Table S4), where the uncertainty derives from error propagation of individual measurements analyzed by MC-ICP-MS. The observation of chlorophyll Mg being distinctly heavier than both the growth solution and total cell Mg supports the assumption in Pokharel et al. (2017) that Mg-bearing organic compounds inside the cell preferentially incorporate the heavier Mg isotopes. A similar trend of heavy Mg isotope incorporation in chlorophyll molecules extracted from leaves is consistent with previous laboratory experiments and theoretical calculations (Black et al., 2007; Moynier and Fujii, 2017).

The question thus arises of why bulk *N. punctiforme* has lower $\delta^{26}Mg$ than the bonded Mg compounds (chlorophyll, ATP, or ribosome), when these compounds are the dominant Mg carriers in the cell. In the following we use a mass balance model to explain the overall low $\delta^{26}Mg$ of the *N. punctiforme* and identify parameters controlling the Mg isotope composition of fungi and higher plants. The mass balance equation for the isotope composition of the total cell is:

$$M_{Cell} \times \delta^{26}Mg_{Cell} = M_{free} \times \delta^{26}Mg_{free} + M_{chlo} \times \delta^{26}Mg_{chlo} + M_{ATP} \times \delta^{26}Mg_{ATP} \quad (1)$$

where M is a mass of Mg and the subscripts Cell, free, chlo and ATP refer to Mg in the total cell, as free cytosolic Mg^{2+}, in chlorophyll and in other non-chlorophyll compounds, respectively, and $\delta^{26}Mg$ their respective isotope composition. The implicit assumption is that these three pools are an adequate representation of the complexities of intracellular Mg physiology. By replacing the values of $\delta^{26}Mg_{chlo}$ and $\delta^{26}Mg_{ATP}$ in eq 1 we get,

$$M_{Cell} \times \delta^{26}Mg_{Cell} = M_{free} \times \delta^{26}Mg_{free} + M_{chlo} \times (\delta^{26}Mg_{free} + \varepsilon_{chlo\text{-}free}) + M_{ATP} \times (\delta^{26}Mg_{free} + \varepsilon_{ATP\text{-}free}) \quad (2)$$

where $\varepsilon_{target\text{-}source}$ is a fractionation factor (in ‰) between a target and a source compartment. The measured isotopic composition of bulk *N. punctiforme* cell ($\delta^{26}Mg_{N.punctiforme}$) is -0.27‰ and $\delta^{26}Mg_{chlo}$ of extracted chlorophyll is 1.85‰. Solving eq 2 for $\delta^{26}Mg_{free}$ by assuming that $\varepsilon_{ATP\text{-}free}$ = 2‰ (Pokharel et al., 2017) and using the respective compartment's mass fractions (Table 2) a $\delta^{26}Mg_{free}$ value of -2.64‰ is obtained. From this value and $\varepsilon_{ATP\text{-}free}$ of 2‰, $\delta^{26}Mg_{ATP}$ and $\varepsilon_{chlo\text{-}free}$ of -0.64‰ and 4.5‰, respectively, can be calculated. The value for $\varepsilon_{chlo\text{-}free}$ is within the range of the value calculated by Moynier and Fujii (2017) and Black et al. (2007) using *ab initio* models. To satisfy the conditions that (i) the bulk *N. punctiforme* cell has a composition of -0.27‰ and (ii) the measured $\delta^{26}Mg_{chlo}$ to be 1.85‰, our calculation requires

that $\varepsilon_{chlo\text{-}free}$ be nearly double that of $\varepsilon_{ATP\text{-}free}$. The various intracellular Mg compartments of *N. punctiforme cells* and their respective Mg isotopic compositions resulting from these considerations are summarized in Table 2.

Table 2: Intracellular Mg compartments with their size and respective Mg isotopic compositions.

Compartment Name	Mass Fraction	Isotope Composition ($\delta^{26}Mg$)
Free Mg	0.05[a]	$\delta^{26}Mg_{free}$[d]
Chlorophyll	0.19[b]	($\delta^{26}Mg_{free} + \varepsilon_{chlo\text{-}free}$[e]) = 1.85 ± 0.14 (2SD)
ATP	0.76[c]	($\delta^{26}Mg_{free} + \varepsilon_{ATP\text{-}free}$[f])

[a]Mass Fraction of free Mg in the cell, assuming that the fraction of bonded (chlorophyll- and ATP-bound) Mg is 0.95.
[b]Chlorophyll-bound Mg fraction; i.e. 20% of bonded Mg (20% of 0.95).(Marschner, 1995; Utkilen, 1982)
[c]Fraction of non-chlorophyll bonded Mg compartment (ATP, and ribosomes) (80% of 0.95).
[d]Mg isotopic composition of intracellular free Mg^{2+}.
[e]Mg isotope fractionation factor between chlorophyll and free Mg in ‰.
[f]Mg isotope fractionation factor between ATP and free Mg, i.e. $\varepsilon_{ATP\text{-}free}$ = 2‰, similar to the assumption made by Pokharel et al. (2017).

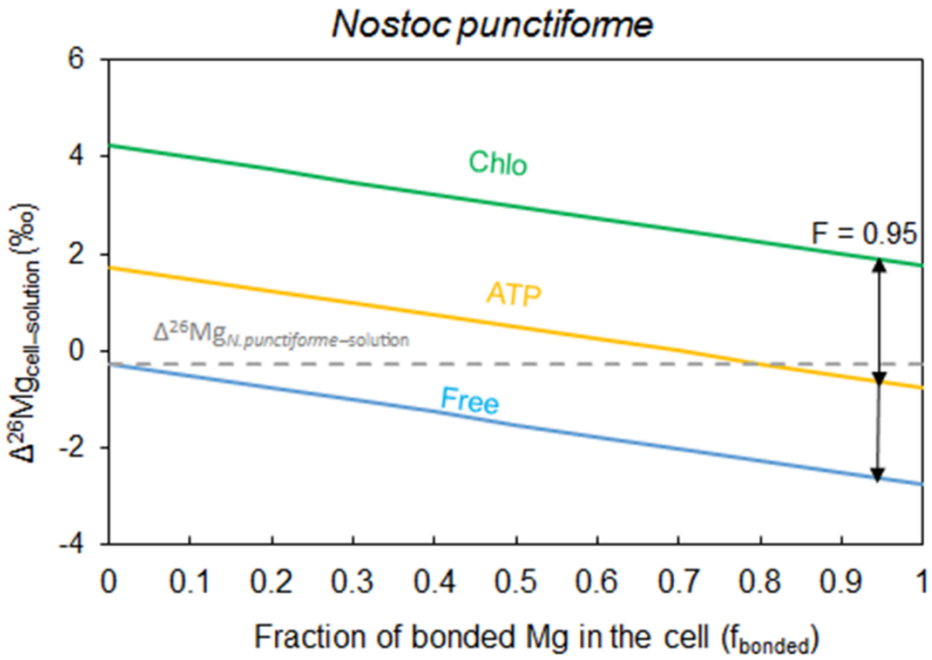

Figure 2: Isotope exchange diagram for cyanobacterium *N. punctiforme* of which the measured bulk cell δ^{26}Mg is -0.27‰ relative to the growth solution (grey dashed line). The solid, blue, orange, and green lines represent Mg isotope values of free-, ATP/ribosome-, and chlorophyll- bonded Mg, respectively (expressed relative to the initial growth solution as $\Delta^{26}Mg_{cell\text{-}solution}$). Here $\varepsilon_{chlo\text{-}free}$ is 4.5‰, and $\varepsilon_{ATP\text{-}free}$ is 2‰. The black dashed arrows indicate the resulting Mg isotope values of free, ATP/ribosome-bound, and chlorophyll-bound Mg if the mass fraction of bonded Mg is 0.95 (5% free Mg and 95% bonded Mg in cells).

We display the relationships among the δ^{26}Mg values of the three Mg compartments that emerge from eq. (2) in a closed-reactor type isotope exchange diagram in which the measured bulk cell δ^{26}Mg is -0.27‰ lower than the growth solution (Figure 2). While this model explains the measured isotope partitioning between the compartments given assumed mass fractions (Table 2), it does not explain the overall lower δ^{26}Mg of *N. punctiforme*. This low isotope ratio can potentially result from either a) a net negative fractionation during uptake (i.e. discriminating against ^{26}Mg) during Mg desolvation of hydrated $Mg^{2+}_{(aq)}$ prior to or during transport across the protein channel; or b) a positive fractionation associated with the efflux of Mg from the cell through the membrane transporter, leaving the residual cellular Mg pool with lower δ^{26}Mg. Ra et al. (2010) indicated that the Mg isotope composition of a coccolithophore cell may be influenced by a preferential supply of light Mg isotopes during cellular uptake due to a kinetic isotope effect and leakage of heavy Mg isotopes across the membrane. For Ca, the discrimination against the heavier isotopes during desolvation and transport through the protein channels has already been identified (Gussone et al., 2003; Gussone et al., 2006; Mejía et al., 2018). To our knowledge, no work on Mg isotope fractionation in membrane transporters has

been done. However, Mg equilibrium isotope fractionation factors between various aqueous Mg species have been determined by Schott et al. (2016) using *ab-initio* calculations. Within the context of magnesite precipitation experiments they predict the $\delta^{26}Mg$ of solvated Mg to be 0.3 to 0.7‰ higher in $\delta^{26}Mg$ than desolvated Mg^{2+} - which is compatible with explanation a) above: isotope fractionation towards lower $\delta^{26}Mg$ before membrane transport into the cell.

3.3.3 Predicting cell $\delta^{26}Mg$ with a flux model

In contrast to the model developed here for *N. punctiforme*, the substantial enrichment of heavy ^{26}Mg observed by Pokharel et al. (2017) in the fungus *Knufia petricola* was interpreted to be due to efflux of free cytosolic Mg low in $\delta^{26}Mg$ after bonding of heavy Mg into ATP. To explore possible mechanisms by which bulk cells obtain $\delta^{26}Mg$ that can be either higher or lower than that of the growth solution, Pokharel et al. (2017) proposed an equation that relates the net isotope fractionation to the relative mass fluxes of Mg into and out of a fungal cell. Their derivation was based on fluxes of Mg in and out of the cell, and is strictly valid only for a cell growing at a constant rate with a constant ratio of bonded and free Mg compartments. The net Mg isotopic difference between bulk cell and growth solution was defined as a function of cellular Mg fluxes:

$$\Delta^{26}Mg_{\text{bulk cell-solution}} = \varepsilon_{\text{bonded–free}} [f_{\text{bonded}} - (R_{\text{bonded}} / R_{\text{in}})] \qquad (3)$$

where R_{in} is the input rate of Mg into the cell [moles sec^{-1}], R_{bonded} is the net bonding rate of Mg into intracellular Mg bonding organic compounds [moles sec^{-1}]; $\varepsilon_{\text{bonded-free}} = \delta^{26}Mg_{\text{ribo+ATP+chlo}} - \delta^{26}Mg_{\text{free}}$ is the lumped isotope fractionation between free Mg^{2+} and Mg bonded (ATP, ribosomes, chlorophyll) and f_{bonded} is the fraction of total cell Mg present in a bonded form compartment in the cell (i.e. $M_{\text{ribo+chlo+ATP}}/M_{\text{cell}}$).

By replacing $R_{bonded} = R_{in} - R_{out} - R_{free}$ (Pokharel et al., 2017), where R_{out} is the rate of Mg efflux from the cell and R_{free} is the rate of Mg transferred into the free cytosolic compartment [moles sec^{-1}] in eq 3, we obtain

$$\Delta^{26}Mg_{\text{cell–solution}} = \varepsilon_{\text{bonded–free}} [f_{\text{bonded}} - (R_{\text{in}} - R_{\text{out}} - R_{\text{free}})/R_{\text{in}}] \qquad (4)$$

$$\Delta^{26}Mg_{\text{cell–solution}} = \varepsilon_{\text{bonded–free}} [f_{\text{bonded}} - [1 - (R_{\text{out}}/R_{\text{in}}) - (R_{\text{free}} / R_{\text{in}})] \qquad (5)$$

Since, R_{free}/R_{in} gives a very small number ($R_{in} >> R_{free}$; see Supporting Information for detailed information) the R_{free} / R_{in} term can be neglected and we obtain an expression relating $\Delta^{26}Mg_{\text{cell–solution}}$ to R_{out},

$$\Delta^{26}Mg_{cell-solution} = \varepsilon_{bonded-free}\,[f_{bonded} - [1 - (R_{out}/R_{in})] \quad (6)$$

The complete derivation of this expression is given in the Supporting Information. Equations 3 and 6 suggest that the isotopic composition of cells is governed by f_{bonded} and R_{bonded}/R_{in} (or alternatively R_{out}/R_{in}), assuming that the fractionation between bonded and cytosolic free Mg is constant. It is well established that intracellular mechanisms tightly regulate the partitioning between free and bonded Mg, and that the bonded Mg is the dominant Mg pool in cells (Alatossava et al., 1985; Gardner, 2003; Moncany and Kellenberger, 1981). Past investigations on bacterial and yeast cells show that the Mg compartment sizes in these species have a restricted range of f_{bonded} values, ranging from about 0.95 to 0.997 under normal growth conditions (Alatossava et al., 1985; Beeler et al., 1997; Nierhaus, 2014). From equation 3, we can deduce that when R_{bonded}/R_{in} is less than f_{bonded}, $\Delta^{26}Mg_{bulkcell-solution}$ is positive. The process by which this comes about is thought to be light Mg in the cell being continuously replaced by unfractionated Mg from fresh intake of bulk growth solution that is isotopically identical to the initial growth solution ($\Delta^{26}Mg$ = 0‰). The cell can be thus considered to be an open reactor with continuous exchange of Mg. Figure 3 shows the resulting isotopic composition for *K. petricola* cells in which Mg is heavier than the growth solution.

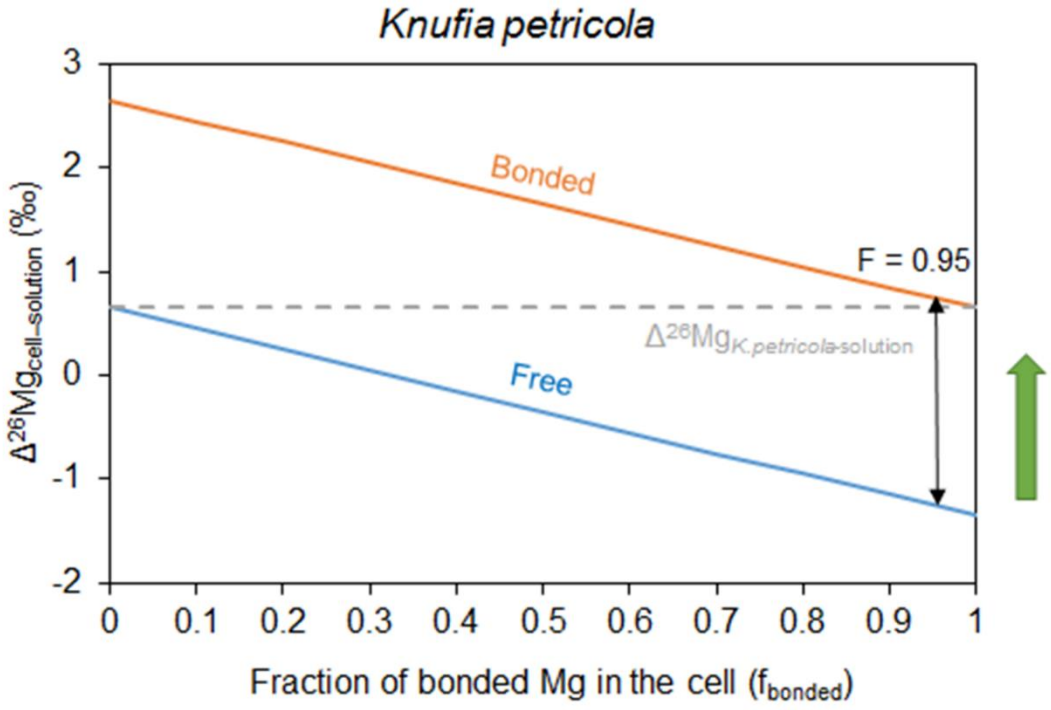

Figure 3: Isotope exchange diagram for fungus *K. petricola* in which bonded and free Mg exchange at chemical and isotopic equilibrium. The solid blue line represents the Mg isotope values of free Mg, the solid orange line that of bonded Mg (expressed relative to the initial growth solutions as $\Delta^{26}Mg_{cell\text{-}solution}$).. A fractionation factor $\varepsilon_{bonded\text{-}free}$ of 2‰ is assumed between free and bonded. The grey dashed line is the measured isotope fractionation between bulk *K. petricola* cell and the initial growth solution measured by Pokharel et al. (2017) ($\Delta^{26}Mg_{k.petricola\text{-}solution}$ = 0.65‰). The green arrow shows the direction of the Mg isotopic shift of free Mg that is continuously being replaced by unfractionated Mg from fresh intake of bulk growth solution that is isotopically identical to the initial growth solution ($\Delta^{26}Mg$ = 0‰). Black arrow shows the resulting isotopic composition of free and bonded Mg, respectively, at a fraction of bonded Mg of 0.95.

We can secondly predict from equation 3 that when R_{bonded}/R_{in} is greater than f_{bonded} then $\Delta^{26}Mg_{bulkcell-solution}$ obtains a value close to zero or slightly lower than the growth solution. In this system Mg enters the cell and is partitioned into 95% of bonded heavy Mg and 5% of free light Mg, but with minimal efflux of light free Mg, unlike in the open system case of *K. petricola* where the efflux is high. We thus speculate the *N. punctiforme* cell behaves as an almost closed system where R_{out} is minimal. Thus although the Mg-bonding organic compounds contain 95% of the cellular Mg in the *N. punctiforme* and the Mg extracted from the chlorophyll molecule had a distinctly higher $\delta^{26}Mg$ value than the growth solution, the bulk cell is close to zero or slightly lower. In this regard it is important to note that *N. punctiforme* incorporated 10 times more Mg (3004 µg/g of dry cell) than the *K. petricola* cell. Attaining large intracellular Mg inventories is consistent with all Mg entering into the cell being utilized to make Mg-bonded compounds and no significant efflux of Mg from the cell. Isotope mass balance requires that if

there is no efflux of isotopically fractionated Mg the cell must take on the isotopic composition of the growth solution, plus any fractionation associated with influx. The slight negative value of -0.27‰ measured in *N. punctiforme* might be due to fractionation prior to Mg entering the cytoplasm. As mentioned above, lighter isotopes may be preferred during interaction of different Mg species in solution, desolvation, or transfer across the protein channel, for example. If present, a slight preference towards uptake of lighter Mg isotopes was not detectable in the *K. petricola* cell as it behaved more like open system containing a dominant compartment being isotopically heavy in Mg.

To summarize, *K. petricola* cells behave as an open system with low R_{bonded} and small intracellular Mg inventories that result in high R_{out} and a high $\Delta^{26}Mg_{bulkcell-solution}$ value. Conversely, *N. punctiforme* cells behave as a closed system with high R_{bonded} and large intracellular Mg quotas due to low R_{out}, resulting in $\Delta^{26}Mg_{bulkcell-solution}$ values close to zero. Figure 4 shows the dependence of $\Delta^{26}Mg_{bulkcell-solution}$ (for both *K. petricola* and *N. punctiforme*) on R_{bonded}/R_{in} within the possible range of f_{bonded} values from 0.95 to 0.997. It can be seen from figure 4 that for the measured Mg isotope composition of *K. petricola*, R_{bonded}/R_{in} is close to 0.7, assuming a $\varepsilon_{bonded-free}$ value of 2.5‰. However, the measured value of *N. punctiforme* is beyond the lower boundary limit of $\Delta^{26}Mg_{bulkcell-solution}$ values calculated using equation 3, further supporting our speculation of Mg isotope fractionation during Mg entering or leaving the cytoplasm of *N. punctiforme.*

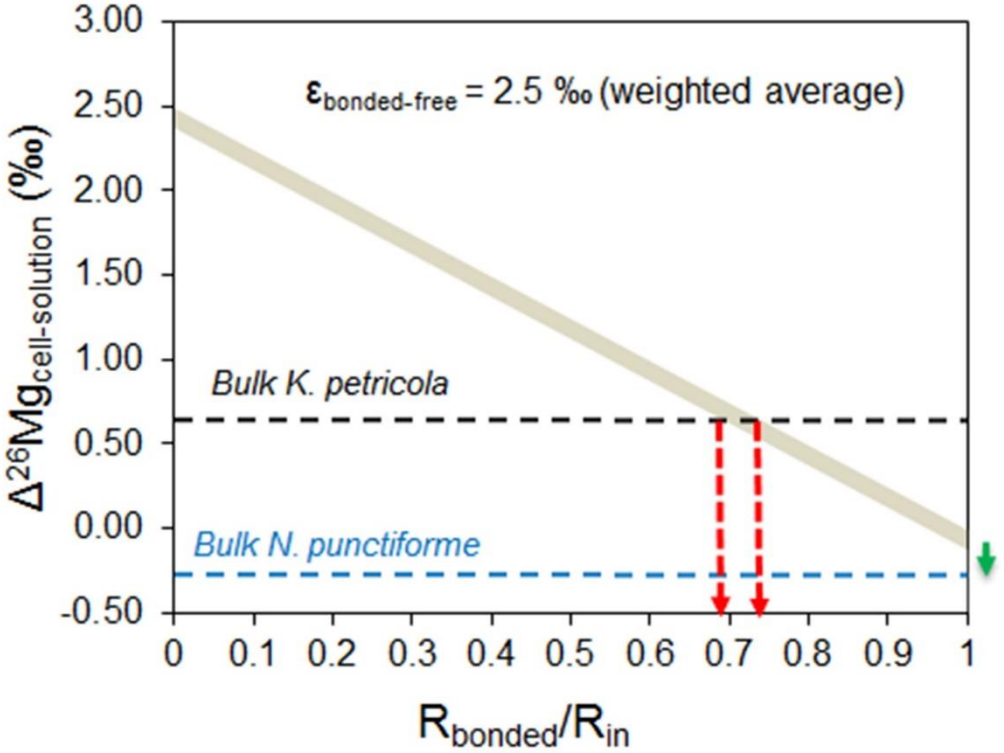

Figure 4: Dependence of $\Delta^{26}Mg_{cell–solution}$ on R_{bonded}/R_{in} following eq (3). The area under the oblique grey line shows this dependence for f_{bonded} values of 0.95 to 0.997, the range typically observed in fungal and cyanobacterial cells. $\varepsilon_{bonded\text{-}free}$ of 2.5‰ was derived by weighing individual fractionation factors ($\varepsilon_{bonded\text{-}free}$) by their respective Mg mass fractions: 20% chlorophyll with $\varepsilon_{chlo\text{-}free}$ of 4.5‰ and 80% ATP with $\varepsilon_{ATP\text{-}free}$ of 2‰. The blue dashed line represents the measured isotopic composition of bulk *N. punctiforme* cell with respect to the growth solution ($\Delta^{26}Mg_{N.punctiforme\text{-}solution}$ = -0.27‰), and the black dashed line that of *K. petricola*, respectively ($\Delta^{26}Mg_{K.petricola\text{-}solution}$ =0.65‰) measured in this study and by Pokharel et al. (2017). The red arrows denote the range of R_{bonded}/R_{in} values derived from the intersection of the measured $\Delta^{26}Mg_{K.petricola\text{-}solution}$ with the grey model line. The measured value of $\Delta^{26}Mg_{N.punctiforme\text{-}solution}$ does not intersect with the oblique grey lines indicating a very high R_{bonded}/R_{in} and minor Mg isotope fractionation during Mg entering or leaving the cytoplasm of *N. punctiforme*, respectively (denoted by a green arrow).

3.3.4 Mg cycling in higher plants

Both laboratory and field experiments have shown that bulk higher plants are enriched in the heavier Mg isotopes over the source from which they obtain their Mg (Black et al., 2008; Bolou-Bi et al., 2010; Bolou-Bi et al., 2012; Mavromatis et al., 2014; Opfergelt et al., 2014; Tipper et al., 2010; Uhlig et al., 2017). Further, the Mg isotope composition of different parts of higher plants shifts due to Mg isotope fractionation during Mg translocation within the plants (Black et al., 2008; Bolou-Bi et al., 2010). Studies by Bolou-Bi et al. (2010) and Bolou-Bi et al. (2012) show that the leaves of plants typically obtain high Mg concentrations and are enriched in the lighter Mg isotopes relative to their roots that have lower Mg concentrations and are enriched in the heavier Mg isotopes. In order to assess whether a relationship between concentration and

Mg isotope composition is universal we compiled all Mg isotope available data on compartments of higher plants (roots, leaves and needles) in addition to fungi, and cyanobacteria (this study), and their Mg sources, measured in both laboratory and field experiments (Figure 5 and Table S2). We excluded Mg isotope data on wood because wood serves as a pathway of Mg from roots to leaves and also as a store of Mg that was resorbed from leaves, for example during autumnal senescence (Bolou-Bi et al., 2010; Kimmig et al., 2018). Given that translocation and precipitation for storage may entail additional isotope fractionation, Mg from wood likely does not reflect the isotope compositions of the cellular processes we explore here. In Figure 5 an inverse relationship between Mg concentration and the Mg isotope composition becomes apparent from both laboratory growth experiments and ecosystem samples. The scatter in the relationship partially reflects discrepancies in identifying the exact composition of the Mg source of species sampled in natural ecosystems. Both laboratory and field data show that low Mg concentrations amounts to high $\Delta^{26}Mg_{species-source}$ values, whereas at high Mg concentrations, $\Delta^{26}Mg_{species-source}$ tends to be closer to zero. This relationship also holds for what we observed for *K. petricola* and *N. punctiforme* cells. With this relationship we can now explain the observation of Fahad et al. (2016), namely that non-mycorrhizal fungi with low Mg concentration features high positive $\Delta^{26}Mg_{species-source}$ values whereas a mycorrhizal fungi with high Mg concentration yields $\Delta^{26}Mg_{species-source}$ close to zero or even slightly negative. In terms of our mass balance model, high Mg concentrations and low $\delta^{26}Mg$ correspond to low R_{out}/R_{in} or high R_{bonded}/R_{in}.

The Mg metabolic pathway that governs the isotopic composition of *K. petricola* and *N. punctiforme* cells, respectively, may thus serve as a model for roots and leaves of higher plants. Within the framework suggested by Pokharel et al. (2017) we suggest that Mg enters the root cell, possibly with a minor isotope fractionation favoring the lighter Mg isotopes during desolvation or in transport channels, that heavy Mg isotopes are incorporated into the 95% of Mg contained in the root cells' bonded compounds (as seen for *K. petricola*), and that the effluxed free Mg thus depleted in heavy Mg isotopes is preferentially transported through the xylem into the leaves. There it becomes further fractionated with preference of light Mg isotopes during desolvation or transport across the protein channel of the leaf cells similar to the fractionation observed in *N. punctiforme* cells. Inside the leaf cells, most of the Mg is partitioned into Mg-ATP, ribosomes and the chlorophyll molecule and thus due to the high requirements of Mg by these bonding compounds there is little efflux of light free Mg^{2+} from the leaf. During growth the leaf thus behaves as a closed system and is thus depleted in ^{26}Mg compared to the roots. This model can explain why the root cells exhibit elevated $\delta^{26}Mg$, while

leaf cells show low δ^{26}Mg. During autumnal senescence some of the Mg present in the leaves is withdrawn into the plants and remobilized during growth seasons, whereas the remaining is returned to the soil as plant litter fall (Kimmig et al., 2018; Proe et al., 2000; Uhlig et al., 2017). We speculate that both the fraction of Mg withdrawn from the leaves during resorption and the fraction returned to soil as litter fall determine the Mg isotope composition of the bulk plants.

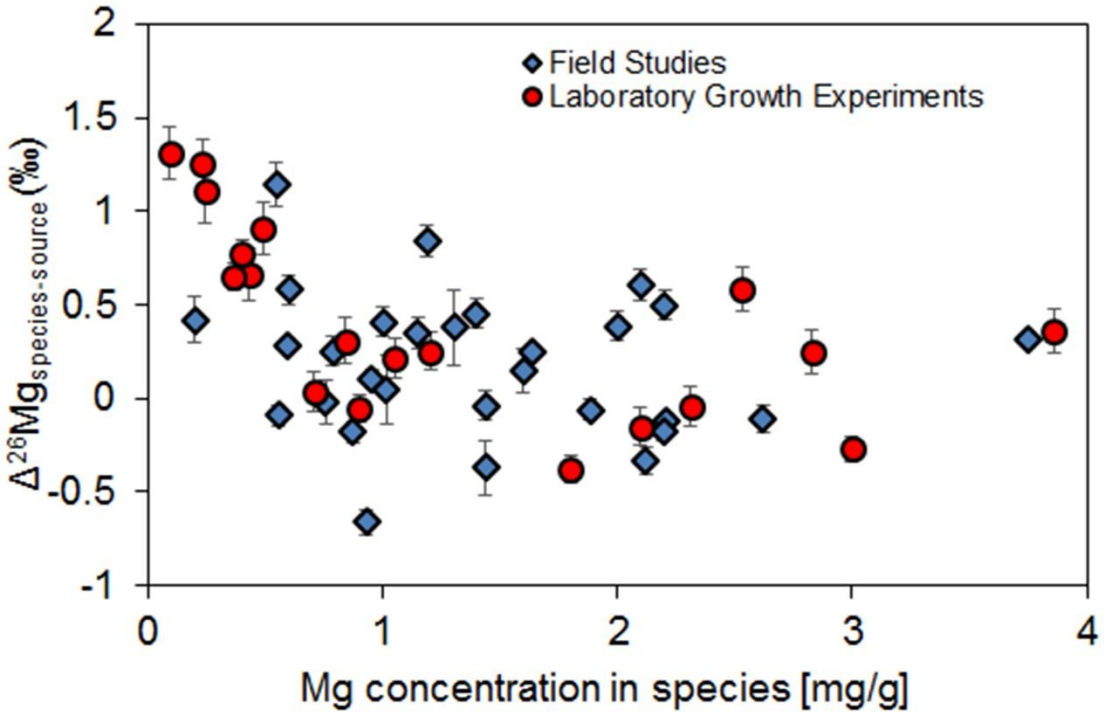

Figure 5: Compilation of Mg isotope composition relative to the Mg source ($\Delta^{26}Mg_{species-source}$) measured in fungal and cyanobacterium cells and the organs of plants with respect to the concentration of Mg in the species from both laboratory growth experiments (red circles) and field studies (blue diamonds). Data are compiled from Bolou-Bi et al. (2010): rye grass and clover (leaves, stem, and shoots); Bolou-Bi et al. (2012): Norway spruce and hair grass (needles, roots, and leaves); Black et al. (2008): wheat (root, leaves and shoot); Uhlig et al. (2017): ponderosa pine, jeffrey pine, manzanita, whitethorn (needles, root, and leaves); Opfergelt et al. (2014): grass; Kimmig et al. (2018): sugar maple (root, leaf); Mavromatis et al. (2014): sphagnum, shrub (leaves), lichen, larch (roots and needles); Fahad et al. (2016): mycorrhizal and non-mycorrhizal fungi; Schuessler et al. (2018): *Eurya japonica, Maesa indica, Neolitsea fuscata, Cestrum aurantiacum, Ixora calycina, Arundinaria debilis* (leaves); Pokharel et al. (2017): *Knufia petricola* and melanin-mutant; this study (*Nostoc punctiforme*). Mg isotope data from woody plant parts was not used as it may be affected by secondary isotope fractionation. Details on the data sources and Mg source compositions are provided in Table S2 in the Supporting Information.

3.4 Environmental Implications

Cyanobacteria are ubiquitous colonizers of natural rock surfaces and building stones. They acidify their environment by releasing organic acids or locally increase the pH by photosynthesis and hence could stimulate weathering of the substrates they inhabit. They take the nutrients released from minerals, use them for photosynthesis and transfer them to fungi

and higher plants through symbiotic relationships. Together with fungi they form lichens that cover about 8% of Earth's terrestrial surface (Chen et al., 2000). Given that large fluxes of mineral nutrients pass through this bacterial and fungal pool, methods that fingerprint the partitioning of nutrients through both species might deliver crucial information for nutrients cycling studies in ecosystems (Gadd, 2010; Landeweert et al., 2001). Mg stable isotope ratios serve to track these cycles. Knowing the fractionations factors and the environmental conditions that set them is an essential prerequisite to their application. We found a fractionation factor of -0.27‰ for uptake of Mg into *Nostoc punctiforme* when grown at circum-neutral conditions. In contrast, uptake of Mg into a black fungus as explored in a previous study involves a fractionation factor of +0.65 and +1.1‰, depending on pH (Pokharel et al., 2017). These results show that in general Mg stable isotope fractionation in ecosystems depend on species and on environmental conditions, including pH, that determine the fluxes of Mg into root cells or symbionts.

More broadly, we inferred that it is the rates of Mg bonding into intracellular compartments relative to the rate of Mg intake into and efflux from the cell that governs the Mg isotopic composition of cells, and here we present a mathematical expression that describes this relationship. A data compilation of Mg isotope fractionation in bacteria, fungi, lichens and higher plants suggests that this relationship holds for a broad range of species, given that Mg isotope fractionation factors are inversely proportional to cellular Mg concentrations. This study thus provides an internally consistent framework of Mg cycling through different types of cells and supplies an explanation for preferred intake of heavy Mg isotopes into plant organs low in Mg, and the apparent absence of isotope fractionation during intake into plant organs high in Mg. Clearly, there are still parameters, pathways and processes that need further attention. For example, the possibility of Mg isotope fractionation during cell influx or efflux, and intracellular fractionation occurring during Mg translocation and resorption mechanism are important next steps to explore.

3.5 Supporting Information

3.5.1 Chlorophyll Extraction, HPLC Separation

For chlorophyll extraction the pellet of *Nostoc punctiforme* cells was resuspended in 1 mL of ultrapure H_2O and chlorophyll and other pigments extracted three-times by 8 mL of methanol. The pooled methanol extracts were first mixed with 1 mL of 5 M NaCl in water and then with 20 mL of hexane. After mixing the solution was incubated for 15 min at room temperature and then centrifuged at 6000 rpm for 5 minutes. The upper hexane phase containing chlorophyll

and other non-polar compounds in the supernatant was taken. The hexane separation procedure was repeated three times. Then the collected hexane solution was evaporated in a vacuum concentrator (Eppendorf Concentrator Plus) at 30 ˚C for 20 minutes. The dried hexane phase was dissolved in 1 mL of methanol and the solution separated by Agilent-1200 HPLC. Separation was carried out isocratically with methanol at 1 mL/min on a reverse phase column (Luna C8, 5 μm, 250 x 10 mm; Phenomenex). The peak corresponding to chlorophyll *a* was collected and dried in a vacuum concentrator.

The isolated chlorophyll (~1 mg) and the initial growth media were dissolved in mixture of HNO_3, and H_2O_2 in screw-top PFA vials on a hotplate for 24 hours. This procedure was repeated multiple times until samples were completely dissolved. Mg purification was done with cation-exchange column chemistry and Mg isotope ratios determined by MC-ICP-MS. Similar procedures (pigment extraction in ethanol, HPLC separation and column chemistry prior to Mg isotope analysis) have been previously applied for Mg in the chlorophyll of phytoplankton (Ra and Kitagawa, 2007; Ra et al., 2010). This established method recover about 99% Mg from chlorophyll of biological species, thus indicating a complete transfer of Mg from one compartment to another during the procedure (Ra and Kitagawa, 2007).

3.5.2 Mass-dependence of Mg isotope analysis

Figure S1 shows that all analysed samples plot on the mass-dependent kinetic or equilibrium isotope fractionation line (the difference between both is unresolvable within analytical uncertainties associated with our data). This dependence shows that none of the three Mg isotopes (^{24}Mg, ^{25}Mg, ^{26}Mg) were affected by isobaric interferences or mass-independent isotope effects.

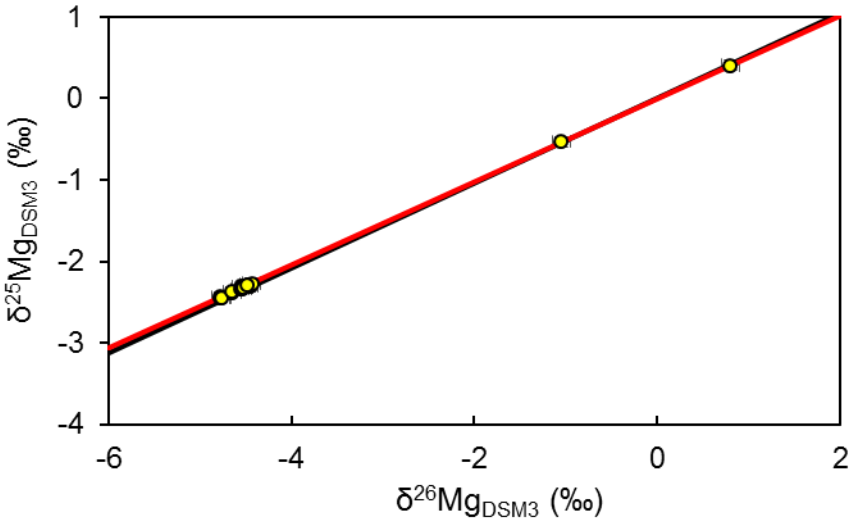

Figure S1: Three isotope plot of $\delta^{26}Mg_{DSM}$ vs $\delta^{25}Mg_{DSM}$ for all samples measured in this study. The solid red line represents the mass-dependent kinetic fractionation line (slope = 0.511) and the solid black line represents the mass-dependent equilibrium fractionation line (slope = 0.521). Error bars in the plot are based on repeated measurement of reference materials processed through the Mg column chemistry and are ±0.10‰ (2SD, $\delta^{26}Mg_{DSM3}$) and ±0.06‰ (2SD, $\delta^{25}Mg_{DSM3}$).

3.5.3 Derivation of cellular Mg flux model

Pokharel et al. (2017) introduced a formalism that relates the net isotope fractionation to the relative mass fluxes of Mg into and out of a cell. Here we expand this mass balance model into a general form that accounts for all cell types in which Mg follows similar metabolic pathways.

The model is based on the following assumptions:

1. The cell is growing at a constant rate.

2. Mg amounts in the bonded and free compartment are increasing with cell growth but at a constant ratio (f_{bonded} to f_{free} of 0.95:0.05) maintained by cellular homeostasis.

3. Bonded and free Mg^{2+} are in chemical and isotopic equilibrium.

4. Equilibrium isotope fractionation factor between bonded and free Mg^{2+} is constant over time.

5. The rate of Mg influx, efflux, bonded Mg formation, free Mg^{2+} formation are invariant with time.

6. There is no fractionation during influx to the cell membrane (although such fractionation factor can be easily added).

The cellular mass balance is given by:

$$\delta^{26}Mg_{cell} \bullet M_{cell} = \delta^{26}Mg_{free} \bullet M_{free} + \delta^{26}Mg_{bonded} \bullet M_{bonded} \quad \text{(eq. 1)},$$

where M_{cell} is the total amount of Mg in the cell [moles]; M_{free} is the amount of Mg^{2+}_{free} in the cell [moles]; M_{bonded} is the amount of Mg in strongly bonded intracellular compounds [moles]; $\delta^{26}Mg_{cell}$ is the Mg isotopic composition of the bulk cell [‰]; $\delta^{26}Mg_{free}$ is the Mg isotope composition of Mg^{2+}_{free} in the cell [‰]; $\delta^{26}Mg_{bonded}$ is the Mg isotopic composition of Mg_{bonded} [‰].

The rate of chance in Mg mass in a cell growing at a constant rate is given by:

$$\frac{dM_{cell}}{dt} = R_{in} - R_{out} = R_{bonded} + R_{free} \qquad \text{(eq. 2)}$$

where R_{in} is the input rate of Mg into the cell [moles sec^{-1}]; R_{bonded} is the bonding rate of Mg into Mg bonding compounds [moles sec^{-1}]; R_{out} is the rate of Mg efflux [moles sec^{-1}]; R_{free} is the rate of free Mg formation [moles sec^{-1}];

Thus,

$$R_{in} = R_{bonded} + R_{free} + R_{out} \qquad \text{(eq. 3)}$$

Introducing corresponding δ-values in eq. 3,

$$R_{in} \bullet \delta^{26}Mg_{solution} = R_{bonded} \bullet \delta^{26}Mg_{bonded} + R_{free} \bullet \delta^{26}Mg_{free} + R_{out} \bullet \delta^{26}Mg_{free} \quad \text{(eq. 4)}$$

where $\delta^{26}Mg_{solution}$ is the Mg isotopic composition of the influx of Mg [‰], here assumed to be unfractionated relative to the growth solution (although a fractionation factor for intake can be easily added).

$$R_{in} \bullet \delta^{26}Mg_{solution} = R_{bonded} \bullet (\delta^{26}Mg_{free} + \varepsilon_{bonded-free}) + R_{free} \bullet \delta^{26}Mg_{free} + R_{out} \bullet \delta^{26}Mg_{free} \quad \text{(eq. 5)}$$

where $\varepsilon_{bonded-free}$ is the constant equilibrium isotope fractionation between bonded and free Mg compounds.

Substituting $R_{out} = (R_{in} - R_{bonded} - R_{free})$ into eq. 5, we derive an equation for $\delta^{26}Mg_{free}$.

$$\delta^{26}Mg_{free} = \delta^{26}Mg_{solution} - (R_{bonded}/R_{in}) \bullet \varepsilon_{bonded-free} \qquad \text{(eq. 6)}$$

Substituting equation 6 to equation 1,

$$\Delta^{26}Mg_{cell-solution} = \varepsilon_{bonded-free}[f_{bonded} - (R_{bonded}/R_{in})] \qquad \text{(eq. 7)}$$

where $\Delta^{26}Mg_{cell-solution}$ is the measured isotopic difference between the bulk cell and growth solution and f_{bonded} is the fraction of Mg in the bonded intracellular compartment (M_{bonded}/M_{cell}).

Substituting $R_{bonded} = R_{in} - R_{out} - R_{free}$ in eq 7 we obtain

$$\Delta^{26}Mg_{cell-solution} = \varepsilon_{bonded-free}\,[f_{bonded} - (R_{in} - R_{out} - R_{free})/R_{in}] \qquad \text{(eq. 8)}$$

$$\Delta^{26}Mg_{cell-solution} = \varepsilon_{bonded-free}\,[f_{bonded} - [1 - (R_{out}/R_{in}) - (R_{free}/R_{in})] \qquad \text{(eq. 9)}$$

Since the fraction of Mg in the free compartment (M_{free}/M_{cell} or f_{free}) is only 0.05, the rate of formation of free Mg is very slow in comparison to the rate of Mg coming into the cell during uptake ($R_{in} >> R_{free}$). Thus, R_{free}/R_{in} is a very small number. We can neglect the right-hand term in eq. 9 to obtain a simplified expression relating $\Delta^{26}Mg_{cell-solution}$ with R_{out}.

$$\Delta^{26}Mg_{cell-solution} = \varepsilon_{bonded-free}\,[f_{bonded} - [1 - (R_{out}/R_{in})] \qquad \text{(eq.10)}$$

We can further derive $\Delta^{26}Mg_{cell-solution}$ in terms of f_{free} as given below

$$\Delta^{26}Mg_{cell-solution} = \varepsilon_{bonded-free}\,[(R_{out}/R_{in}) - f_{free}] \qquad \text{(eq. 11)}$$

Table S1: Composition[a] of modified BG-11 media as growth solution

Species	Concentration (mM)
NaEDTA	0.0027
NH_4Fe citrate	0.0229
Citrate*H_2O	0.0204
$CaCl_2$*$2H_2O$	0.2449
$MgSO_4$*$7H_2O$	0.15
K_2HPO_4*$3H_2O$	0.1753
H_3BO_3	0.0463
$MnCl_2$*$4H_2O$	0.0058
$ZnSO_4$*$7H_2O$	0.0008
$CuSO_4$*$5H_2O$	0.0003
$CoCl_2$*$6H_2O$	0.0002
$NaMoO_4$*H_2O	0.0019

[a]The BG 11 media were diluted to 1 L with MilliQ water. Then 0.75 g of $NaNO_3$ (8.82 mM), 0.75 g of NH_4NO_3 (9.37 mM) and 0.02 g of Na_2CO_3 (0.189 mM) was added. The pH of the solution was adjusted to 6 and then autoclaved. After autoclaving, 2000 mg filtered, sterilized glucose*H_2O (11.22 mM) was added. Finally, 10662 mg filter sterilized MES*H_2O (54.62 mM) was added as a pH buffer. This data in this table is from Pokharel et al. (2017).

Table S2: Compilation of available Mg concentration and isotope ratios in plants and growth experiments

Article	Condition	Species	Compartment	Mg concentration (mg/g)	Compartment $\delta^{26}Mg_{DSM3}$ (‰)	Source	Source $\delta^{26}Mg_{DSM3}$ (‰)	$\Delta^{26}Mg_{compartment-source}$[a] (‰)	SD[b]
Bolou-Bi et al. (2010)	Laboratory	Rye grass	Shoot	0.43	-0.56	mineral	-1.22	0.66	0.14
		Rye grass	Root	0.09	0.09	mineral	-1.22	1.31	0.14
		Clover	Leaf	0.49	-0.31	mineral	-1.22	0.91	0.14
		Clover	Root	0.23	0.03	mineral	-1.22	1.25	0.14
		Rye grass	Shoot	2.83	-0.72	Growth solution	-0.97	0.25	0.12
		Rye grass	Root	0.84	-0.66	Growth solution	-0.97	0.31	0.12
		Clover	Leaf	3.86	-0.61	Growth solution	-0.97	0.36	0.12
		Clover	Root	2.53	-0.39	Growth solution	-0.97	0.58	0.12
Bolou-Bi et al. (2012)	Field	Norway spruce	Needle (avg)	0.76	-0.66	Exchangeable soil solution (avg)	-0.64	-0.02	0.12
		Norway spruce	Roots (avg)	0.55	0.51	Exchangeable soil solution (avg)	-0.64	1.15	0.12
		Norway spruce	Leaf	1.60	-0.49	Exchangeable soil solution (avg)	-0.64	0.15	0.12
		Norway spruce	Roots	0.20	-0.22	Exchangeable soil solution (avg)	-0.64	0.42	0.12
Black et al. (2008)	Laboratory	Wheat	Root	2.31	-0.15	Growth solution	-0.11	-0.04	0.11
			Leaf	1.05	0.11	Growth solution	-0.11	0.22	0.11
			Shoot	0.71	-0.07	Growth solution	-0.11	0.04	0.11
Uhlig et al. (2017)	Field	Panderosa pine	Needle	1.44	-0.72	Exchangeable soil solution	-0.68	-0.04	0.08
		Jeffrey pine	Needle	0.79	-0.43	Exchangeable soil solution	-0.68	0.25	0.08

		Manzanita	Leaf	0.60	-0.33	Exchangeable soil solution	-0.68	0.35	0.08
		Manzanita	Root	1.19	0.01	Exchangeable soil solution	-0.68	0.69	0.08
		Whitehorn	Leaf	1.15	-0.10	Exchangeable soil solution	-0.68	0.58	0.08
Opfergelt et al. (2014)	Field	HA-grass	Bulk	2.10	-0.18	Exchangeable soil solution (avg)	-0.79	0.61	0.08
		H-grass	Bulk	2.00	-0.28	Exchangeable soil solution (avg)	-0.67	0.385	0.08
		BA-grass	Bulk	1.40	-0.18	Exchangeable soil solution (avg)	-0.64	0.455	0.07
		GA-grass	Bulk	2.20	-0.25	Exchangeable soil solution (avg)	-0.75	0.5	0.07
		V-grass	Bulk	1.00	-0.50	Exchangeable soil solution (avg)	-0.91	0.41	0.08
Kimming et al. (2018)	Field	Sugar Maple	Root-Autumn	1.02	-0.60	Soil solution (avg)	-0.65	0.05	0.19
			Leaf-Autumn	1.44	-1.02	Soil solution (avg)	-0.65	-0.37	0.15
			Leaf-Spring	1.30	-0.27	Soil solution (avg)	-0.65	0.38	0.20
Mavromatis et al. (2014)	Field	Spagnum (live)green	Bulk	0.87	-0.57	Avg-Soil Solution-North facing slope	-0.39	-0.18	0.06
		Spagnum (live)green	Bulk	0.95	-0.49	Avg-Soil Solution-South facing slope	-0.60	0.11	0.05
		Larix gmelinii/	Root	0.60	-0.31	Avg-Soil Solution-South facing slope	-0.60	0.29	0.03

		Larix gmelinii	Needle	2.21	-0.51	Avg-Soil Solution-North facing slope	-0.39	-0.12	0.04
		Larix gmelinii	Needle	1.88	-0.45	Avg-Soil Solution-North facing slope	-0.39	-0.06	0.05
		Larix gmelinii	Needle	3.75	-0.28	Avg-Soil Solution-South facing slope	-0.60	0.32	0.03
		Larix gmelinii	Needle	1.64	-0.35	Avg-Soil Solution-Southside	-0.60	0.25	0.02
		Dwarf Shrub (*V. uliginosum*)	Leaf	2.20	-0.57	Avg-Soil Solution-North facing slope	-0.39	-0.18	0.05
		Lichen (*Cladonia stellaris*)	Bulk	0.55	-0.48	Avg-Soil Solution-North facing slope	-0.39	-0.09	0.06
Fahad et al. (2016)	Laboratory	Mycorrhizal (avg)	Bulk	1.80		Mineral		-0.38	0.075
		Non-mycorrhizal (avg)	Bulk	0.90		Mineral		-0.05	0.075
	Laboratory	Mycorrhizal (avg)	Bulk	2.10		Growth solution		-0.15	0.1
		Non-mycorrhizal (avg)	Bulk	1.20		Growth solution		0.25	0.1
Pokharel et al. (2017)	Laboratory	*Knufia petricola*	Bulk	0.37	-3.85	Growth solution	-4.5	0.65	0.07
	Laboratory	*Knufia petricola*	Bulk	0.25	-3.34	Growth solution	-4.45	1.11	0.175
	Laboratory	melanin-mutant	Bulk	0.40	-3.72	Growth solution	-4.5	0.78	0.07
Schuessler et al. (2018)	Field	*Eurya japonica*	Leaf	4.22	-1.04	soil solution (avg)	-0.70	-0.34	0.09

		Maesa indica	Leaf	2.12	-1.03	soil solution (avg)	-0.70	-0.33	0.09
		Neolitsea fuscata	Leaf	6.27	-1.06	soil solution (avg)	-0.70	-0.36	0.09
		Cestrum aurantiacum	Leaf	6.39	-0.79	soil solution (avg)	-0.70	-0.09	0.09
		Ixora calycina	Leaf	0.93	-1.36	soil solution (avg)	-0.70	-0.66	0.09
		Arundinaria debilis	Leaf	2.62	-0.81	soil solution (avg)	-0.70	-0.11	0.09
This study	Laboratory	*Nostoc punctiforme*	Bulk	3.00	-4.77	Growth solution	-4.5	-0.27	0.07

Compilation of Mg concentrations and isotope compositions measured for various plants and their compartments (root, leaf, and needles), fungal and cyanobacterium species for both experimental and field studies (Black et al., 2008; Bolou-Bi et al., 2010; Bolou-Bi et al., 2012; Fahad et al., 2016; Kimmig et al., 2018; Mavromatis et al., 2014; Opfergelt et al., 2014; Pokharel et al., 2017; Schuessler et al., 2018; Uhlig et al., 2017). Available wood data was not plotted because wood is a pathway of Mg from roots to leaves and is also a storage of Mg from the leaves for example during autumnal senescence, and therefore does not yield the isotopic endmember compositions of the cellular processes we postulate.

[a] $\Delta^{26}Mg_{compartment\ –\ source}$ represents the isotopic difference between the $\delta^{26}Mg$ value of the respective biological compartment and the $\delta^{26}Mg$ value of the source.

[b] SD represents the uncertainty in $\Delta^{26}Mg_{compartment\text{-}source}$ derived from error propagation of the standard deviations provided in the corresponding literature.

Table S3: Concentration and Mg isotope measurements of biomass and growth solution

			Growth solution							Bulk cell *N. punctiforme*		Isotopic difference (*N. punctiforme* – solution)
Experiment	**Replicate experiment number**	**Time (Days)**	**pH**	**Mg[c] (mM)**	**Fe[c] (mM)**	**K[c] (mM)**	**P[c] (mM)**	**$\delta^{25}Mg_{DSM3}$ (‰)**	**$\delta^{26}Mg_{DSM3}$ (‰)**	**$\delta^{25}Mg_{DSM3}$ (‰)**	**$\delta^{26}Mg_{DSM3}$ (‰)**	**$\Delta^{26}Mg_{cell-solution}$[d] (‰)**
Abiotic Experiment	Initial BG-11 growth solution	0	5.86	0.149	0.017	0.397	0.169	-2.31 ± 0.06[a]	-4.50 ± 0.10[a]			
	Exp 1	0.08	5.89	0.150	0.018	0.401	0.170	-2.31 ± 0.06[a]	-4.46 ± 0.10[a]			
	Exp 2	0.08	5.86	0.149	0.018	0.401	0.171	-2.31 ± 0.06[a]	-4.54 ± 0.10[a]			
	Exp 3	0.08	5.85	0.149	0.018	0.396	0.172					
	Mean		**5.87**	**0.149**	**0.018**	**0.399**	**0.171**	**-2.31**	**-4.50**			
	2SD[b]		**0.04**	**0.001**	**0**	**0.006**	**0.002**	**0**	**0.10**			
	Exp 1	3	5.90	0.149	0.004	0.398	0.160					
	Exp 2	3	5.87	0.149	0.003	0.400	0.160					
	Exp 3	3	5.85	0.149	0.004	0.395	0.163					
	Mean		**5.87**	**0.149**	**0.004**	**0.398**	**0.161**					
	2SD[b]		**0.06**	**0.000**	**0**	**0.006**	**0.004**					
	Exp 1	5	5.90	0.150	0.002	0.403	0.160					
	Exp 2	5	5.87	0.150	0.003	0.404	0.160	-2.31 ± 0.06[a]	-4.54 ± 0.10[a]			
	Exp 3	5	5.86	0.149	0.003	0.398	0.161					
	Mean		**5.88**	**0.150**	**0.003**	**0.402**	**0.160**					
	2SD[b]		**0.04**	**0.002**	**0**	**0.006**	**0.002**					
	Exp 1	7	5.90	0.149	0.002	0.396	0.157					
	Exp 2	7	5.87	0.150	0.002	0.401	0.160					
	Exp 3	7	5.86	0.150	0.002	0.398	0.161					
	Mean		**5.88**	**0.149**	**0.002**	**0.398**	**0.159**					
	2SD[b]		**0.04**	**0.001**	**0**	**0.007**	**0.003**					
	Exp 1	10	5.86	0.150	0.001	0.399	0.158	-2.38 ± 0.06[a]	-4.65 ± 0.10[a]			
	Exp 2	10	5.83	0.151	0.002	0.403	0.160	-2.31 ± 0.06[a]	-4.51 ± 0.10[a]			
	Exp 3	10	5.81	0.149	0.002	0.396	0.160					

		Mean		**5.83**	**0.150**	**0.002**	**0.399**	**0.159**	**-2.35**	**-4.58**		
		2SD[b]		**0.05**	**0.001**	**0**	**0.007**	**0.003**	**0.1**	**0.20**		
Biotic Experiment	Exp 1		0.08	5.82	0.150	0.018	0.399	0.171	-2.37 ± 0.06[a]	-4.65 ± 0.10[a]		
	Exp 2		0.08	5.83	0.150	0.017	0.398	0.172	-2.33 ± 0.06[a]	-4.54 ± 0.10[a]		
	Exp 3		0.08	5.83	0.148	0.018	0.390	0.171				
		Mean		**5.83**	**0.149**	**0.017**	**0.396**	**0.171**				
		2SD[b]		**0.01**	**0.002**	**0.001**	**0.010**	**0.001**				
	Exp 1		3	5.82	0.146	0.003	0.390	0.149				
	Exp 2		3	5.83	0.146	0.002	0.390	0.151				
	Exp 3		3	5.83	0.145	0.003	0.384	0.150				
		Mean		**5.83**	**0.146**	**0.003**	**0.388**	**0.150**				
		2SD[b]		**0.01**	**0.002**	**0.000**	**0.007**	**0.002**				
	Exp 1		5	5.81	0.139	0.002	0.376	0.132	-2.34 ± 0.06[a]	-4.56 ± 0.10[a]		
	Exp 2		5	5.82	0.142	0.001	0.382	0.142	-2.32 ± 0.06[a]	-4.52 ± 0.10[a]		
	Exp 3		5	5.82	0.141	0.002	0.378	0.141				
		Mean		**5.82**	**0.141**	**0.002**	**0.379**	**0.138**				
		2SD[b]		**0.01**	**0.004**	**0.001**	**0.006**	**0.010**				
	Exp 1		7	5.79	0.132	0.001	0.370	0.118	-2.29 ± 0.06[a]	-4.47 ± 0.10[a]		
	Exp 2		7	5.79	0.136	0.001	0.373	0.128	-2.27 ± 0.06[a]	-4.44 ± 0.10[a]		
	Exp 3		7	5.79	0.135	0.002	0.372	0.127				
		Mean		**5.79**	**0.134**	**0.001**	**0.372**	**0.124**				
		2SD[b]		**0.00**	**0.003**	**0.000**	**0.003**	**0.011**				
	Exp 1		10	5.76	0.115	0.001	0.351	0.090	-2.29 ± 0.06[a]	-4.48 ± 0.10[a]	-2.44 ± 0.06[a]	-4.77 ± 0.10[a]	-0.27 ± 0.14[d]
	Exp 2		10	5.76	0.119	0.001	0.352	0.100	-2.29 ± 0.06[a]	-4.48 ± 0.10[a]	-2.45 ± 0.06[a]	-4.78 ± 0.10[a]	-0.28 ± 0.14[d]
	Exp 3		10	5.77	0.119	0.001	0.349	0.101			-2.45 ± 0.06[a]	-4.77 ± 0.10[a]	-0.27 ± 0.14[d]
		Mean		**5.76**	**0.117**	**0.001**	**0.350**	**0.097**				
		2SD[b]		**0.01**	**0.004**	**0.000**	**0.003**	**0.012**				

[a]Uncertainties given after each individual result are analytical uncertainties for each individual experiment analyzed by MC-ICP-MS. These are estimated based on repeat reference material measurements processed through the Mg column chemistry and are ±0.10‰ (2SD, $\delta^{26}Mg$) and ±0.06 ‰ (2SD, $\delta^{25}Mg$). Multiple MC-

ICP-MS measurements of each sample solution were always repeatable within the stated uncertainties. All δ-values are reported relative to the international measurement standard DSM3.

[b]Both abiotic and biotic experiment were ran in triplicates in parallel (indicated by exp. 1, 2, and 3). For each experiment type, where more than one of the triplicates was analyzed by ICP-OES and MC-ICP-MS after Mg column separation, the experimental mean and 2SD is reported.

[c]Element concentrations were measured by ICP-OES with analytical uncertainties estimated to be ± 5% relative (95% confidence) based on repeat measurements of quality control standards. The following emission wavelengths were used: Mg (280.270 nm), Fe (238.204 nm), K (766.491 nm) and P (213.618 nm) and calibration of the ICP-OES was made with matrix-matched multi-elements standard solutions.

[d]$\Delta^{26}Mg_{cell-solution}$ represents the isotopic difference between the $\delta^{26}Mg$ value of biomass *N. punctiforme* at the end of each experiment and the $\delta^{26}Mg$ value of the growth solution. The growth solution stayed constant in $\delta^{26}Mg_{DSM3}$ over the entire experiment duration with a mean $\delta^{26}Mg_{DSM3}$ of -4.50 ‰ ± 0.1‰ (2SD uncertainty in $\Delta^{26}Mg_{cell-solution}$ is derived from error propagation of individual measurement uncertainties).

Table S4: Mg isotope measurements of growth experiments for chlorophyll extraction

Growth solution		**Chlorophyll *N. punctiforme***		**Isotopic difference (chlorophyll – solution)**
$\delta^{25}Mg_{DSM3}$ (‰)	$\delta^{26}Mg_{DSM3}$ (‰)	$\delta^{25}Mg_{DSM3}$ (‰)	$\delta^{26}Mg_{DSM3}$ (‰)	$\Delta^{26}Mg_{chlorophyll-solution}$[b] (‰)
-0.53 ± 0.06[a]	-1.05 ± 0.10[a]	0.41 ± 0.06[a]	0.80 ± 0.10[a]	1.85 ± 0.14[b]

[a]Uncertainties given after each individual result are analytical uncertainties (2SD) for each individual experiment analyzed by MC-ICP-MS.

[b]$\Delta^{26}Mg_{chlorophyll-solution}$ represents the isotopic difference between the $\delta^{26}Mg$ value of Mg extracted from chlorophyll and the $\delta^{26}Mg$ value of the growth solution.

Uncertainty in $\Delta^{26}Mg_{chlorophyll-solution}$ is the 2SD derived from error propagation of individual measurement uncertainties.

Chapter 4

Mechanisms of olivine dissolution by rock-inhabiting fungi explored using magnesium stable isotopes

Abstract

To disclose the dissolution mechanisms of olivine by a rock-inhabiting fungus we determined the stable isotope ratios of Mg on solutions released in a laboratory experiment. We found that in the presence of the fungus *Knufia petricola* the olivine dissolution rates were about seven-fold higher (1.04×10^{-15} mol cm^{-2} s^{-1}) than those in the abiotic experiments (1.43×10^{-16} mol cm^{-2} s^{-1}) conducted under the same experimental condition (pH 6, 25°C, 94 days). Supernatant solutions in both the biotic and the abiotic experiment followed a dissolution trend characterized by initial non-stoichiometric release of Mg and Si and preferential release of ^{24}Mg over ^{26}Mg, followed by a later phase of stoichiometric release of Mg and Si, as well as isotopically congruent Mg release. We attribute the initial non-stoichiometric phase to the rapid replacement of Mg^{2+} in the olivine with H^{+} along with simultaneous polymerization of Si tetrahedra, resulting in high dissolution rates, and the stoichiometric phase to be influenced by the accumulation of a Si-rich amorphous layer that slowed olivine dissolution. We attribute the accelerated dissolution of olivine during the biotic experiment to physical attachment of *K. petricola* to the Si-rich amorphous layer of olivine which potentially results in its direct exposure to protons released by the fungal cells. These additional protons can diffuse through the Si-rich amorphous layer into the crystalline olivine. Our results also show the ability of *K. petricola* to dissolve Fe precipitates in the Si-rich amorphous layer either by protonation, or by Fe(III) chelation with siderophores. Such dissolution of Fe precipitates increases the porosity of the Si-rich amorphous layer and hence enhances olivine dissolution. The demonstration of an initial phase of preferential ^{24}Mg release suggests that Mg isotopes are a sensitive tracer of the initial stages of rock weathering. The acceleration of mineral dissolution in the presence of a rock-dissolving fungus further suggests that its presence in surficial CO_2 sequestration plants may aid to accelerate CO_2 binding.

4.1 Introduction

Fungi are ubiquitous in the terrestrial environment and can live in soils and rocks, or be in symbiosis with plant roots or other microbes (Burford et al., 2003a; Burford et al., 2003b; Harley and Smith, 1983; Hawksworth, 1988; Warcup, 1951). Several studies confirm the ability of fungi to increase silicate mineral dissolution rates (Banfield et al., 1999; Bonneville et al., 2009; Ehrlich, 1996; Gadd, 2007; Hagerberg et al., 2003; Henderson and Duff, 1963; Rosling et al., 2004). For example, laboratory studies by Balogh-Brunstad et al. (2008) and Bonneville et al. (2011) showed that an ectomycorrhizal (ECM) fungus accelerated biotite dissolution by direct (e.g. tunneling into the mineral and excreting protons and ligands in the contact zone) and indirect (e.g. lowering the pH of the solution by exuding organic acids and by producing CO_2 via respiration) mechanisms. Another study on dissolution of lizardite by the fungus *Talaromyces flavus* in lab experiments concluded that biogenic dissolution accounted for about 40% - 50% of total weathering at steady-state conditions (Li et al., 2016). A contrasting observation by Oelkers et al. (2015) showed that the preferential growth of fungi and bacteria on the surface of Mg silicate minerals potentially slows dissolution rates. These observations call for the role of fungi to be elucidated and quantified in field studies of silicate weathering.

However, in bio-weathering systems a major challenge lies in the need to separate the effects of biotic from abiotic processes that often occur simultaneously. Application of metal stable isotopes can help to tackle this challenge. For example, Mg isotopes fractionate during both abiotic (mineral dissolution, secondary mineral formation, carbonate precipitation and ion exchange) (Maher et al., 2016; Opfergelt et al., 2014; Pearce et al., 2012; Ryu et al., 2016; Schott et al., 2016; Wimpenny et al., 2014; Wimpenny et al., 2010) and biotic (uptake and translocation by microbes and higher plants) processes (Black et al., 2008; Bolou-Bi et al., 2010; Bolou-Bi et al., 2012; Fahad et al., 2016; Kimmig et al., 2018; Mavromatis et al., 2014; Moynier and Fujii, 2017; Pokharel et al., 2017; Pokharel et al., 2018; Ra and Kitagawa, 2007; Ra et al., 2010; Schmitt et al., 2012; Shirokova et al., 2011; Tipper et al., 2010; Uhlig et al., 2017). In an abiotic dissolution experiment of olivine at pH 2-3 by Wimpenny et al. (2010) showed the preferential release of lighter ^{24}Mg, where after 3 days the dissolved phase was -0.36‰ lower in $^{26}Mg/^{24}Mg$ than the original olivine. An opposite trend was observed by Oelkers et al. (2015) during olivine dissolution in presence of microbes at neutral pH, where the dissolved phase was enriched in the ^{26}Mg, such that after 5 years the solution was 0.25‰ higher in $^{26}Mg/^{24}Mg$ than the dissolving olivine. Maher et al. (2016) interpreted Mg isotope fractionation during experimental forsterite dissolution with a surface kinetic model. During the early stages of olivine dissolution the enrichment of the solution in ^{24}Mg, where its

$^{26}Mg/^{24}Mg$ ratio was -0.36‰ lower in than that of the original olivine, was attributed to a surface kinetic effect. At a later stage, a phase called steady state dissolution, the bulk solution attained the isotopic composition of the original olivine. Several studies indicate that Mg isotopes are fractionated during uptake by fungi. A study by Fahad et al. (2016) showed ectomycorrhizal fungus incorporate lighter Mg isotopes from the growth solution where the fungus was about -0.15‰ lower in $^{26}Mg/^{24}Mg$ than the growth solution, whereas a non-mycorrhizal fungus preferentially incorporated heavier Mg isotopes and its Mg was enriched about 0.3‰ in its $^{26}Mg/^{24}Mg$ ratio. A study by Pokharel et al. (2017) showed that rock-inhabiting black fungus *Knufia petricola* preferentially incorporate heavier Mg isotopes during growth and observed a pH-dependence on Mg isotope fractionation: $^{26}Mg/^{24}Mg$ in the fungus was 0.65‰ and 1.11‰ higher in than the growth solution at pH 6 and pH 3 respectively. Given these previous results, we expect that during mineral dissolution Mg isotopes in the solutions track either or both of the following processes: 1) uptake of Mg into organisms, provided a significant fraction of the Mg released is partitioned into their biomass; 2) the kinetics of mineral dissolution, provided that the fraction of Mg transferred into and remaining in organisms is low.

Here we apply stable isotopes of Mg to a laboratory microcosm batch experiments comprised of the rock-inhabiting microcolonial fungus *Knufia petricola* A95 and the mineral olivine to investigate biogenic mineral dissolution. We chose *K. petricola* as it is commonly found in sub-aerial environments, has the ability to dissolve rocks (Seiffert et al., 2016), and also has been shown to preferentially incorporate the heavier Mg isotopes from a growth solution (Pokharel et al., 2017). The main objectives of this study are to: 1) quantify fungal olivine dissolution rates, and 2) explore the mechanism of biogenic olivine dissolution. We show that in the presence of *K. petricola* dissolution rates increases seven-fold over the abiotic control, and discuss mechanisms that can lead to this acceleration.

4.2 Materials and Methods

4.2.1 Components of batch experiments

Olivine, $(Mg,Fe)_2SiO_4$, is an orthosilicate, with $[SiO_4]^{4-}$ tetrahedra. Forsterite is its Mg-rich endmember, whereas fayalite is the Fe(II)-rich endmember of the solid-solution series (Kolesov and Geiger, 2004). During weathering of olivine only one ionic Mg-O-bond is broken, and unlike in other silicate minerals, no Si-O-Si bond is broken. Due to this feature olivine is one of the fastest dissolving silicate minerals (Oelkers et al., 2018), making it well-suited for mineral dissolution studies. The natural olivine mineral used in this study was from San Carlos,

Arizona. The olivine mineral grains of ~ 0.5 cm in size were ground with an agate mortar and pestle and a size fraction of 63 to 125 µm was separated by sieving. This fraction was ultrasonically cleaned multiple times with acetone and deionized water (Merck Millipore) to remove fine particles and then dried at 65°C for 24 hours. The surface area of the cleaned olivine was measured at Bundesanstalt für Materialforschung und -prüfung (BAM) in Berlin, Germany, by BET (ASAP2020, Micromeritics, USA) and was 1470 ± 260 (2SD) $cm^2\ g^{-1}$. The chemical composition measured by electron microprobe (JXA 8200, JEOL, USA) at Freie *Universität Berlin* indicates that the average composition of the olivine was $Mg_{1.86}Fe_{0.19}SiO_4$.

The growth media (prepared in bulk volume of 5 liters) comprised 0.3 mM Na_2SO_4, 0.173 mM K_2HPO_4, 9.95 µM thiamine hydrochloride, and 18.5 mM NH_4NO_3. The media was autoclaved prior to addition of filter-sterilized glucose as a carbon source (9.96 mM final concentration). Finally 2-(*N*-morpholino) ethanesulfonic acid (MES) (11.1 mM final concentration) was added as a pH buffer.

The fungus used in this study was a relatively fast growing rock-inhabiting microcolonial fungus *Knufia petricola* A95 (formerly known as *Sarcinomyces petricola*). This species is ubiquitous in the terrestrial environment and its geographic distribution ranges from the Mediterranean to the Artic (Gorbushina et al., 2008; Wollenzien et al., 1997). This particular strain was isolated from weathered marble monument in Athens, Greece. The DNA sequence of this fungus has been well-studied (Nai et al., 2013). This species is both biologically relevant due to its ability to form symbiosis with cyanobacteria and geologically important due to its mineral weathering ability (Gorbushina et al., 2008; Seiffert et al., 2016). A detailed description of the cultivation of the strain is given in Nai et al. (2013) and Noack-Schönmann et al. (2014). Prior to cultivation in the batch experiment setup, the fungal biomass strain was washed with EDTA and then the batch supernatant media to remove surficial contamination.

4.2.2 Dissolution Experiment

All dissolution experiments were done as batch experiments. Four grams of ground olivine powder were distributed over six pre-cleaned 500 ml polycarbonate Erlenmeyer flasks with vented caps which were then autoclaved for microbial sterilization. 400 ml of growth media was placed in each of the Erlenmeyer flask. In each of three Erlenmeyer flasks, 4 mg dry weight of *K. petricola* was inoculated and the remaining three flasks were not inoculated thus representing the abiotic dissolution experiment. All experiments were run in triplicates. The Erlenmeyer flasks were placed in a climate chamber at constant temperature (25°C), constant light source (90 µmol photon $m^{-2}\ s^{-1}$) and were shaken at 140 rpm min^{-1}. To support the fungus'

carbon demand an additional 0.4 g of filter sterile glucose was added on day 65 of the experiment. The experiments were ran for 94 days.

Periodic sampling (5 ml) of the supernatant with a pipette while manually shaking the flask was done during the course of the experiment. The manual shaking was done to homogenise the components of the Erlenmeyer flasks, to have roughly similar amounts of mineral, liquid and biomass pipetted at each sampling interval and thus maintain a constant mineral:liquid:biomass ratio over the course of the experiment. Prior tests indicated a loss of about 0.05g of olivine powder from the Erlenmeyer flask at each sampling point. The sampled supernatant aliquots were filtered with a 0.22 µm filter, and a part was used for pH measurement while the rest was acidified and stored at 4^{o}C for further elemental and isotopic analysis. The filtrate consisting of biomass and olivine powders were separated from the filter. The DNA of the fungal biomass was extracted for qPCR analysis to measure fungal growth at each sampling point in the batch reactor.

4.2.3 Analysis

Microbial growth rates were determined by extracting the DNA and then quantified using quantitative PCR at BAM using the protocol of Martin-Sanchez et al. (2016). For a detailed description of the procedure the reader is referred to that article.

A part of the acidified supernatant sample was used for elemental analysis using Inductively Coupled Plasma Optical Emission Spectrometry (ICP-OES, Varian 720-ES) at the Helmholtz Laboratory for the Geochemistry of the Earth Surface (HELGES) at GFZ Potsdam (von Blanckenburg et al., 2016). The analysis was performed following the procedure described in Schuessler et al. (2016). Briefly, all samples and standards (ICP multi element solution) were diluted 1:3 using 0.3 M quartz-distilled HNO_3 acid and 1 mg/g Cs for matrix matching the samples to the calibration standards within 5% relative. Samples were doped with known concentrations of In and Sc to check for instrument stability during the measurements. A quality control solution (in 0.3 M HNO_3 and 1 mg/g Cs, made from Merck CertiPUR multi element standards with certified concentrations traceable to NIST reference materials) matrix-matched to that of the samples and solution was prepared. This solution and blanks were analyzed every 12 samples to assess measurement uncertainty and verify absence of contamination during the run. Based on repeated measurement of the quality control standards, the analytical uncertainty was estimated to be less than 5.2 %. See supporting information (Table S1) for details on quality controls samples preparation and analysis.

The Mg isotope composition of the initial bulk solid olivine and the acidified supernatant solutions (sampled at different times during the experiments) were determined by

Multicollector Inductively Coupled Plasma Mass Spectrometry (MC-ICP-MS, Thermo Scientific Neptune) after Mg separation from the sample matrix. All samples and standards for Mg isotopes analysis were processed in the HELGES clean lab facility using ultrapure acids. Blanks and reference materials were processed in parallel with the samples to quantify measurement accuracy and potential cross contamination. The reference materials Cambridge-1 and BHVO-2 were prepared in both pure and doped form. Doped solutions indicate that pure Mg solutions (500 ng/ml Mg) were doped in the input solution. The blanks, samples and reference material were first treated with a mixture of concentrated HNO_3, HCl, H_2O_2 and HF (HF was used only for dissolving olivine) on a hotplate at 150°C in PFA vials. The samples were evaporated and re-dissolved multiple times in acids until completely dissolved. Finally the samples were dissolved in 1M HNO_3 prior to Mg separation by cation exchange column chromatography. The protocols for the column separation procedure along with instrument settings for Mg isotopes analysis by MC-ICP-MS are given in Pokharel et al. (2017). Results are expressed in the δ-notation as the part per thousand (‰) deviation of the $^{26}Mg/^{24}Mg$ ratio from the international measurement standard DSM3, $\delta^{x}Mg_{sample} = [((^{x}Mg/^{24}Mg)_{sample} / (^{x}Mg/^{24}Mg)_{DSM3}) - 1 \times 1000]$, where x = 26 or 25. Based on repeated measurements of reference materials (both pure and doped), the uncertainty in $\delta^{26}Mg$ and $\delta^{25}Mg$ is estimated at ± 0.1‰ (2SD) and ± 0.06‰ (2SD), respectively. See supporting information for details on reference materials measurements and uncertainties (Table S2).

4.3 Results

Figure 1 shows the evolution of pH, elemental Mg, Si, and Fe concentrations in the supernatant, fungal DNA analysis for estimating growth, and the olivine dissolution rate with experimental run time for both abiotic and biotic experiments. The pH was maintained constant at around 6.2 by the MES buffer for both abiotic and biotic experiments (Figure 1a; Table 1). DNA analysis of the supernatant showed that fungal cells increased from 230 to 2350 DNA ng/ml over the 94 days of the runs (Figure 1b; Table 1), where most of the growth occurred between day 40 and 94. Despite the consistent pH between the biotic and abiotic experiments, the release of both Mg and Si varied between them: the biotic experiments liberated higher amounts of both these elements (Figure 1c). In both experiments, there was a rapid initial release of both Mg and Si during the first two days, after which the release slowed down. Fe was initially released into the solution but was rapidly removed in the first 20 days in both experiments (Figure 1d) - likely as Fe(III) precipitates. In the abiotic experiment, the amount of Fe remained constant in the solution after 20 days (slight changes were within the analytical uncertainty), whereas in the

biotic experiment, the concentrations of dissolved Fe increased with time. Details of Mg, Si, and Fe concentrations in the supernatant along with the respective uncertainties are provided in the supporting information (Table S3). A constant dissolution rate for Mg and Si was not attained by the end of this experiment. A PHREEQC calculation showed that Mg and Si were undersaturated in the bulk solution with respect to any Mg- or Si-bearing secondary minerals. The relative amount of Mg released from the olivine was low for both abiotic and biotic experiments, 0.75% and 1.65% respectively. The Mg dissolution rate from the olivine mineral at each sampling interval was calculated following the mineral dissolution study by Daval et al. (2011).

$$r[t] = \frac{\Delta[i]}{SSA \times \Delta t \times \eta[i]} \qquad \text{(eq. 1)}$$

where r[t] is the dissolution rate (mol cm^{-2} s^{-1}) of olivine at time t, i.e. between two consecutive sampling points (calculated from supernatant Mg or Si concentrations); Δ[i] is the difference in molar amount of solute i (Mg or Si; mol) sampled between two sampling points; SSA is the specific surface area of the olivine (cm^2; due to experimental limitations we were not able to determine the changes in surface area induced by the presence of *K. petricola* or any structural changes in olivine during the course of the experiment. Therefore, we used the initial surface area of the olivine but accounted for the changes in the amount of olivine caused by pipetting at each sampling interval as explained in the method section); Δt is the time interval between two sampling points (s); η[i] is the stoichiometric coefficient ratio of solute i (1.86 for Mg and 1 for Si as measured by electron microprobe).

The olivine dissolution rate calculated from Mg concentrations at the end of 94 days for the biotic experiment (1.04×10^{-15} mol cm^{-2} s^{-1}) was seven times higher than that of the abiotic dissolution experiment (1.43×10^{-16} mol cm^{-2} s^{-1}) (Table 1; Figure 1e). Detailed calculation of the dissolution rates using the parameters in equation 1 is provided in the supporting information (Table S4).

Table 1: Summary of the results obtained for the abiotic and biotic dissolution experiments

Experiment	Time (Days)	pH	DNA (ng ml^{-1})	±[b]2SD	Mg (moles)	±[b]2SD	[a]Olivine Dissolution Rates (mol cm^{-2} s^{-1})	±[b]2SD	$\delta^{25}Mg_{DSM3}$ (‰)	±[b]2SD	$\delta^{26}Mg_{DSM3}$ (‰)	±[b]2SD
Abiotic	0	6.21	0		0	0						
	0.04	6.24			3.44E-05	0.63E-05	8.74E-13	1.64E-13	-0.37	0.05	-0.71	0.13
	0.25	6.25			5.30E-05	0.50E-05	9.62E-14	2.70E-14	-0.31	0.06	-0.62	0.12
	1	6.28			6.61E-05	0.72E-05	1.90E-14	0.43E-14	-0.27	0.10	-0.54	0.18
	2	6.26			7.04E-05	0.65E-05	4.67E-15	1.05E-15	-0.26	0.06	-0.52	0.10
	6	6.30	0.004	0.008	7.91E-05	0.65E-05	2.43E-15	0.46E-15	-0.25	0.08	-0.50	0.16
	15	6.30			8.60E-05	0.76E-05	8.62E-16	1.62E-16	-0.22	0.06	-0.43	0.10
	28	6.29	0.034	0.067	9.15E-05	0.80E-05	4.89E-16	0.92E-16	-0.26	0.06	-0.49	0.10
	41	6.28	0.001	0.002	9.51E-05	0.80E-05	3.16E-16	0.60E-17	-0.23	0.06	-0.47	0.12
	94	6.20	0.008	0.015	1.02E-04	0.08E-04	1.43E-16	0.38E-16	-0.19	0.06	-0.38	0.10
Biotic	0	6.21	228	114	0							
	0.04	6.23			2.91E-05	0.50E-05	7.40E-13	1.39E-13	-0.36	0.07	-0.70	0.13
	0.25	6.25			4.45E-05	1.20E-05	7.95E-14	3.62E-14	-0.28	0.06	-0.54	0.10
	1	6.26			5.60E-05	1.36E-05	1.67E-14	0.31E-14	-0.27	0.13	-0.53	0.21
	2	6.26			6.26E-05	1.43E-05	7.28E-15	1.36E-15	-0.24	0.07	-0.48	0.10
	6	6.25	126	239	7.80E-05	1.49E-05	4.29E-15	0.80E-15	-0.29	0.06	-0.55	0.10
	15	6.19			9.68E-05	1.62E-05	2.36E-15	0.44E-15	-0.24	0.13	-0.46	0.23
	28	6.16	527	287	1.59E-04	0.13E-04	5.48E-15	2.35E-15	-0.23	0.09	-0.46	0.20
	41	6.15	535	574	1.77E-04	0.09E-04	1.61E-15	1.14E-15	-0.22	0.15	-0.44	0.27
	94	6.08	2304	571	2.24E-04	0.18E-04	1.04E-15	0.24E-15	-0.18	0.10	-0.36	0.19

[a]Instantaneous olivine dissolution rates calculated between two consecutive sampling points (calculated from supernatant Mg concentrations using equation 1).
[b]2SD represents the analytical uncertainty for an individual measurement or uncertainty derived from the repeatability of three independent experiments, whichever was larger (see Table S3 for all individual analyses).

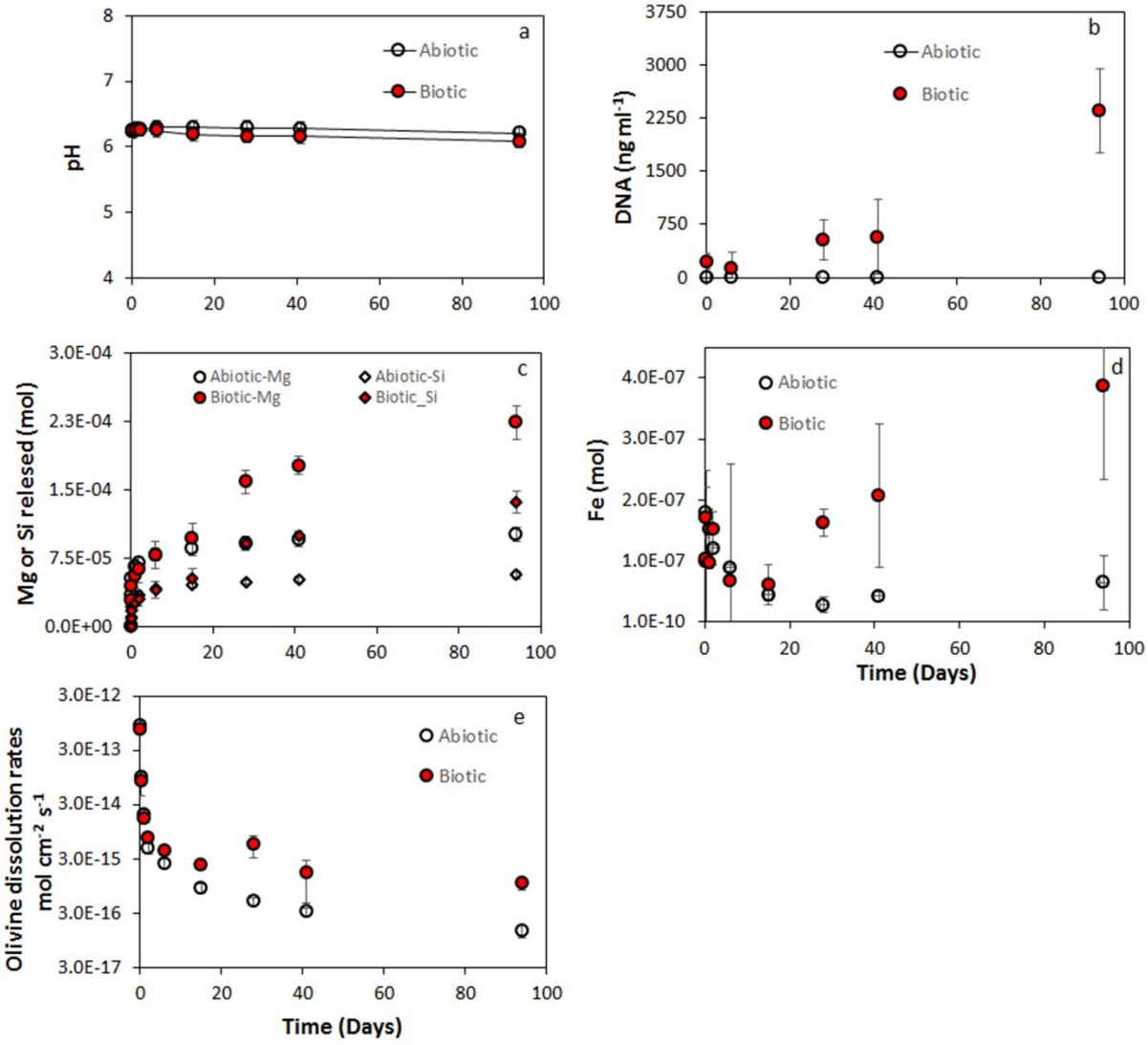

Figure 1: Temporal evolution of a) pH; b) DNA concentration; c) Mg and Si released; d) Fe released; e) instantaneous olivine dissolution rates calculated from Mg concentrations (eq. 1) during dissolution experiments. The Y-axis of Figure (e) is plotted on a logarithmic scale of base 10. All uncertainty bars represent 2SD. 2SD on graph (a) represent analytical uncertainty, whereas on graphs b, c, d and e represents the analytical uncertainty for an individual measurement or uncertainty derived from the repeatability of three independent experiments, whichever was larger. For plots where no uncertainty is shown, the uncertainty is smaller than the symbols. See Table 1, Table S3 and Table S4 for detailed information

All measured isotopic data showed mass-dependent isotope fractionation. Based on the slope in a three-isotope-plot (Young and Galy, 2004) and the deviation of δ^{25}Mg from the mass-dependent fractionation line typical for equilibrium fractionation (Δ^{25}Mg', Fig. 2b), an equilibrium isotope effect could not be singled-out from a kinetic effect from the slope of the mass-dependent fractionation line (Figure 2a and 2b), given the uncertainty of these values and the low spread in δ^{26}Mg. The temporal evolution of the Mg isotopic ratio of the supernatant did

not differ between abiotic and biotic experiments, despite differences in the amounts of Mg released.

Both experiments showed an initial preferential release of ^{24}Mg over ^{26}Mg during the early stages of the experiment, but at the later stages $\delta^{26}Mg$ of the solution approached a value identical to the initial unreacted olivine (Figure 3). Any possible differences in $\delta^{26}Mg$ of the solution between the abiotic and biotic experiment were within the analytical uncertainty of the MC-ICP-MS (±0.1‰) and thus are not detectable. All $\delta^{26}Mg$ data for each of the independent experiments is presented in the supporting information (Table S3).

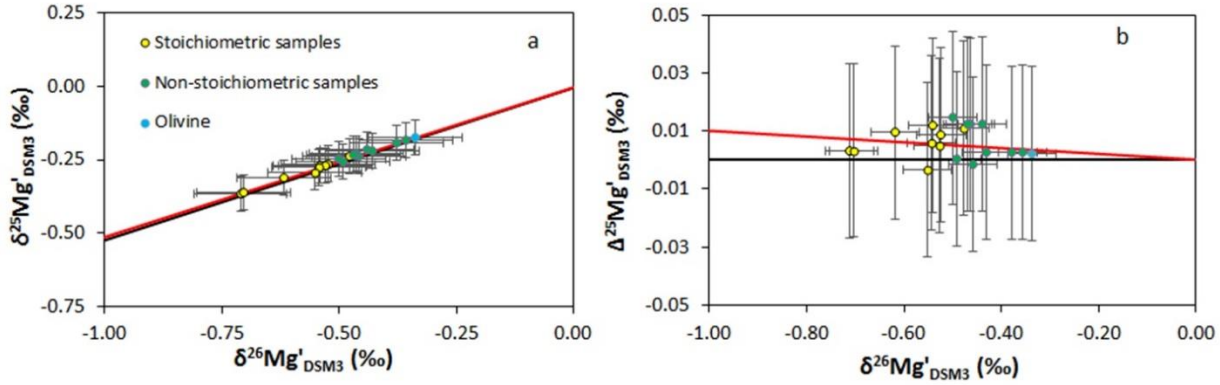

Figure 2: Three-isotope plot diagram for samples measured in this study. The solid red line represents the kinetic fractionation line (slope = 0.511) and the solid black line represent the equilibrium fractionation line (slope = 0.521). For both graphs, yellow circles show the samples measured during the non-stoichiometric dissolution phase (up to day 2), green circles are the sample measured during the stoichiometric dissolution phase, and blue circle is the initial olivine. (a) $\delta^{26}Mg'_{DSM3}$ vs $\delta^{25}Mg'_{DSM3}$ plot as defined in Young and Galy (2004). Uncertainty in the plot are based on repeated measurement of reference materials processed through the Mg column chemistry and are ±0.10‰ (2SD, $\delta^{26}Mg'_{DSM3}$) and ±0.06‰ (2SD, $\delta^{25}Mg'_{DSM3}$). (b) $\Delta^{25}Mg'$ and $\delta^{26}Mg'$ graph for the samples. The uncertainty for $\Delta^{25}Mg'$ was ±0.03 (1SD) and was based on equation 19 in Young and Galy (2004). The uncertainty for $\delta^{26}Mg'_{DSM3}$ was ±0.05 (1SD).

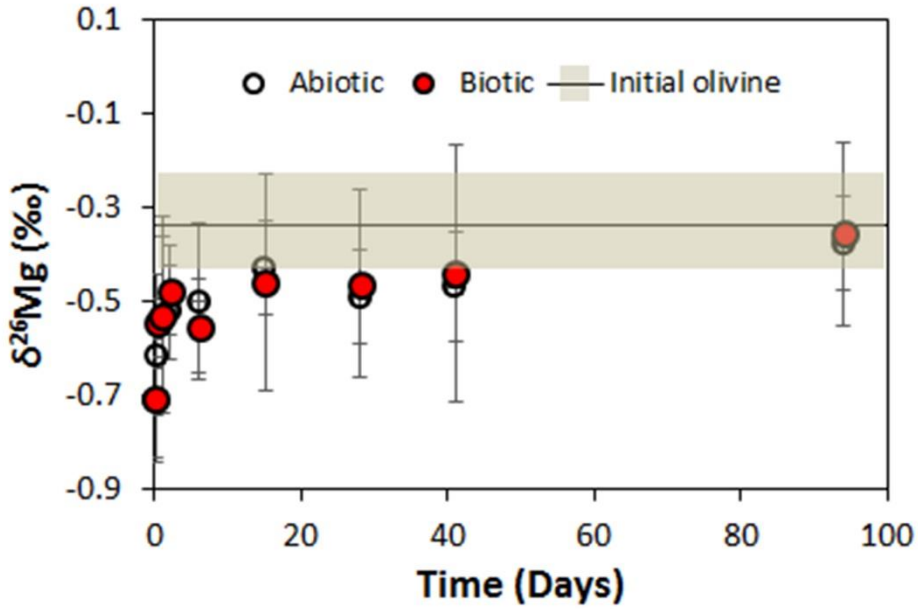

Figure 3: Mg isotopic composition of the bulk dissolved phase for the abiotic and biotic experiments as a function of experiment run time. The error bars (2SD) in the graph was either derived from the analytical uncertainty from the individual measurements by MC-ICPMS or the uncertainty from the repeatability of independent growth experiments, whichever was larger. The Mg isotopic composition (δ^{26}Mg) of the initial olivine was measured to be -0.34 ±0.10‰ (2SD). The grey area represents the 2SD of δ^{26}Mg of the initial olivine.

A similar picture emerged from the evolution of the supernatants Mg/Si ratios. Figure 4 shows that the olivine dissolution can be separated into two stages: (i) an initial non-stoichiometric dissolution stage yielding a high Mg/Si ratio in the supernatant followed by (ii) a stoichiometric stage yielding an Mg/Si ratio that was identical to Mg/Si of the dissolving olivine.

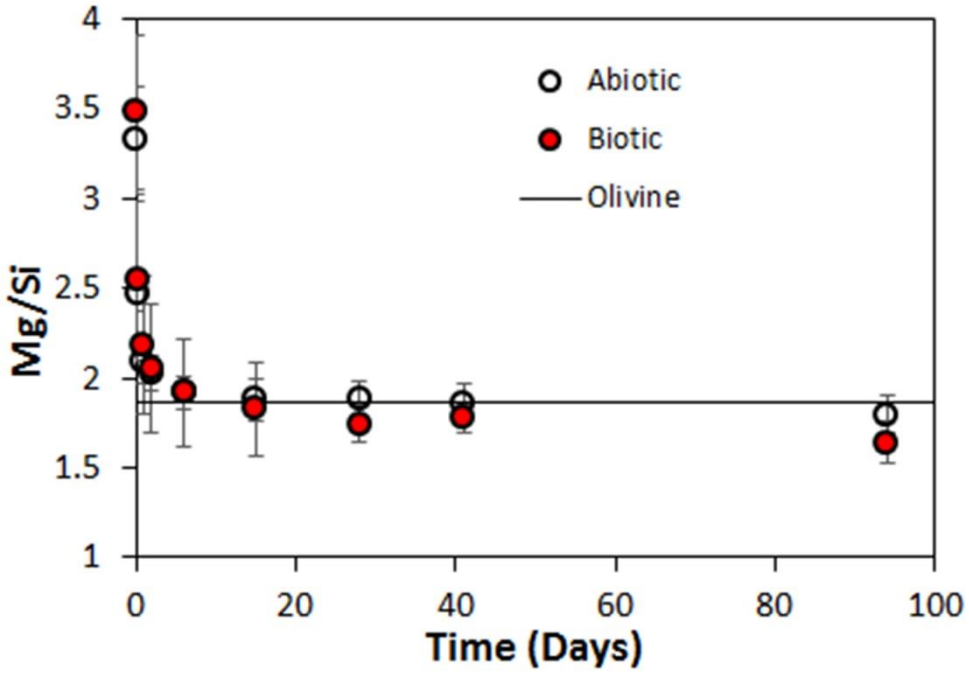

Figure 4: Mg/Si molar ratio in the dissolved phase of the abiotic and biotic experiments, where the solid line denotes the molar Mg/Si ratio of initial olivine (1.86). The uncertainty in the figure is 2SD and is based on error propagation of uncertainties in measured Si and Mg concentrations.

4.4 Discussion

4.4.1 Dissolution stages, processes and isotope fractionation

The olivine structure is made of individual silicon-tetrahedra linked by Mg atoms each of which are in octahedral coordination (Birle et al., 1968). At acidic conditions, protons are transported to the olivine surface either by diffusion or advection. The initial non-stoichiometric stage of dissolution is attributed to rapid exchange of protons with Mg^{2+} atoms in the olivine surface along with simultaneous polymerization of silica tetrahedra (eq. 2) (Daval et al., 2011; Johnson et al., 2014; Maher et al., 2016; Pokrovsky and Schott, 2000a, b). The silica tetrahedra simultaneously dissolve as silicic acid (eq. 3) but with a slower reaction kinetics than the Mg^{2+} release hydrolysis reaction (Maher et al., 2016).

$$Mg_2SiO_4 + 4H^+ \rightarrow 2Mg^{2+} + SiO_2 + 2H_2O \qquad \text{(eq. 2)}$$

$$SiO_2 + 2H_2O \rightarrow H_4SiO_4\,(aq) \qquad \text{(eq. 3)}$$

Due to the differences in reaction kinetics for Mg and Si release, Mg is depleted in the surface of olivine in comparison to amorphous Si. The measured high Mg/Si molar ratio (in comparison to the stoichiometric molar ratio of the unreacted olivine) in the bulk solution during the initial non-stoichiometric phase confirms this (Figure 4). The formed surface layer

thus is low in Mg and high in Si, and has been previously termed as the "active layer" or the "leached layer" (Maher et al., 2016; Pokrovsky and Schott, 2000a). We refer to this surface layer as "Si-rich amorphous layer". Hellmann et al. (2012) proposed a different mechanism whereby interfacial dissolution/precipitation processes take place at the thin-fluid film contacting the olivine surface. They postulated that the chemistry of this thin-fluid film differs from the bulk solution, and thus in this layer the precipitation of amorphous silica takes place even if the bulk solution is undersaturated with respect to amorphous silica. Regardless of the mode of formation of this layer, once the Si-rich amorphous layer has formed, the dissolution of surface silica is always governed by reaction 3 (Maher et al., 2016).

We thus infer that in the initial non-congruent dissolution phase such Si-rich amorphous surface layer is formed and Mg is not any further present at the surface for protonation. The Si-rich amorphous layer can slow down the release of Mg and Si, thereby significantly decreasing the olivine dissolution rates. The parabolic nature of the dissolution rate curve observed is due to this effect (Figure 1d). As these surface layer are porous, protons can diffuse through this layer onto the olivine surface (Pokrovsky and Schott, 2000a). The dissolution rate at this stage is therefore controlled by transport through the Si-rich amorphous layer. As the proton reacts with the crystalline olivine in the inner edge of the amorphous layer, Mg^{2+} is released (following eq. 2) and diffuses through the porous surface layer into the solution. Simultaneously new Si tetrahedra are released by H^+ at the inner edge of the amorphous surface layer. In the stoichiometric phase the Si release from the olivine surface balances the rate of dissolution of the external amorphous Si layer (following eq. 3) which thus maintains constant thickness (Hellmann et al., 2012; Maher et al., 2016). The Si-rich amorphous layer moves inward at a rate controlled by both the rate of Mg exchange according to the reaction given in eq. (2) and the net release of Si via the reaction given in eq. (3), resulting in stoichiometric release of these two elements (Figure 4) (Maher et al., 2016). We observed a decrease in the olivine dissolution rates as the reaction progressed from initial non-stoichiometric to the stoichiometric stage (Figure 1d) that amounted to two to three orders of magnitude. A similar decrease was observed by Daval et al. (2011) in solutions undersaturated in both Mg and Si.

The molar ratio of Fe/Mg in the supernatant was non-stoichiometric with respect to the initial olivine over the course of both biotic and abiotic experiments (Table S3). The Fe/Mg ratios in the supernatants were 1-2 orders of magnitude lower than the initial olivine ratio of 0.1. This incongruent release of Fe and Mg from the surface of olivine might be due to oxidation of Fe(II) released from olivine followed by precipitation due to the low solubility of Fe(III). During the non-stoichiometric dissolution phase the precipitation of Fe(III) phases is indicated

by the decrease in the dissolved Fe amount in the solution (Figure 1d). This Fe was released from the fayalite component of olivine initially as Fe(II) which upon entering the solution was fast oxidized to insoluble Fe(III) which was precipitated as Fe(III)oxy-hydroxides. Past studies have indicated that Fe(III) precipitates contribute to additional protection in the Si-rich amorphous layer and reduce the porosity of the layer by clogging (Saldi et al., 2013; Schott and Berner, 1983; Sissmann et al., 2013; Torres et al., 2014). Their presence thus potentially slows down olivine dissolution even further.

Within this framework we now explore the causes of the faster Mg and Si release in the presence of *K. petricola*. Fungi are known to break mineral structures by two mechanisms, 1) biomechanical weathering; and 2) biochemical weathering (Adeyemi and Gadd, 2005; Balogh-Brunstad et al., 2008; Bonneville et al., 2009; Callot et al., 1987; Chizhikova et al., 2016; Daghino et al., 2010; Duane, 2006; Gadd, 2007, 2010; Hirsch et al., 1995; Hoffland et al., 2004; Krumbein and Jens, 1981). Both these processes are triggered by physical attachment of *K. petricola* to the mineral surface. Biomechanical weathering is caused by fungal hyphae penetration into weak spots of rocks like cracks and mineral cleavage to acquire nutrients. After attachment, fungal hyphae can generate an internal turgor pressure as high of 0.4 MPa (4 bars) to 8 MPa (80 bars) through osmosis that facilitates them to penetrate hard rock surfaces (Bechinger et al., 1999; Bonneville et al., 2009; Harold, 2002). However, *K. petricola* has a short torulose hyphae with smaller surface area that limits its biomechanical weathering ability. Hence in *K. petricola* it is the biochemical weathering processes that have a greater influence on releasing metals from the rock surface. Biochemical fungal weathering is thought to take place by two processes, (I) proton-based and (II) ligand-based (Gadd, 2007, 2010; Hoffland et al., 2004). Protons acidify the microenvironment of the fungi. They are excreted through the plasma membrane as H^+-ATPase, are produced from carbonic acid as a by-product of respiration, or are produced from organic acids (Balogh-Brunstad et al., 2008; Bonneville et al., 2009; Burford et al., 2003a). Pokharel et al. (2017) showed that in unbuffered conditions *K. petricola* lowered the pH of the growth solution by 3-4 units over the course of only a few days. Although in our experiment the MES buffer stabilized the pH of the solution, we speculate that a local pH change might have arisen that acidified the surface of the mineral in direct contact with *K. petricola*. Ligand-based weathering processes include release of for example siderophores, carboxylic acids, amino acids, phenolic compounds that potentially complex metals from the mineral surfaces (Gadd, 2007, 2010; Hoffland et al., 2004). Through all these reactions weathering rates are accelerated at the zone of contact between mineral and fungi (Balogh-Brunstad et al., 2008; Li et al., 2016).

The similarity between both experiments in the early stages of the dissolution experiment indicates that the abiotic incongruent dissolution dominates the initial phase of dissolution. Measured DNA amounts show slow fungal growth during this period. In both experiments the initial formation of the amorphous Si surface layer appears to limit the rate of Mg release, and this process appears to be insensitive to the presence of the fungus. However, after 20 days cell numbers as quantified by DNA mass (Fig. 1c) increase substantially, and accelerate the release of Mg and Si in comparison to the abiotic experiments (Fig. 4). Although the presence of *K. petricola* enhances the release of Mg and Si, the release is still congruent in terms of $^{26}Mg/^{24}Mg$ and stoichiometric in terms of Mg/Si as in the abiotic experiments. We speculate that *K. petricola* acidifies the micro-environment of the mineral supplying more protons to diffuse through the Si-rich amorphous layer. This additional provision of protons by *K. petricola* accelerates the olivine dissolution rate which however follows the same net reactions for congruent Mg and Si release as in the abiotic process previously described. We note that the Fe amount in the bulk solution increases in the later phase of the biotic experiment. The Fe release in the presence of *K. petricola* could be either due to the dissolution of the Fe(III) phase by micro-environment acidification of the Si-rich amorphous layer, or to the release of siderophores to form soluble Fe(III) complexes. Regardless of the cause, the dissolution of precipitated Fe(III) phases increases the permeability of the Si-rich amorphous layer. This increased permeability, induced by the presence of *K. petricola*, in turn contributes to the faster olivine dissolution in the biotic experiment.

Despite the differences in dissolution rate the isotopic composition of the bulk solution did not differ between the abiotic and biotic experiment. The initial enrichment of ^{24}Mg in the growth solution indicates preferential release of light Mg isotopes during the proton exchange reactions (eq. 2). The preferred release of light ^{24}Mg over ^{26}Mg is attributed to a surface kinetic effect where the irreversible detachment of Mg in the active layer (eq. 2) is a fast forward reaction entailing this isotope effect (DePaolo, 2011; Maher et al., 2016). As stated in section 3 an equilibrium isotope effect could not be resolved from a kinetic effect from the slope of the mass-dependent fractionation line (Figure 2a and 2b). When the dissolution reaction progresses towards the stoichiometric Mg and Si release stage, the isotopic composition of the bulk solution approaches that of bulk olivine too (Figure. 3). At this stage, steady-state dissolution develops, where the dissolution of ^{26}Mg outwards in the active layer counterbalances the preferential release of ^{24}Mg inwards in the layer as was observed for Fe, Mg, and, Si isotopes in mineral dissolution studies (Brantley et al., 2004; Wiederhold et al., 2006; Wimpenny et al., 2010; Ziegler et al., 2005). We can exclude that the shift towards high $\delta^{26}Mg$ is due to uptake

of Mg by the fungus. First, Pokharel et al. (2017) has observed that *K. petricola* incorporates heavier Mg isotope from the growth solution, which is the opposite direction. Secondly, Pokharel et al. (2017) showed that a gram of dry cells of *K. petricola* incorporates about 365 µg of Mg. Considering that the dry weight of *K. petricola* at the end of 94 days was only about 41 mg indicates that the amount of Mg uptake by the fungi from the growth solution is negligible (less than 1%) when compared to the amount released by olivine. To summarize, that the temporal evolution of the chemistry and the isotope ratios released do not differ between the biotic and the abiotic dissolution experiment shows that the fungus does not directly affect the release of Mg. That the release rates differ nevertheless shows that it is the interaction of the fungus with the amorphous silica layer that indirectly accelerates olivine dissolution.

4.4.2 Comparing olivine dissolution rates

Literature data (laboratory experimental studies and review articles) on abiotic olivine dissolution rates measured at near neutral pH (6-8), average Earth surface temperature (19^{o} C to 25^{o} C) and under low CO_2 conditions, range from 10^{-14} - $10^{-16.4}$ mol cm^{-2} s^{-1} (Brantley et al., 2008; Crundwell, 2014; Gislason et al., 2014; Golubev et al., 2005; Luce et al., 1972; Pokrovsky and Schott, 2000b; Renforth et al., 2015; Rimstidt et al., 2012; Wogelius and Walther, 1991), whereas the dissolution rates measured in our experiments in the congruent phase are 10^{-15} mol cm^{-2} s^{-1} for the biotic and 10^{-16} mol cm^{-2} s^{-1} for the abiotic experiment. However, it is important to discuss whether mineral weathering rates calculated from a short-term (< 1 yr) controlled laboratory experiment can be used to predict weathering rates in the complex environment of the Earth's surface. Comparison between laboratory and field silicate mineral weathering rates shows significant differences, with laboratory experiment typically being orders of magnitude higher than field rates (Gruber et al., 2014; White and Brantley, 2003). Differences in parameters like surface area, solution composition, fluid residence time, and covering of primary by secondary minerals cause these discrepancies. Also the presence of organisms can induce such differences. Oelkers et al. (2015) conducted a 5 year long forsterite mineral dissolution. The results showed that dissolution of forsterite is slowed by an order of magnitude from the short-term dissolution rates and they attributed this to the growth of microbial communities on the surface of olivine. The second observation in that study was that the batch solution isotope composition was isotopically heavier in Mg than the dissolving forsterite, a contradiction from what is typically observed in short-term laboratory experiments and field sites. The contradicting nature of these observations question whether, and what type of closed-system laboratory batch experiment setup correctly represent processes taking place in natural field settings that evolve over thousands of years.

4.4.3 Implications for soil pore water isotope composition

Weathering isotope models typically assume isotopically congruent dissolution over time scales of decades to millennia over which soil formation, weathering and erosion shape landscapes, meaning that solutes released from primary minerals obtain the isotope ratios of the primary mineral (Bouchez et al., 2013). At the first sight the initial release of Mg low in δ^{26}Mg found in this and other studies (Maher et al., 2016; Oelkers et al., 2015) seems to invalidate this assumption. Further, in most weathering settings the dissolved Mg in soil pore water and rivers tends to be slightly lower in δ^{26}Mg relative to the dissolving rock (Mavromatis et al., 2014; Opfergelt et al., 2014; Tipper et al., 2010; Uhlig et al., 2017), which apparently supports incongruent release of light Mg isotopes. However, it is likely that this fractionation occurs during clay formation where the heavier Mg isotopes are preferentially incorporated into the clay structure (Ryu et al., 2016; Wimpenny et al., 2014), or by uptake of Mg into higher plants and/or fungi (Black et al., 2008; Bolou-Bi et al., 2010; Kimmig et al., 2018; Pokharel et al., 2017; Uhlig et al., 2017). However, the experimental results in this and in previous studies (mentioned above) also show that the initial isotope effect subsides after a few days or weeks. Hence, it is more likely that during slow natural weathering processes steady state mineral dissolution is attained over long time scales. Only during very low fluid/rock ratios and initial exposure of mineral surfaces to solutions, such as in deep fracture flow or in minerals or aquifers used for CO_2 sequestration might this effect become apparent.

4.4.4 Implications for CO_2 storage

Artificial dispersal of silicate mineral like olivine onto the Earth's surface or injection of CO_2 into ultramafic rock structures has been proposed as a means of CO_2 sequestration ("enhanced weathering") (Johnson et al., 2014; Moosdorf et al., 2014; Schuiling et al., 1986; Schuiling and Krijgsman, 2006; Taylor et al., 2015). The formation of an amorphous Si layer significantly decreases release of Mg from the olivine mineral, hence limiting the pool of readily available Mg^{2+} for storage of CO_2 through carbonation reactions. However our short-term laboratory experiment indicates that the presence of *K. petricola* accelerated Mg release rates by a factor of seven in comparison to the abiotic controls. If valid over the 100 years scale of CO_2 sequestration our results suggest the that addition of a rock-inhabiting black fungus with the ground olivine in the "enhanced weathering" settings could provide a more efficient way to withdraw CO_2 from the atmosphere.

4.5 Conclusion

Laboratory dissolution experiments with the black fungus *K. petricola* enhanced olivine dissolution rates seven times over those in the abiotic controls. Despite faster Mg and Si release, the biotic experiment followed the same trend as the abiotic experiment in terms of the initial non-stoichiometric to the later stoichiometric Mg and Si release from the dissolving olivine, and the initial preferential release of isotopically light Mg to the later release of Mg that is isotopically congruent in its $^{26}Mg/^{24}Mg$ ratio. The initial non-stoichiometric phase was attributed to rapid exchange of Mg^{2+} with H^{+} along with simultaneous polymerization of Si tetrahedra causing higher dissolution rates, whereas the stoichiometric phase was influenced by the buildup of the Si-rich amorphous layer that slowed the dissolution rates. The absence of differences in the temporal evolution of both the Mg/Si released and isotope ratio of the Mg released between the biotic and abiotic experiment indicates that in the presence of the fungi, olivine dissolves in the same way as in the abiotic process. We suggest the accelerated dissolution rate during the stoichiometric phase in the presence of *K. petricola* is due to provision of additional protons by fungal biochemical processes that acidify the micro-environment of the Si-rich amorphous surface layer to which *K. petricola* is attached. These additional protons will diffuse inwards into the amorphous Si layer where they react with the olivine surface, and eventually release Mg and Si into the solution. Our results also indicate that the presence of Fe precipitates in the Si-rich amorphous phase retards olivine dissolution rates. Through biomechanical and biochemical mechanism *K. petricola* dissolves the Fe precipitates, thereby making the Si-rich amorphous layer more porous which increases the olivine dissolution rates. Our Mg isotope study shows a distinct initial phase of ^{24}Mg release and indicates that Mg isotopes can trace incipient rock weathering. The enhanced biotic dissolution rates suggest that the presence of a rock-dissolving fungus in weathering settings or in CO_2 sequestration experiments may aid to accelerate CO_2 binding.

4.6 Supporting Information

Table S1: Analysis of quality control standards for ICP-OES

Name	In (µg/g)	Sc (µg/g)	Mg (µg/g)	Fe (µg/g)
Standard 1: Reference value (Stock: Merck Certipur Multi-element standard)	1.01	0.46	1.01	1.01
Measured value (n=12)	1.02	0.47	1.01	1.00
2SD	0.01	0.01	0.04	0.02
Measured deviation from reference value (%)	**0.7**	**1.8**	**0.3**	**-0.4**
Standard 2: Reference value (Stock: Merck Certipur Multi-element standard)			0.88	0.88
Measured value (n=2)			0.83	0.86
2SD			0.01	0.01
Measured deviation from reference value (%)			**-5.2**	**-2.1**

Results of concentration analysis of reference material by Inductively Coupled Plasma Optical Emission Spectrometry (ICP-OES, Varian 720-ES). Reference materials were prepared from manually diluting and weighing the ICP multiple element standard solutions. Both standards were prepared in 0.3 M HNO3 and 1 mg/g Cs, made from Merck Certipur multi-element standards with certified concentrations traceable to NIST reference materials. The mean results of n replicates are given together with 2SD (representing 95% of the population). The measured deviation from the reference value is a quantitative indication of accuracy.

Table S2: Mg isotope analysis of pure and doped standards

Standards	δ^{26}Mg (‰) ± 2SD	Runs
Cam-1 Pure	-2.70 ± 0.1	45
BHVO-2 Pure	-0.26 ± 0.1	16
Cam-1-doped	-2.88 ± 0.1	8
BHVO-2 doped	-0.27 ± 0.1	8

Results of Mg isotopes analysis of reference material used. All reference material solutions were diluted to 500 ng/ml Mg for MC-ICP-MS analysis and were measured by sample-standard bracketing with DSM3 solution of the same concentration. Doped solutions indicate that pure Mg solutions (500 ng/ml Mg) were doped with the input solution. The mean δ^{26}Mg values of n replicate analysis is given relative to DSM3 (= 0‰). Analytical repeatability of each reference material was within the uncertainty of the MC-ICP-MC analytical method, estimated at ± 0.10‰ for δ^{26}Mg.

Table S3: Concentration and Mg isotope measurements of biomass and growth solution

				Solution					
Experiment	**Replicate number**	**Time (Days)**		**pH**	**[a]Mg (moles)**	**[a]Si (moles)**	**[a]Fe (moles)**	**[b]$\delta^{25}Mg_{solution,DSM3}$ (‰)**	**[b]$\delta^{26}Mg_{solution,DSM3}$ (‰)**
Abiotic	**Initial growth solution**		0	5.86	0	0	0		
	1		0.04	6.24	3.02E-05	1.05E-05	1.22E-07	-0.37	-0.73
	2		0.04		3.77E-05	1.17E-05	1.05E-07	-0.39	-0.77
	3		0.04		3.52E-05	8.75E-06	7.22E-08	-0.34	-0.64
		Mean			3.44E-05	1.03E-05	9.98E-08	-0.37	-0.71
		2SD			0.63E-05	0.24E-05	4.15E-08	0.05	0.13
	1		0.25	6.25	5.02E-05	2.12E-05	1.93E-07	-0.29	-0.56
	2		0.25		5.27E-05	2.19E-05	1.91E-07	-0.30	-0.61
	3		0.25		5.62E-05	2.13E-05	1.55E-07	-0.35	-0.68
		Mean			5.30E-05	2.15E-05	1.80E-07	-0.31	-0.62
		2SD			0.50E-05	0.05E-05	0.35E-07	0.06	0.12
	1		1	6.28	6.13E-05	3.04E-05	1.50E-07		
	2		1		6.73E-05	3.25E-05	1.68E-07	-0.30	-0.60
	3		1		6.98E-05	3.19E-05	1.35E-07	-0.24	-0.48
		Mean			6.61E-05	3.16E-05	1.51E-07	-0.27	-0.54
		2SD			0.72E-05	0.18E-05	0.27E-07	0.10	0.18
	1		2	6.26	6.61E-05	3.39E-05	1.23E-07		
	2		2		7.11E-05	3.48E-05	1.23E-07	-0.29	-0.53
	3		2		7.39E-05	3.51E-05	1.17E-07	-0.24	-0.51
		Mean			7.04E-05	3.46E-05	1.21E-07	-0.26	-0.52
		2SD			0.65E-05	0.11E-05	0.05E-07	0.06	0.03
	1		6	6.3	7.46E-05	4.00E-05	8.28E-08	-0.22	-0.44
	2		6		8.03E-05	4.21E-05	9.54E-08	-0.27	-0.56
	3		6		8.23E-05	4.16E-05	8.95E-08		
		Mean			7.91E-05	4.12E-05	8.92E-08	-0.25	-0.50
		2SD			0.65E-05	0.18E-05	1.03E-08	0.08	0.16
	1		15	6.3	8.07E-05	4.32E-05	3.57E-08		
	2		15		8.75E-05	4.68E-05	4.80E-08	-0.23	-0.46
	3		15		8.96E-05	4.71E-05	4.93E-08	-0.21	-0.40
		Mean			8.60E-05	4.57E-05	4.44E-08	-0.22	-0.43
		2SD			0.76E-05	0.35E-05	1.22E-08	0.04	0.08
	1		28	6.29	8.61E-05	4.69E-05	2.52E-08		
	2		28		9.28E-05	4.88E-05	2.47E-08	-0.25	-0.47
	3		28		9.57E-05	5.02E-05	3.33E-08	-0.26	-0.51
		Mean			9.15E-05	4.86E-05	2.77E-08	-0.26	-0.49
		2SD			0.80E-05	0.27E-05	0.79E-08	0.02	0.05
	1		41	6.28	8.96E-05	4.87E-05	2.41E-08	-0.21	-0.43
	2		41		9.65E-05	5.21E-05	2.76E-08	-0.22	-0.44
	3		41		9.90E-05	5.26E-05	7.35E-08	-0.26	-0.54
		Mean			9.51E-05	5.11E-05	4.17E-08	-0.23	-0.47
		2SD			0.80E-05	0.35E-05	4.50E-08	0.05	0.12
	1		94	6.20	9.65E-05	5.41E-05	3.98E-08	-0.18	-0.34
	2		94		1.02E-04	5.67E-05	8.58E-08	-0.19	-0.39
	3		94		1.06E-04	5.86E-05	6.66E-08	-0.21	-0.40
		Mean			1.02E-04	5.65E-05	6.41E-08	-0.19	-0.38
		2SD			0.08E-04	0.37E-05	3.77E-08	0.03	0.06
Biotic	**Initial growth solution**		0	5.86	0	0	0		

1		0.04	6.23	2.75E-05	6.08E-06	1.01E-07	-0.34	-0.66
2		0.04		3.26E-05	9.96E-06	1.38E-07	-0.40	-0.78
3		0.04		2.71E-05	8.99E-06	2.70E-07	-0.35	-0.67
	Mean			2.91E-05	8.35E-06	1.70E-07	-0.36	-0.70
	2SD			0.50E-05	3.30E-06	1.45E-07	0.07	0.13
1		0.25	6.25	4.03E-05	1.40E-05	9.83E-08	-0.27	-0.51
2		0.25		5.30E-05	2.15E-05	1.09E-07	-0.30	-0.60
3		0.25		4.03E-05	1.69E-05	1.01E-07	-0.26	-0.52
	Mean			4.45E-05	1.75E-05	1.03E-07	-0.28	-0.54
	2SD			1.20E-05	0.61E-05	0.09E-07	0.05	0.09
1		1	6.26	5.05E-05	2.15E-05	7.68E-08	-0.19	-0.41
2		1		6.56E-05	3.07E-05	1.10E-07	-0.30	-0.59
3		1		5.20E-05	2.48E-05	1.01E-07	-0.31	-0.59
	Mean			5.60E-05	2.57E-05	9.60E-08	-0.27	-0.53
	2SD			1.36E-05	0.76E-05	2.82E-08	0.13	0.21
1		2	6.26	5.66E-05	2.57E-05	7.63E-08	-0.22	-0.44
2		2		7.27E-05	3.59E-05	9.41E-08	-0.28	-0.53
3		2		5.87E-05	2.96E-05	2.87E-07	-0.21	-0.45
	Mean			6.26E-05	3.04E-05	1.52E-07	-0.24	-0.48
	2SD			1.43E-05	0.84E-05	1.90E-07	0.07	0.10
1		6	6.25	7.16E-05	3.55E-05	6.43E-08		
2		6		8.85E-05	4.67E-05	8.95E-08	-0.29	-0.55
3		6		7.40E-05	3.95E-05	5.01E-08		
	Mean			7.80E-05	4.06E-05	6.79E-08	-0.29	-0.55
	2SD			1.50E-05	0.93E-05	3.27E-08		
1		15	6.19	9.01E-05	4.77E-05	7.67E-08	-0.20	-0.38
2		15		1.08E-04	6.00E-05	5.15E-08	-0.20	-0.40
3		15		9.21E-05	5.12E-05	5.46E-08	-0.32	-0.59
	Mean			9.68E-05	5.30E-05	6.09E-08	-0.24	-0.46
	2SD			1.62E-05	1.03E-05	2.25E-08	0.13	0.23
1		28	6.16	1.68E-04	9.54E-05	2.42E-07	-0.18	-0.35
2		28		1.54E-04	8.80E-05	9.91E-08	-0.26	-0.54
3		28		1.55E-04	8.95E-05	1.49E-07	-0.25	-0.50
	Mean			1.59E-04	9.10E-05	1.63E-07	-0.23	-0.46
	2SD			0.13E-04	0.63E-05	1.18E-07	0.09	0.20
1		41	6.15	1.80E-04	1.02E-04	3.07E-07	-0.13	-0.28
2		41		1.81E-04	1.02E-04	1.22E-07	-0.25	-0.50
3		41		1.70E-04	9.58E-05	1.92E-07	-0.27	-0.53
	Mean			1.77E-04	9.98E-05	2.07E-07	-0.22	-0.44
	2SD			0.09E-04	0.56E-05	1.52E-07	0.15	0.27
1		94	6.08	2.35E-04	1.44E-04	5.61E-07	-0.13	-0.24
2		94		2.25E-04	1.36E-04	2.65E-07	-0.20	-0.41
3		94		2.12E-04	1.29E-04	3.33E-07	-0.22	-0.42
	Mean			2.24E-04	1.36E-04	3.87E-07	-0.18	-0.36
	2SD			0.18E-04	0.12E-04	2.53E-07	0.10	0.19

[a]Element concentrations were measured by ICP-OES with analytical uncertainties estimated to be about ± 5% relative (95% confidence) based on repeat measurements of quality control standards. Calibration of the ICP-OES was made with multi-elements standard solutions.

[b]Mg isotopes measurement (δ^{25}Mg and δ^{26}Mg) using MC-ICPMS. analytical uncertainties for each individual experiment are estimated based on repeat reference material measurements processed through

the Mg column chemistry and are ±0.10‰ (2SD, δ^{25}Mg) and ±0.06‰ (2SD, δ^{26}Mg). Multiple MC-ICP-MS measurements of each sample solution were always repeatable within the stated uncertainties. All d-values are reported relative to the international measurement standard DSM3.

Table S4: Olivine dissolution rate calculation at each sampling point for both abiotic and biotic dissolution experiments

Experiment	Time (Days)	Volume of solution (mL)	[a]Amount of olivine (g)	pH of solution	[e]2SD	Mg amount in solution (moles)	[f]2SD	[b]Surface area olivine (cm^2)	[e]2SD	[c]Oiivine stoichiometric factor Mg	[e]2SD	[d]Olivine Dissolution Rates (mol cm^{-2} s^{-1})	[f]2SD
Abiotic	0	400	4	6.21	0.02	0	0	5872	1057	1.86	0.03		
	0.04	400	4	6.24	0.02	3.44E-05	0.63E-05	5872	1057	1.86	0.03	8.74E-13	1.64E-13
	0.25	395	3.95	6.25	0.02	5.30E-05	0.50E-05	5799	1044	1.86	0.03	9.62E-14	2.70E-14
	1	390	3.9	6.28	0.02	6.61E-05	0.72E-05	5725	1031	1.86	0.03	1.90E-14	0.43E-14
	2	385	3.85	6.26	0.02	7.04E-05	0.65E-05	5652	1017	1.86	0.03	4.67E-15	1.05E-15
	6	380	3.8	6.30	0.02	7.91E-05	0.65E-05	5578	1004	1.86	0.03	2.43E-15	0.46E-15
	15	375	3.75	6.30	0.02	8.60E-05	0.76E-05	5505	991	1.86	0.03	8.62E-16	1.62E-16
	28	370	3.7	6.29	0.02	9.15E-05	0.80E-05	5432	978	1.86	0.03	4.89E-16	0.92E-16
	41	365	3.65	6.28	0.02	9.51E-05	0.80E-05	5358	964	1.86	0.03	3.16E-16	0.60E-17
	94	360	3.6	6.20	0.02	1.02E-04	0.08E-04	5285	951	1.86	0.03	1.43E-16	0.38E-16
Biotic	0	400	4	6.21	0.02	0	0	5872	1057	1.86	0.03		
	0.04	400	4	6.23	0.02	2.91E-05	0.50E-05	5872	1057	1.86	0.03	7.40E-13	1.39E-13
	0.25	395	3.95	6.25	0.02	4.45E-05	1.20E-05	5799	1044	1.86	0.03	7.95E-14	3.62E-14
	1	390	3.9	6.26	0.02	5.60E-05	1.36E-05	5725	1031	1.86	0.03	1.67E-14	0.31E-14
	2	385	3.85	6.26	0.02	6.26E-05	1.43E-05	5652	1017	1.86	0.03	7.28E-15	1.36E-15
	6	380	3.8	6.25	0.02	7.80E-05	1.49E-05	5578	1004	1.86	0.03	4.29E-15	0.80E-15
	15	375	3.75	6.19	0.02	9.68E-05	1.62E-05	5505	991	1.86	0.03	2.36E-15	0.44E-15
	28	370	3.7	6.16	0.02	1.59E-04	0.13E-04	5432	978	1.86	0.03	5.48E-15	2.35E-15
	41	365	3.65	6.15	0.02	1.77E-04	0.09E-04	5358	964	1.86	0.03	1.61E-15	1.14E-15
	94	360	3.6	6.08	0.02	2.24E-04	0.18E-04	5285	951	1.86	0.03	1.04E-15	0.24E-15

[a]Amount of olivine in the batch experiment accounted for the loss of 0.05g at each sampling point.
[b]Surface area of the olivine at the respective sampling time. It is calculated my multiplying the initial (unreacted) olivine surface area with the amount of olivine present in the batch experiment.[c]The stoichiometric factor of the initial olivine measured using electron microprobe.

[d]Instantaneous olivine dissolution rates calculated between two consecutive sampling points.
[e]2SD represents the analytical uncertainty for individual measurement.
[f]2SD represents analytical uncertainty for an individual measurement or uncertainty derived from the repeatability of three independent experiments, whichever was larger.

References

Adeyemi, A.O. and Gadd, G.M. (2005) Fungal degradation of calcium-, lead- and silicon-bearing minerals. Biometals 18, 269-281.

Alatossava, T., Jütte, H., Kuhn, A. and Kellenberger, E. (1985) Manipulation of intracellular magnesium content in polymyxin B nonapeptide-sensitized Escherichia coli by ionophore A23187. Journal of Bacteriology 162, 413-419.

Balogh-Brunstad, Z., Kent Keller, C., Thomas Dickinson, J., Stevens, F., Li, C.Y. and Bormann, B.T. (2008) Biotite weathering and nutrient uptake by ectomycorrhizal fungus, Suillus tomentosus, in liquid-culture experiments. Geochimica et Cosmochimica Acta 72, 2601-2618.

Banfield, J.F., Barker, W.W., Welch, S.A. and Taunton, A. (1999) Biological impact on mineral dissolution: Application of the lichen model to understanding mineral weathering in the rhizosphere. Proceedings of the National Academy of Sciences 96, 3404-3411.

Bardgett, R.D., Wardle, D.A. and Yeates, G.W. (1998) Linking above-ground and below-ground interactions: how plant responses to foliar herbivory influence soil organisms. Soil Biology and Biochemistry 30, 1867-1878.

Bechinger, C., Giebel, K.-F., Schnell, M., Leiderer, P., Deising, H.B. and Bastmeyer, M. (1999) Optical Measurements of Invasive Forces Exerted by Appressoria of a Plant Pathogenic Fungus. Science 285, 1896.

Beeler, T., Bruce, K. and Dunn, T. (1997) Regulation of cellular Mg2+ by Saccharomyces cerevisiae. Biochimica et Biophysica Acta (BBA) - Biomembranes 1323, 310-318.

Bigeleisen, J. and Mayer, M.G. (1947a) Calculation of Equilibrium Constants for Isotopic Exchange Reactions. Journal of Chemical Physics 15, 261-267.

Bigeleisen, J. and Mayer, M.G. (1947b) Calculation of Equilibrium Constants for Isotopic Exchange Reactions. The Journal of Chemical Physics 15, 261-267.

Bindeman, I.N., Lundstrom, C.C., Bopp, C. and Huang, F. (2013) Stable isotope fractionation by thermal diffusion through partially molten wet and dry silicate rocks. Earth and Planetary Science Letters 365, 51-62.

Birle, J.D., Gibbs, G.V., Moore, P.B. and Smith, J.V. (1968) Crystal structures of natural olivines. American Mineralogist 53, 807-824.

Black, J., Emanuel Epstein, William D. Rains, Yin, Q.-z. and Casey, W.H. (2008) Magnesium-Isotope Fractionation During Plant Growth. Environmental Science & Technology 42, 7831-7836.

Black, J.R., Yin, Q.-z. and Casey, W.H. (2006) An experimental study of magnesium-isotope fractionation in chlorophyll-a photosynthesis. Geochimica et Cosmochimica Acta 70, 4072-4079.

Black, J.R., Yin, Q.-z., Rustad, J.R. and Casey, W.H. (2007) Magnesium Isotopic Equilibrium in Chlorophylls. Journal of the American Chemical Society 129, 8690-8691.

Bohn, T., Walczyk, T., Leisibach, S. and Hurrell, R.F. (2004) Chlorophyll-bound Magnesium in Commonly Consumed Vegetables and Fruits: Relevance to Magnesium Nutrition. Journal of Food Science 69, S347-S350.

Bolou-Bi, E.B., Poszwa, A., Leyval, C. and Vigier, N. (2010) Experimental determination of magnesium isotope fractionation during higher plant growth. Geochimica et Cosmochimica Acta 74, 2523-2537.

Bolou-Bi, E.B., Vigier, N., Brenot, A. and Poszwa, A. (2009) Magnesium Isotope Compositions of Natural Reference Materials. Geostandards and Geoanalytical Research 33, 95-109.

Bolou-Bi, E.B., Vigier, N., Poszwa, A., Boudot, J.-P. and Dambrine, E. (2012) Effects of biogeochemical processes on magnesium isotope variations in a forested catchment in the Vosges Mountains (France). Geochimica et Cosmochimica Acta 87, 341-355.

Bonneville, S., Mark M. Smits, Andrew Brown, John Harrington, Jonathan R. Leake, Rik Brydson and Benning, L.G. (2009) Plant-driven fungal weathering: Early stages of mineral alteration at the nanometer scale. Geology 37, 4.

Bonneville, S., Morgan, D.J., Schmalenberger, A., Bray, A., Brown, A., Banwart, S.A. and Benning, L.G. (2011) Tree-mycorrhiza symbiosis accelerate mineral weathering: Evidences from nanometer-scale elemental fluxes at the hypha–mineral interface. Geochimica et Cosmochimica Acta 75, 6988-7005.

Bouchez, J., von Blanckenburg, F. and Schuessler, J.A. (2013) Modeling novel stable isotope ratios in the weathering zone. American Journal of Science 313(4), 267-308.

Brantley, S., Kubicki, J. and F White, A. (2008) Kinetics of Water-Rock Interaction. Springer, New York, NY.

Brantley, S.L., Liermann, L.J., Guynn, R.L., Anbar, A., Icopini, G.A. and Barling, J. (2004) Fe isotopic fractionation during mineral dissolution with and without bacteria1. Geochimica et Cosmochimica Acta 68, 3189-3204.

Brown, G.E., Trainor, T.P. and Chaka, A.M. (2008) Chapter 7 - Geochemistry of Mineral Surfaces and Factors Affecting Their Chemical Reactivity, in: Nilsson, A., Pettersson, L.G.M., Nørskov, J.K. (Eds.), Chemical Bonding at Surfaces and Interfaces. Elsevier, Amsterdam, pp. 457-509.

Burford, E.P., Fomina, M. and Gadd, G.M. (2003a) Fungal involvement in bioweathering and biotransformation of rocks and minerals. Mineralogical Magazine 67, 1127-1155.

Burford, E.P., Kierans, M. and Gadd, G.M. (2003b) Geomycology: fungi in mineral substrata. Mycologist 17, 98-107.

Callot, G., Maurette, M., Pottier, L. and Dubois, A. (1987) Biogenic etching of microfractures in amorphous and crystalline silicates. Nature 328, 147.

Campbell, E. and Meeks, J.C. (1992) Evidence for plant-mediated regulation of nitrogenase expression in the Anthoceros-Nostoc symbiotic association.

Chang, V.T.C., Williams, R.J.P., Makishima, A., Belshawl, N.S. and O'Nions, R.K. (2004) Mg and Ca isotope fractionation during CaCO3 biomineralisation. Biochemical and Biophysical Research Communications 323, 79-85.

Chapela Lara, M., Buss, H.L., Pogge von Strandmann, P.A.E., Schuessler, J.A. and Moore, O.W. (2017) The influence of critical zone processes on the Mg isotope budget in a tropical, highly weathered andesitic catchment. Geochimica et Cosmochimica Acta 202, 77-100.

Chen, J., Blume, H.-P. and Beyer, L. (2000) Weathering of rocks induced by lichen colonization — a review. CATENA 39, 121-146.

Chizhikova, N., Lessovaia, S. and Gorbushina, A. (2016) Biogenic Weathering of Mineral Substrates (Review). Springer

Cooper, D.C., Picardal, F.F. and Coby, A.J. (2006) Interactions between Microbial Iron Reduction and Metal Geochemistry: Effect of Redox Cycling on Transition Metal Speciation in Iron Bearing Sediments. Environmental Science & Technology 40, 1884-1891.

Coplen, T.B. (2011) Guidelines and recommended terms for expression of stable-isotope-ratio and gas-ratio measurement results. Rapid Communications in Mass Spectrometry 25, 2538-2560.

Criss, R.E. (1999) Principles of Stable Isotope Distribution. . Oxford University Press.

Crundwell, F.K. (2014) The mechanism of dissolution of forsterite, olivine and minerals of the orthosilicate group. Hydrometallurgy 150, 68-82.

Daghino, S., Martino, E. and Perotto, S. (2010) Fungal weathering and implications in the solubilization of metals from soil and from asbestos fibres.

Daval, D., Sissmann, O., Menguy, N., Saldi, G.D., Guyot, F., Martinez, I., Corvisier, J., Garcia, B., Machouk, I., Knauss, K.G. and Hellmann, R. (2011) Influence of amorphous silica layer formation on the dissolution rate of olivine at 90°C and elevated pCO2. Chemical Geology 284, 193-209.

DePaolo, D.J. (2011) Surface kinetic model for isotopic and trace element fractionation during precipitation of calcite from aqueous solutions. Geochimica et Cosmochimica Acta 75, 1039-1056.

Drever, J.I. (1994) The effect of land plants on weathering rates of silicate minerals. Geochimica et Cosmochimica Acta 58, 2325-2332.

Duane, M.J. (2006) Coeval biochemical and biophysical weathering processes on Quaternary sandstone terraces south of Rabat (Temara), northwest Morocco. Earth Surface Processes and Landforms 31, 1115-1128.

Ehrlich, H.L. (1996) How microbes influence mineral growth and dissolution. Chemical Geology 132, 5-9.

Ekman, M., Picossi, S., Campbell, E.L., Meeks, J.C. and Flores, E. (2013) A Nostoc punctiforme Sugar Transporter Necessary to Establish a Cyanobacterium-Plant Symbiosis. Plant Physiology 161, 1984-1992.

Fahad, Z.A., Bolou-Bi, E.B., Köhler, S.J., Finlay, R.D. and Mahmood, S. (2016) Fractionation and assimilation of Mg isotopes by fungi is species dependent. Environmental Microbiology Reports 8, 956-965.

Finlay, R., Wallander, H., Smits, M., Holmstrom, S., van Hees, P., Lian, B. and Rosling, A. (2009) The role of fungi in biogenic weathering in boreal forest soils. Fungal Biology Reviews 23, 101-106.

Flatman, P. (1984) Magnesium transport across cell membranes. J Membr Biol 80, 1-14.

Froschauer, E.M., Kolisek, M., Dieterich, F., Schweigel, M. and Schweyen, R.J. (2004) Fluorescence measurements of free [Mg2+] by use of mag-fura 2 in Salmonella enterica. FEMS Microbiology Letters 237, 49-55.

Gadd, G.M. (2007) Geomycology: biogeochemical transformations of rocks, minerals, metals and radionuclides by fungi, bioweathering and bioremediation. Mycological Research 111, 3-49.

Gadd, G.M. (2010) Metals, minerals and microbes: geomicrobiology and bioremediation. Microbiology 156, 609-643.

Gadd, G.M. (2017) Fungi, Rocks, and Minerals. Elements 13, 171-176.

Galy, A., Bar-Matthews, M., Halicz, L. and O'Nions, R.K. (2002) Mg isotopic composition of carbonate: insight from speleothem formation. Earth and Planetary Science Letters 201, 105-115.

Gao, T., Ke, S., Teng, F.-Z., Chen, S., He, Y. and Li, S.-G. (2016) Magnesium isotope fractionation during dolostone weathering. Chemical Geology 445, 14-23.

Gardner, R.C. (2003) Genes for magnesium transport. Current Opinion in Plant Biology 6, 263-267.

Gislason, S.R., Broecker, W.S., Gunnlaugsson, E., Snæbjörnsdóttir, S., Mesfin, K.G., Alfredsson, H.A., Aradottir, E.S., Sigfusson, B., Gunnarsson, I., Stute, M., Matter, J.M., Arnarson, M.T., Galeczka, I.M., Gudbrandsson, S., Stockman, G., Boenisch, D.W., Stefansson, A., Ragnheidardottir, E., Flaathen, T., Gysi, A.P., Olssen, J., Didriksen, K., Stipp, S., Menez, B. and Oelkers, E.H. (2014) Rapid solubility and mineral storage of CO2 in basalt. Energy Procedia 63, 4561-4574.

Golubev, S.V., Pokrovsky, O.S. and Schott, J. (2005) Experimental determination of the effect of dissolved CO2 on the dissolution kinetics of Mg and Ca silicates at 25 °C. Chemical Geology 217, 227-238.

Gorbushina, A.A. (2007) Life on the rocks. Environmental Microbiology 9, 1613-1631.

Gorbushina, A.A. and Broughton, W.J. (2009) Microbiology of the Atmosphere-Rock Interface: How Biological Interactions and Physical Stresses Modulate a Sophisticated Microbial Ecosystem. Annual Review of Microbiology 63, 431-450.

Gorbushina, A.A., Kotlova, E.R. and Sherstneva, O.A. (2008) Cellular responses of microcolonial rock fungi to long-term desiccation and subsequent rehydration. Studies in Mycology 61, 91-97.

Groisman, E.A., Hollands, K., Kriner, M.A., Lee, E.-J., Park, S.-Y. and Pontes, M.H. (2013) Bacterial Mg(2+) Homeostasis, Transport, and Virulence. Annual review of genetics 47, 625-646.

Grubbs, R.D. (2002) Intracellular magnesium and magnesium buffering. Biometals 15, 251-259.

Gruber, C., Zhu, C., Georg, R.B., Zakon, Y. and Ganor, J. (2014) Resolving the gap between laboratory and field rates of feldspar weathering. Geochimica et Cosmochimica Acta 147, 90-106.

Gussone, N., Eisenhauer, A., Heuser, A., Dietzel, M., Bock, B., Böhm, F., Spero, H.J., Lea, D.W., Bijma, J. and Nägler, T.F. (2003) Model for kinetic effects on calcium isotope fractionation (δ44Ca) in inorganic aragonite and cultured planktonic foraminifera. Geochimica et Cosmochimica Acta 67, 1375-1382.

Gussone, N., Langer, G., Thoms, S., Nehrke, G., Eisenhauer, A., Riebesell, U. and Wefer, G. (2006) Cellular calcium pathways and isotope fractionation in Emiliania huxleyi. Geology 34, 625-628.

Hagerberg, D., Thelin, G. and Wallander, H. (2003) The production of ectomycorrhizal mycelium in forests: Relation between forest nutrient status and local mineral sources. Plant and Soil 252, 279-290.

Harley, J.L. and Smith, S.E. (1983) Mycorrhizal symbiosis. Academic Press Inc., London; New York, USA.

Harold, F.M. (2002) Force and compliance: rethinking morphogenesis in walled cells. Fungal genetics and biology : FG & B 37, 271-282.

Hawkesford, M., Horst, W., Kichey, T., Lambers, H., Schjoerring, J., Møller, I.S. and White, P. (2012) Chapter 6 - Functions of Macronutrients A2 - Marschner, Petra, Marschner's Mineral Nutrition of Higher Plants (Third Edition). Academic Press, San Diego, pp. 135-189.

Hawksworth, D.L. (1988) The variety of fungal-algal symbioses, their evolutionary significance, and the nature of lichens. Botanical Journal of the Linnean Society 96, 3-20.

Hellmann, R., Wirth, R., Daval, D., Barnes, J.-P., Penisson, J.-M., Tisserand, D., Epicier, T., Florin, B. and Hervig, R.L. (2012) Unifying natural and laboratory chemical weathering with interfacial dissolution–reprecipitation: A study based on the nanometer-scale chemistry of fluid–silicate interfaces. Chemical Geology 294–295, 203-216.

Henderson, M.E.K. and Duff, R.B. (1963) The release of metallic and silicate ions from minerals, rocks, and soils by fungal activity. Journal of Soil Science 14, 236-246.

Hendry, K.R. and Robinson, L.F. (2012) The relationship between silicon isotope fractionation in sponges and silicic acid concentration: Modern and core-top studies of biogenic opal. Geochimica et Cosmochimica Acta 81, 1-12.

Hirsch, P., Eckhardt, F.E.W. and Palmer Jr, R.J. (1995) Fungi active in weathering of rock and stone monuments. Canadian Journal of Botany 73, 1384-1390.

Hochella, M.F. (2002) Sustaining Earth: Thoughts on the present and future roles of mineralogy in environmental science. Mineralogical Magazine 66, 627-652.

Hoffland, E., Kuyper, T.W., Wallander, H., Plassard, C., Gorbushina, A.A., Haselwandter, K., Holmström, S., Landeweert, R., Lundström, U.S., Rosling, A., Sen, R., Smits, M.M., van Hees, P.A.W. and van Breemen, N. (2004) The role of fungi in weathering. Frontiers in Ecology and the Environment 2, 258-264.

Jacoby, R., Peukert, M., Succurro, A., Koprivova, A. and Kopriva, S. (2017) The Role of Soil Microorganisms in Plant Mineral Nutrition—Current Knowledge and Future Directions. Frontiers in Plant Science 8, 1617.

Johnson, C.M., Beard, B.L. and Albarède, F. (2004) Overview and General Concepts. Reviews in Mineralogy and Geochemistry 55, 1-24.

Johnson, D. and Gilbert, L. (2015) Interplant signalling through hyphal networks. New Phytologist 205, 1448-1453.

Johnson, N.C., Thomas, B., Maher, K., Rosenbauer, R.J., Bird, D. and Brown, G.E., Jr. (2014) Olivine dissolution and carbonation under conditions relevant for in situ carbon storage. Chemical Geology 373, 93-105.

Katz, J.J. (1968) Coordination Properties of Magnesium in Chlorophyll from IR and NMR Spectra, in: Baer, W.K., Perkins, A.J., Grove, E.L. (Eds.), Developments in Applied Spectroscopy: Selected papers from the Eighteenth Annual Mid-America Spectroscopy Symposium Held in Chicago, Illinios May 15–18, 1967. Springer US, Boston, MA, pp. 201-218.

Kehres, D.G. and Maguire, M.E. (2002) Structure, properties and regulation of magnesium transport proteins. Biometals 15, 261-270.

Kendall, C. and Caldwell, E.A. (1998) Chapter 2 - Fundamentals of Isotope Geochemistry, in: Kendall, C., McDonnell, J.J. (Eds.), Isotope Tracers in Catchment Hydrology. Elsevier, Amsterdam, pp. 51-86.

Kennedy, A.C. and de Luna, L.Z. (2005) RHIZOSPHERE, in: Hillel, D. (Ed.), Encyclopedia of Soils in the Environment. Elsevier, Oxford, pp. 399-406.

Kimmig, S.R., Holmden, C. and Bélanger, N. (2018) Biogeochemical cycling of Mg and its isotopes in a sugar maple forest in Québec. Geochimica et Cosmochimica Acta 230, 60-82.

Kirkby, E. (2012) Chapter 1 - Introduction, Definition and Classification of Nutrients A2 - Marschner, Petra, Marschner's Mineral Nutrition of Higher Plants (Third Edition). Academic Press, San Diego, pp. 3-5.

Köhler, I., Konhauser, K. and Kappler, A. (2010) Role of microorganisms in banded iron formations. In Geomicrobiology: Molecular and Environmental Perspective, pp. 309–324. Edited by L. Barton, M. Mandl & A. Loy. Berlin: Springer.

Kolesov, B.A. and Geiger, C.A. (2004) A Raman spectroscopic study of Fe–Mg olivines. Physics and Chemistry of Minerals 31, 142-154.

Krumbein, W.E. and Jens, K. (1981) Biogenic rock varnishes of the negev desert (Israel) an ecological study of iron and manganese transformation by cyanobacteria and fungi. Oecologia 50, 25-38.

Landeweert, R., Hoffland, E., Finlay, R.D., Kuyper, T.W. and van Breemen, N. (2001) Linking plants to rocks: ectomycorrhizal fungi mobilize nutrients from minerals. Trends in Ecology & Evolution 16, 248-254.

Lareen, A., Burton, F. and Schäfer, P. (2016) Plant root-microbe communication in shaping root microbiomes. Plant Molecular Biology 90, 575-587.

Li, L., Tutone, A.F., Drummond, R.S.M., Gardner, R.C. and Luan, S. (2001) A Novel Family of Magnesium Transport Genes in Arabidopsis. The Plant Cell 13, 2761-2775.

Li, Z., Liu, L., Chen, J. and Teng, H. (2016) Cellular dissolution at hypha- and spore-mineral interfaces revealing unrecognized mechanisms and scales of fungal weathering. Geology 44, 319-322.

Lindberg, P., Schütz, K., Happe, T. and Lindblad, P. (2002) A hydrogen-producing, hydrogenase-free mutant strain of Nostoc punctiforme ATCC 29133. International Journal of Hydrogen Energy 27, 1291-1296.

Liu, D., Liu, Y., Fang, S. and Tian, Y. (2015) Tree species composition influenced microbial diversity and nitrogen availability in rhizosphere soil. Plant, Soil and Environment 61, 438-443.

Liu, X.-M., Teng, F.-Z., Rudnick, R.L., McDonough, W.F. and Cummings, M.L. (2014) Massive magnesium depletion and isotope fractionation in weathered basalts. Geochimica et Cosmochimica Acta 135, 336-349.

Lovley, D.R., Holmes, D.E. and Nevin, K.P. (2004) Dissimilatory Fe(III) and Mn(IV) Reduction, Advances in Microbial Physiology. Academic Press, pp. 219-286.

Luce, R.W., Bartlett, R.W. and Parks, G.A. (1972) Dissolution kinetics of magnesium silicates. Geochimica et Cosmochimica Acta 36, 35-50.

Maguire, M. and Cowan, J. (2002) Magnesium chemistry and biochemistry. Biometals 15, 203-210.

Maguire, M.E. (2006) Magnesium transporters: properties, regulation and structure. Frontiers in bioscience : a journal and virtual library 11, 3149-3163.

Maher, K., Johnson, N.C., Jackson, A., Lammers, L.N., Torchinsky, A.B., Weaver, K.L., Bird, D.K. and Brown Jr, G.E. (2016) A spatially resolved surface kinetic model for forsterite dissolution. Geochimica et Cosmochimica Acta 174, 313-334.

Maroto-Valer, M.M., Fauth, D.J., Kuchta, M.E., Zhang, Y. and Andrésen, J.M. (2005) Activation of magnesium rich minerals as carbonation feedstock materials for CO2 sequestration. Fuel Processing Technology 86, 1627-1645.

Marschner, H. (1995) 8 - Functions of Mineral Nutrients: Macronutrients, Mineral Nutrition of Higher Plants (Second Edition). Academic Press, London, pp. 229-312.

Martin-Sanchez, P.M., Gorbushina, A.A., Kunte, H.-J. and Toepel, J. (2016) A novel qPCR protocol for the specific detection and quantification of the fuel-deteriorating fungus Hormoconis resinae. Biofouling 32, 635-644.

Mavromatis, V., Pearce, C.R., Shirokova, L.S., Bundeleva, I.A., Pokrovsky, O.S., Benezeth, P. and Oelkers, E.H. (2012) Magnesium isotope fractionation during hydrous magnesium carbonate precipitation with and without cyanobacteria. Geochimica et Cosmochimica Acta 76, 161-174.

Mavromatis, V., Prokushkin, A.S., Pokrovsky, O.S., Viers, J. and Korets, M.A. (2014) Magnesium isotopes in permafrost-dominated Central Siberian larch forest watersheds. Geochimica et Cosmochimica Acta 147, 76-89.

McClelland, H.L.O., Bruggeman, J., Hermoso, M. and Rickaby, R.E.M. (2017) The origin of carbon isotope vital effects in coccolith calcite. Nature Communications 8, 14511.

Meeks, J.C. (1998) Symbiosis between Nitrogen-Fixing Cyanobacteria and Plants. BioScience 48, 266-276.

Meeks, J.C., Elhai, J., Thiel, T., Potts, M., Larimer, F., Lamerdin, J., Predki, P. and Atlas, R. (2001) An overview of the genome of Nostoc punctiforme, a multicellular, symbiotic cyanobacterium. Photosynthesis Research 70, 85-106.

Mejía, L.M., Paytan, A., Eisenhauer, A., Böhm, F., Kolevica, A., Bolton, C., Méndez-Vicente, A., Abrevaya, L., Isensee, K. and Stoll, H. (2018) Controls over δ44/40Ca and Sr/Ca variations in coccoliths: New perspectives from laboratory cultures and cellular models. Earth and Planetary Science Letters 481, 48-60.

Milligan, A.J., Varela, D.E., Brzezinski, M.A. and Morel, F.M.M. (2004) Dynamics of silicon metabolism and silicon isotopic discrimination in a marine diatomas a function of pCO2. Limnology and Oceanography 49, 322-329.

Moncany, M.L.J. and Kellenberger, E. (1981) High magnesium content ofEscherichia coli B. Experientia 37, 846-847.

Moomaw, A.S. and Maguire, M.E. (2008) The Unique Nature of Mg(2+) Channels. Physiology (Bethesda, Md.) 23, 275-285.

Moosdorf, N., Renforth, P. and Hartmann, J. (2014) Carbon Dioxide Efficiency of Terrestrial Enhanced Weathering. Environmental Science & Technology 48, 4809-4816.

Moulton, K.L., West, J. and Berner, R.A. (2000) Solute flux and mineral mass balance approaches to the quantification of plant effects on silicate weathering. American Journal of Science 300, 539-570.

Moynier, F. and Fujii, T. (2017) Theoretical isotopic fractionation of magnesium between chlorophylls. Scientific Reports 7, 6973.

Müller, D.B., Vogel, C., Bai, Y. and Vorholt, J.A. (2016) The Plant Microbiota: Systems-Level Insights and Perspectives. Annual Review of Genetics 50, 211-234.

Nai, C., Wong, H.Y., Pannenbecker, A., Broughton, W.J., Benoit, I., de Vries, R.P., Gueidan, C. and Gorbushina, A.A. (2013) Nutritional physiology of a rock-inhabiting, model microcolonial fungus from an ancestral lineage of the Chaetothyriales (Ascomycetes). Fungal Genetics and Biology 56, 54-66.

Nelson, D.L. and Kennedy, E.P. (1971) Magnesium Transport in Escherichia coli : INHIBITION BY COBALTOUS ION. Journal of Biological Chemistry 246, 3042-3049.

Nierhaus, K.H. (2014) Mg(2+), K(+), and the Ribosome. Journal of Bacteriology 196, 3817-3819.

Noack-Schönmann, S., Bus, T., Banasiak, R., Knabe, N., Broughton, W.J., Den Dulk-Ras, H., Hooykaas, P.J.J. and Gorbushina, A.A. (2014) Genetic transformation of Knufia petricola A95 - a model organism for biofilm-material interactions. AMB Express 4, 80-85.

Oelkers, E.H., Benning, L.G., Lutz, S., Mavromatis, V., Pearce, C.R. and Plümper, O. (2015) The efficient long-term inhibition of forsterite dissolution by common soil bacteria and fungi at Earth surface conditions. Geochimica et Cosmochimica Acta 168, 222-235.

Oelkers, E.H., Declercq, J., Saldi, G.D., Gislason, S.R. and Schott, J. (2018) Olivine dissolution rates: A critical review. Chemical Geology https://doi.org/10.1016/j.chemgeo.2018.10.008.

Okorokov, L.P., Kholodenko, V.P., Kadomtseva, V.M., Petrikevich, S.B., Zaichkin, E.I. and Karimova, A.M. (1975) Free and Bound Magnesium in Fungi and Yeasts. Folia Microbiologica 20, 460-466.

Opfergelt, S., Burton, K.W., Georg, R.B., West, A.J., Guicharnaud, R.A., Sigfusson, B., Siebert, C., Gislason, S.R. and Halliday, A.N. (2014) Magnesium retention on the soil exchange complex controlling Mg isotope variations in soils, soil solutions and vegetation in volcanic soils, Iceland. Geochimica et Cosmochimica Acta 125, 110-130.

Opfergelt, S., Georg, R.B., Delvaux, B., Cabidoche, Y.M., Burton, K.W. and Halliday, A.N. (2012) Mechanisms of magnesium isotope fractionation in volcanic soil weathering sequences, Guadeloupe. Earth and Planetary Science Letters 341-344, 176-185.

Pasternak, J., Kocot, J. and Horecka, A. (2010) Biochemistry of magnesium. Journal of Elementology 15, 601-616.

Pearce, C.R., Saldi, G.D., Schott, J. and Oelkers, E.H. (2012) Isotopic fractionation during congruent dissolution, precipitation and at equilibrium: Evidence from Mg isotopes. Geochimica et Cosmochimica Acta 92, 170-183.

Pogge von Strandmann, P.A.E., Elliott, T., Marschall, H.R., Coath, C., Lai, Y.-J., Jeffcoate, A.B. and Ionov, D.A. (2011) Variations of Li and Mg isotope ratios in bulk chondrites and mantle xenoliths. Geochimica et Cosmochimica Acta 75, 5247-5268.

Pokharel, R., Gerrits, R., Schuessler, J.A., Floor, G.H., Gorbushina, A.A. and von Blanckenburg, F. (2017) Mg Isotope Fractionation during Uptake by a Rock-Inhabiting, Model Microcolonial Fungus Knufia petricola at Acidic and Neutral pH. Environmental Science & Technology 51, 9691-9699.

Pokharel, R., Gerrits, R., Schuessler, J.A., Frings, P.J., Sobotka, R., Gorbushina, A.A. and von Blanckenburg, F. (2018) Magnesium stable isotope fractionation on a cellular level explored by cyanobacteria and black fungi with implications for higher plants. Environmental Science & Technology.

Pokrovsky, O.S. and Schott, J. (2000a) Forsterite surface composition in aqueous solutions: a combined potentiometric, electrokinetic, and spectroscopic approach. Geochimica et Cosmochimica Acta 64, 3299-3312.

Pokrovsky, O.S. and Schott, J. (2000b) Kinetics and mechanism of forsterite dissolution at 25°C and pH from 1 to 12. Geochimica et Cosmochimica Acta 64, 3313-3325.

Proe, M.F., Midwood, A.J. and Craig, J. (2000) Use of Stable Isotopes to Quantify Nitrogen, Potassium and Magnesium Dynamics in Young Scots Pine (Pinus sylvestris). The New Phytologist 146, 461-469.

Quamme, G.A. (2010) Molecular identification of ancient and modern mammalian magnesium transporters. American Journal of Physiology-Cell Physiology 298, C407-C429.

Ra, K. and Kitagawa, H. (2007) Magnesium isotope analysis of different chlorophyll forms in marine phytoplankton using multi-collector ICP-MS. Journal of Analytical Atomic Spectrometry 22, 817-821.

Ra, K., Kitagawa, H. and Shiraiwa, Y. (2010) Mg isotopes in chlorophyll-a and coccoliths of cultured coccolithophores (Emiliania huxleyi) by MC-ICP-MS. Marine Chemistry 122, 130-137.

Renforth, P., Pogge von Strandmann, P.A.E. and Henderson, G.M. (2015) The dissolution of olivine added to soil: Implications for enhanced weathering. Applied Geochemistry 61, 109-118.

Rimstidt, J.D., Brantley, S.L. and Olsen, A.A. (2012) Systematic review of forsterite dissolution rate data. Geochimica et Cosmochimica Acta 99, 159-178.

Romani, A. and Scarpa, A. (1992) Regulation of cell magnesium. Archives of Biochemistry and Biophysics 298, 1-12.

Rosling, A., Lindahl, B.D., Taylor, A.F.S. and Finlay, R.D. (2004) Mycelial growth and substrate acidification of ectomycorrhizal fungi in response to different minerals. FEMS Microbiology Ecology 47, 31-37.

Ryu, J.-S., Vigier, N., Decarreau, A., Lee, S.-W., Lee, K.-S., Song, H. and Petit, S. (2016) Experimental investigation of Mg isotope fractionation during mineral dissolution and clay formation. Chemical Geology 445, 135-145.

Saldi, G.D., Daval, D., Morvan, G. and Knauss, K.G. (2013) The role of Fe and redox conditions in olivine carbonation rates: An experimental study of the rate limiting reactions at 90 and 150°C in open and closed systems. Geochimica et Cosmochimica Acta 118, 157-183.

Sand-Jensen, K. (2014) Ecophysiology of gelatinous Nostoc colonies: unprecedented slow growth and survival in resource-poor and harsh environments. Annals of Botany 114, 17-33.

Schauble, E.A. (2004) Applying Stable Isotope Fractionation Theory to New Systems. Reviews in Mineralogy and Geochemistry 55, 65-111.

Schauble, E.A. (2007) Role of nuclear volume in driving equilibrium stable isotope fractionation of mercury, thallium, and other very heavy elements. Geochimica et Cosmochimica Acta 71, 2170-2189.

Schmitt, A.-D., Vigier, N., Lemarchand, D., Millot, R., Stille, P. and Chabaux, F. (2012) Processes controlling the stable isotope compositions of Li, B, Mg and Ca in plants, soils and waters: A review. Comptes Rendus: Geoscience 344, 704-722.

Schott, J. and Berner, R.A. (1983) X-ray photoelectron studies of the mechanism of iron silicate dissolution during weathering. Geochimica et Cosmochimica Acta 47, 2233-2240.

Schott, J., Mavromatis, V., Fujii, T., Pearce, C.R. and Oelkers, E.H. (2016) The control of carbonate mineral Mg isotope composition by aqueous speciation: Theoretical and experimental modeling. Chemical Geology 445, 120-134.

Schuessler, J.A., Kämpf, H., Koch, U. and Alawi, M. (2016) Earthquake impact on iron isotope signatures recorded in mineral spring water. Journal of Geophysical Research: Solid Earth 121, 8548-8568.

Schuessler, J.A., von Blanckenburg, F., Bouchez, J., Uhlig, D. and Hewawasam, T. (2018) Nutrient cycling in a tropical montane rainforest under a supply-limited weathering regime traced by elemental mass balances and Mg stable isotopes. Chemical Geology 497, 74-87.

Schuiling, R.D., Herk, J. and Pietersen, H.S. (1986) A potential process for the neutralisation of industrial waste acids by reaction with olivine. Geologie & Mijnbouw 65, 243-246.

Schuiling, R.D. and Krijgsman, P. (2006) Enhanced Weathering: An Effective and Cheap Tool to Sequester Co2. Climatic Change 74, 349-354.

Schüßler, A., Martin, H., Cohen, D., Fitz, M. and Wipf, D. (2007) Arbuscular Mycorrhiza: Studies on the Geosiphon Symbiosis Lead to the Characterization of the First Glomeromycotan Sugar Transporter. Plant Signaling & Behavior 2, 431-434.

Schwartzman, D.W. and Volk, T. (1989) Biotic enhancement of weathering and the habitability of Earth. Nature 340, 457.

Seiffert, F., Bandow, N., Bouchez, J., von Blanckenburg, F. and Gorbushina, A.A. (2014) Microbial Colonization of Bare Rocks: Laboratory Biofilm Enhances Mineral Weathering. Procedia Earth and Planetary Science 10, 123-129.

Seiffert, F., Bandow, N., Kalbe, U., Milke, R. and Gorbushina, A.A. (2016) Laboratory Tools to Quantify Biogenic Dissolution of Rocks and Minerals: A Model Rock Biofilm Growing in Percolation Columns. Frontiers in Earth Science 4.

Selbmann, L., Zucconi, L., Isola, D. and Onofri, S. (2015) Rock black fungi: excellence in the extremes, from the Antarctic to space. Current Genetics 61, 335-345.

Shalev, N., Farkaš, J., Fietzke, J., Novák, M., Schuessler, J.A., Pogge von Strandmann, P.A.E. and Törber, P.B. (2018) Mg Isotope Interlaboratory Comparison of Reference Materials from Earth-Surface Low-Temperature Environments. Geostandards and Geoanalytical Research 42, 205-221.

Shaul, O. (2002) Magnesium transport and function in plants: the tip of the iceberg. Biometals 15, 307-321.

Shirokova, L.S., Mavromatis, V., Bundeleva, I., Pokrovsky, O.S., Bénézeth, P., Pearce, C., Gérard, E., Balor, S. and Oelkers, E.H. (2011) Can Mg isotopes be used to trace cyanobacteria-mediated magnesium carbonate precipitation in alkaline lakes? Biogeosciences Discussions 8, 6473-6517.

Sigfusson, B., Gislason, S.R. and Paton, G.I. (2008) Pedogenesis and weathering rates of a Histic Andosol in Iceland: Field and experimental soil solution study. Geoderma 144, 572-592.

Silver, S. (1969) Active transport of magnesium in Escherichia coli Proceedings of the National Academy of Sciences 62, 764-771.

Sissmann, O., Daval, D., Brunet, F., Guyot, F., Verlaguet, A., Pinquier, Y., Findling, N. and Martinez, I. (2013) The deleterious effect of secondary phases on olivine carbonation yield: Insight from time-resolved aqueous-fluid sampling and FIB-TEM characterization. Chemical Geology 357, 186-202.

Sommer, M., Kaczorek, D., Kuzyakov, Y. and Breuer, J. (2006) Silicon pools and fluxes in soils and landscapes—a review. Journal of Plant Nutrition and Soil Science 169, 310-329.

Staley, J.T., Palmer, F. and Adams, J.B. (1982) Microcolonial Fungi: Common Inhabitants on Desert Rocks? Science 215, 1093-1095.

Stein, A. and Crothers, D.M. (1976) Equilibrium binding of magnesium(II) by Escherichia coli tRNAfMet. Biochemistry 15, 157-160.

Sulzman, W.K. (1995) Stable Isotope Chemistry and Measurement: a Primer in: Lajtha, K., Michener, R. (Eds.), Stable Isotopes in Ecology and Environmental Science, Second Edition. Blackwell Publishing.

Taylor, L.L., Quirk, J., Thorley, R.M.S., Kharecha, P.A., Hansen, J., Ridgwell, A., Lomas, M.R., Banwart, S.A. and Beerling, D.J. (2015) Enhanced weathering strategies for stabilizing climate and averting ocean acidification. Nature Climate Change 6, 402.

Tipper, E.T., Gaillardet, J., Louvat, P., Capmas, F. and White, A.F. (2010) Mg isotope constraints on soil pore-fluid chemistry: Evidence from Santa Cruz, California. Geochimica et Cosmochimica Acta 74, 3883-3896.

Tipper, E.T., Lemarchand, E., Hindshaw, R.S., Reynolds, B.C. and Bourdon, B. (2012) Seasonal sensitivity of weathering processes: Hints from magnesium isotopes in a glacial stream. Chemical Geology 312, 80-92.

Torres, M.A., West, A.J. and Nealson, K. (2014) Microbial Acceleration of Olivine Dissolution via Siderophore Production. Procedia Earth and Planetary Science 10, 118-122.

Uhlig, D., Schuessler, J.A., Bouchez, J., Dixon, J.L. and von Blanckenburg, F. (2017) Quantifying nutrient uptake as driver of rock weathering in forest ecosystems by magnesium stable isotopes. Biogeosciences 14, 3111-3128.

Utkilen, H.C. (1982) Magnesium-limited Growth of the Cyanobacterium Anacystis nidulans. Microbiology 128, 1849-1862.

Verrecchia, E. (2000) Fungi and Sediments, In: Riding R.E., Awramik S.M. (eds) Microbial Sediments. Springer, Berlin, Heidelberg, pp. 68-75.

von Blanckenburg, F., Wittmann, H. and Schuessler, J.A. (2016) HELGES: Helmholtz Laboratory for the Geochemistry of the Earth Surface. Journal of large-scale research facilities 2, A84.

Walker, J.C.G., Hays, P.B. and Kasting, J.F. (1981) A negative feedback mechanism for the long-term stabilization of Earth's surface temperature. Journal of Geophysical Research: Oceans 86, 9776-9782.

Warcup, J.H. (1951) The ecology of soil fungi. Transactions of the British Mycological Society 34, 376-399.

White, A.F. and Brantley, S.L. (2003) The effect of time on the weathering of silicate minerals: why do weathering rates differ in the laboratory and field? Chemical Geology 202, 479-506.

Wiederhold, J.G. (2015) Metal Stable Isotope Signatures as Tracers in Environmental Geochemistry. Environmental Science & Technology 49, 2606-2624.

Wiederhold, J.G., Kraemer, S.M., Teutsch, N., Borer, P.M., Halliday, A.N. and Kretzschmar, R. (2006) Iron Isotope Fractionation during Proton-Promoted, Ligand-Controlled, and Reductive Dissolution of Goethite. Environmental Science & Technology 40, 3787-3793.

Wille, M., Sutton, J., Ellwood, M.J., Sambridge, M., Maher, W., Eggins, S. and Kelly, M. (2010) Silicon isotopic fractionation in marine sponges: A new model for understanding silicon isotopic variations in sponges. Earth and Planetary Science Letters 292, 281-289.

Wimpenny, J., Colla, C.A., Yin, Q.-Z., Rustad, J.R. and Casey, W.H. (2014) Investigating the behaviour of Mg isotopes during the formation of clay minerals. Geochimica et Cosmochimica Acta 128, 178-194.

Wimpenny, J., Gíslason, S.R., James, R.H., Gannoun, A., Pogge Von Strandmann, P.A.E. and Burton, K.W. (2010) The behaviour of Li and Mg isotopes during primary phase dissolution and secondary mineral formation in basalt. Geochimica et Cosmochimica Acta 74, 5259-5279.

Wogelius, R.A. and Walther, J.V. (1991) Olivine dissolution at 25°C: Effects of pH, CO2, and organic acids. Geochimica et Cosmochimica Acta 55, 943-954.

Wolf, F.I. and Cittadini, A. (2003) Chemistry and biochemistry of magnesium. Molecular Aspects of Medicine 24, 3-9.

Wollenzien, U., de Hoog, G.S., Krumbein, W. and Uijthof, J.M.J. (1997) Sarcinomyces petricola, a new microcolonial fungus from marble in the Mediterranean basin. Antonie van Leeuwenhoek 71, 281-288.

Wombacher, F., Eisenhauer, A., Böhm, F., Gussone, N., Regenberg, M., Dullo, W.C. and Rüggeberg, A. (2011) Magnesium stable isotope fractionation in marine biogenic calcite and aragonite. Geochimica et Cosmochimica Acta 75, 5797-5818.

Young, E.D. and Galy, A. (2004) The Isotope Geochemistry and Cosmochemistry of Magnesium. Reviews in Mineralogy and Geochemistry 55, 197-230.

Yurlova, N.A., de Hoog, G.S. and Fedorova, L.G. (2008) The influence of ortho- and para-diphenoloxidase substrates on pigment formation in black yeast-like fungi. Studies in Mycology 61, 39-49.

Zhang, G., Dong, H., Jiang, H., Kukkadapu, R.K., Kim, J., Eberl, D. and Xu, Z. (2009) Biomineralization associated with microbial reduction of Fe3+ and oxidation of Fe2+ in solid minerals. American Mineralogist 94, 1049-1058.

Zhang, T., Wang, N.-F., Liu, H.-Y., Zhang, Y.-Q. and Yu, L.-Y. (2016) Soil pH is a Key Determinant of Soil Fungal Community Composition in the Ny-Ålesund Region, Svalbard (High Arctic). Frontiers in Microbiology 7, DOI 10.3389/fmicb.2016.00227.

Ziegler, K., Chadwick, O.A., Brzezinski, M.A. and Kelly, E.F. (2005) Natural variations of δ30Si ratios during progressive basalt weathering, Hawaiian Islands. Geochimica et Cosmochimica Acta 69, 4597-4610.

Zitomer, R.S. and Flaks, J.G. (1972) Magnesium dependence and equilibrium of the Escherichia coli ribosomal subunit association. Journal of Molecular Biology 71, 263-279.